

Design and Development of Hydro-Squeeze Classifier Assisted Grinding Ball Mill for Narrow Size Particle Separation

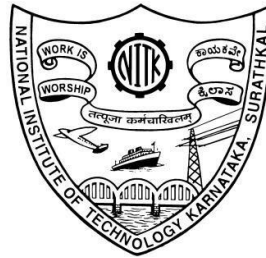
Thesis

Submitted in partial fulfilment of the requirements for the degree of

DOCTOR OF PHILOSOPHY

by

HARISH H



DEPARTMENT OF MINING ENGINEERING
NATIONAL INSTITUTE OF TECHNOLOGY KARNATAKA,
SURATHKAL, MANGALORE-575025

SEPTEMBER, 2022

DECLARATION

by the Ph.D. Research Scholar

I hereby *declare* that the Research Thesis entitled “**Design and Development of Hydro-Squeeze Classifier Assisted Grinding Ball Mill for Narrow Size Particle Separation**” which is being submitted to the National Institute of Technology Karnataka, Surathkal in partial fulfillment of the requirements for the award of the Degree of **Doctor of Philosophy in Mining Engineering** is a *bonafide report of the research work carried out by me*. The material contained in this Research Thesis has not been submitted to any University or Institution for the award of any degree.



Harish H

Reg.No.:165072MN16F01

Department of Mining Engineering

Place: NITK-Surathkal

Date: 06/09/2022

CERTIFICATE

This is to certify that the Research Thesis entitled “**Design and Development of Hydro-Squeeze Classifier Assisted Grinding Ball Mill for Narrow Size Particle Separation**” submitted by **Mr. Harish H (Register Number: 165072MN16F01)** as the record of the research work carried out by him, is *accepted as the Research Thesis submission* in partial fulfillment of the requirements for the award of degree of Doctor of Philosophy.


Prof. Harsha Vardhan


Prof. Govinda Raj

Research Guides

Department of Mining Engineering
National Institute of Technology Karnataka,
Surathkal



Dr. Mangalpady Aruna

Associate Professor, Head and Chairman, DRPC
Department of Mining Engineering
National Institute of Technology Karnataka, Surathkal

Chairman - DRPC
Department of Mining Engineering
National Institute of Technology Karnataka, Surathkal.
P.O. Srinivasnagar 575 025, Mangalore
Karnataka State, India.

Date: 06.09.2022

*Dedicated to my wife Mrs.Nandini G V
and my daughter Yadhya H*

ACKNOWLEDGEMENTS

The research work, which is presented in this dissertation, is more of teamwork and I would like to thank many who have contributed their time and energy for the study.

First and foremost, I am grateful to my advisors Prof. Harsha Vardhan and Prof. Govinda Raj, Department of Mining Engineering, National Institute of Technology Karnataka, Surathkal (NITK) as they consistently kept me motivated and instilled good thoughts not only for research but for life as well. Their constant and enthusiastic support throughout is the root cause for the research work to see its logical end.

I wish to thank all the members of the Research Program Assessment Committee (RPAC) including Dr. A. K. Tripathi, Assistant Professor, Department of Mining Engineering, NITK, Surathkal and Prof. Ampar Chitharanjan Hegde, Professor, Department of Chemistry, NITK, Surathkal for their unbiased appreciation, support and suggestions provided during the various discussions which has certainly helped in the betterment of this research work.

I am thankful to Dr. Aruna M, Associate Professor, Head & DRPC Chairman, Department of Mining Engineering, NITK, Surathkal. I extend my gratitude to the authorities of NITK, Surathkal and Staff of Department of Mining Engineering for their help which ensured the satisfactory progress of my research work.

I am thankful to Sri. Pandey, Former Vice President, Mining Department, JSW Steel Ltd., Toranagallu, Bellary, Karnataka for getting permission for my research work in JSW R&D Centre.

I owe my deepest gratitude to JSW Steel Ltd., Toranagallu, Bellary, Karnataka for their collaboration with NITK Surathkal related to this research work. I extend my gratitude to the management of JSW Steels for providing accommodation during my stay in JSW R&D Centre.

I am thankful to Dr. Marutiram Kaza, Former Head of the R&D Department, JSW Steel Ltd., Toranagallu, Bellary, Karnataka for his excellent guidance and moral support throughout the research work. His constant encouragement, help and review of the entire work during the course of the investigation are invaluable. Also, I owe my deepest gratitude to Sri. Rameshwar Sah, General Manager, R&D Department, JSW Steel Ltd., Toranagallu, Bellary, Karnataka for his support during my stay in JSW Steel Ltd.

I am thankful to Sri. Roy, Head of the I-Shop Department, JSW Steel Ltd., Toranagallu, Bellary, Karnataka for his guidance and helping in fabrication of new machine which is related to my research work. I extend my thanks to employees of I-Shop Department, JSW Steel Ltd., Sri.Takor, Sri.Chitanya, Sri.Suhas, Sri.Ram Prasad Sri.Harish, Sri.Nagaraj, Sri.Naveen and other helper for their continued effort which helped me to fabricate and run the new machine successful.

I thank Sri. M Varma Raju and Sri.Suribabu Pandiri Assistant Manager, R&D and SS Department for their help in conducting experiments in JSW Steel Ltd. I extend my thanks to JSW R&D and SS Department for their support in conducting experiments. I extend my thanks to internship students in R&D and SS department, Sri.Raju, Sri.Karthik, Sri. Narappa, Sri.Lokesh, Sri.Abishak, Sri.Satyam, Sri.Subash, Sri.Kuber, Sri.Chakraverty for helping me to conduct experiments on the new machine.

I would also like to thank the management of the Hutti Gold Mines Company Ltd. & Karnataka State Mineral Corporation Ltd. for their partial financial support for this work.

I would like to thank my friends Mr. Bharath Kumar, Mr. Harish Kumar N S, Mr. Vijay Kumar S, Mr. Balaji Rao K, Mrs. Gayana B C, Mr. N V Sarathbabu Goriparti, Mr. Ch. Vijay Kumar, Mr. Balaraju Jakulla, Mr. Abhishek Kumar Tripathi, Mr. Raghu Chandra Garimella,, Mr. Tejeswaran K M, Mr. and M. Sasi Kiran, who have helped in various stages of the project at NITK, Surathkal, and made my stay feel comfortable.

I express my heartfelt thanks to all the non-teaching staff of the Department of Mining Engineering, NITK, Surathkal who helped me in one way or the other during the course

of my work. Also, I thank NITK, Surathkal, for providing financial assistance and all the necessary facilities to make this research successful.

I owe my deepest gratitude to my parents Mr.Hanumanthappa V and Mrs.Rajamma K P and my in-laws Late Mr. Vasudeva G and Mrs.Vimalamma for their support. Last but not the least; I owe my gratitude to my spouse Mrs.Nandini G V and my daughter Yadhya H who has been very patient and supportive at all times. She has been strong and steady source of inspiration for me and there have been countless moments while pursuing my research that, without her, I feel I would have succumbed to defeat. I thank all of them from the bottom of my heart for the undivided support and being a witness for every step of the way. I thank them for all the sacrifices they have gone through to give me the best of the best things in life.

Place: NITK, Surathkal

Date: 06/09/2022

Harish H

ABSTRACT

In the iron and steel industry, the production of desired particle size distribution (PSD) for pellet feed making from the iron ore is very difficult. This study is carried out to achieve desired pellet feed particle size distribution from the iron ore. The iron ores have been collected from three different sources (mines in Karnataka state) and milled. Iron ore obtained from different sources differ in their chemical and physical properties. These variations make the process of grinding a difficult task. The work carried out in this context focuses on three different samples of iron ore, viz., High Silica High Alumina (HSHA), Low Silica High Alumina (LSHA), and Low Silica low Alumina (LSLA).

The grinding process for all the three iron ores is carried out individually in Bond's ball mill and the total retention time taken by each iron ore sample is calculated. The present investigation focuses on utilizing the calculated retention time of the iron ore as a standard grinding reference time to the laboratory ball mill for optimizing the grinding time of each ore. The desired P_{80} (150 μm) with an acceptable range of hematite liberation ($>75\%$) was obtained in laboratory ball mill after reducing 6 min from the total retention time taken in the Bond's ball mill. The blend as iron ore feed sample was prepared by using High Silica High Alumina, Low Silica High Alumina, and Low Silica low Alumina iron samples, in various proportions.

The iron ore blend feed sample is analyzed in the Optical Microscope (OM) and QEMSCAN (Quantitative Evaluation of Minerals by Scanning Electron Microscopy) to understand the PSD and percentage of hematite liberation. A new approach was adapted to identify the retention time (RT) of the iron ore blend in the mill, and the total retention time (TRT) taken for the blend sample in the Bond's ball mill (BBM) was considered as the reference grinding time for milling in the Laboratory Ball Mill (LBM). The desired PSD ($-150 \mu\text{m}$) with acceptable hematite liberation was achieved at an optimal grinding time of 7 min in the LBM.

The discharge end design of a ball mill plays an important role in discharging the desired particle sizes ($-150 + 10 \mu\text{m}$) and the percentage of recirculating load from the discharge end of the ball mill. In continuous wet ball mills, the composition of feed (hard ore or soft ore) to the mill varies continuously, leading to uncontrolled grinding in the mill. In view of this, a new design of the discharge mechanism has been implemented to remove the ground particles of desired particle size fraction with minimum recirculating load ($+150 \mu\text{m}$).

The results from the discharge end with lifters (closed and open) show that the particle size fraction obtained from the discharge end has a maximum percentage of desired particle size fraction when the mill is operating at 60% critical speed. Discharge end without lifters has an uncontrolled particle size distribution in the discharge and the percentage of desired-size particles discharged was found to be very less. Also, the percentage of the recirculating load is minimum in the case of discharge end with lifter design compared with discharge end without a lifter. Hence, a new design of lifters in the discharge end leads to the discharge of the desired particle size fraction with minimum recirculating load.

A new ball mill hydro-squeeze classifier has been developed for particle size reduction and wet classification of different particle sizes. The mill classifier consists of milling and classification sections with a squeezing disc with a mesh of $150 \mu\text{m}$. This study analyses the size of particles discharged from the ball mill and the efficiency of hydro-squeeze classifier in separating oversize particles from undersize particles. The ball mill hydro-squeeze classifier was tested at different iron ore feed slurry concentrations and the ball mill operating discharge end opening time. A significant increase in coarse particle discharge from the mill to the classification section was achieved at a higher (75%) slurry solid concentration. The squeezing of the slurry increases the recirculating load to the mill. The squeezing efficiency is maximum (84.8%) at a solid slurry concentration of 55% at a mill discharge opening time of 150 s. The separated particles in the hydro-squeeze classifier consist of 100% $-150 \mu\text{m}$ particles. Further, these particles can be directly used for downstream processing without any classification. The results obtained are applicable for the pilot-

scale development of a new ball mill hydro-squeeze classifier unit for wet grinding and classification process.

Key words: Particle Size Distribution, Retention time, Bond Work Index and Circulating load, Optical Microscope, QEMSCAN

ACRONYMS

PSD	Particle Size Distribution
OM	Optical Microscope
QEMSCAN	Quantitative Evaluation of Minerals by Scanning Electron Microscopy
RT	Retention Time
TRT	Total Retention Time
BBM	Bond's ball mill
BWI	Bond Work Index
LBM	Laboratory Ball Mill
HSHA	High Silica High Alumina
LSHA	Low Silica High Alumina
LSLA	Low Silica low Alumina
C_s	Critical speed of the mill
D	Mill diameter in meters
M_H	Material mass holdup in kg
ψ_s	Fractional cross sectional area opened for discharge at mill
V_{op}	Mill opening velocity of material discharge in m/s
M_{Ho}	Mill retained mass of the material at F=0 in kg
F	Mass feed rate in kg/s
L	Mill length in m
C_1	Constant expressing the discharge properties at the mill exit
θ_{pool}	Power Function
C, k	Fitting Parameters
SAG	Semi-Autogenous Grinding
AG	Autogenous Grinding
$A_1, A_2, A_3,$	Constants depend on the mill speed and ball filling
B	Constant depend on the ore properties
U^*	Slurry filling before pool formation when net power draw is maximum
$B_1, B_2, B_3,$	Constants depend on the mill speed and slurry properties
d	Constants depend on ball filling

C*	Slurry concentration for maximum net power draw
RTD	Residence Time Distribution
AR	Attainable Region technique
MRT	Mean Residence Time
DEM	Discrete Element Method
XRF	X-ray fluorescence
LALLS	Low Angle Laser Light Scattering
T	Total retention time taken by the BBM for each iron ore sample
R	Total number of revolutions taken by each ore sample in the BBM
F ₈₀	80% passing particle size of the feed in μm
P ₈₀	80% passing particle size of the final grinding cycle product in μm
A	Mesh size of the test in m,
G _{bp}	Grindability of the undersized product produced per mill revolution
T%	Degree of liberation in the iron ore sample
L%	Apparent degree of liberation
SEM	Scanning Electron Microscope
EDS	Energy-dispersive X-ray spectroscopy
η	Efficiency of classifier disc
G	Goethite
H	Hematite
K	Kaolinite
A	Fe Ox-Al Silicate interface
Q	Quartz
L	Limonite
BMA	Bulk Mineral Analysis
PMA	Particle Mineral Analysis

TABLE OF CONTENTS

ACKNOWLEDGEMENTS	i
ABSTRACT	i
ACRONYMS	v
TABLE OF CONTENTS	vii
LIST OF FIGURES	xii
LIST OF TABLES	xix
CHAPTER 1	1
1 INTRODUCTION	1
1.1 General	1
1.2 Organization of Thesis	3
CHAPTER 2	5
2 LITERATURE REVIEW AND OBJETIVES OF THE RESEARCH WORK	5
2.1 General	5
2.2 Characterization Studies	6
2.3 Assessing Ball Mill Response Based on Mill Performance	7
2.3.1 Energy consumption	8
2.3.1.1 Feed rate	8
2.3.1.2 Speed of the mill	8
2.3.2 Mill hold-up	9
2.3.2.1 Variation of slurry hold-up based on time	10
2.3.2.2 Effect of mill feed rate	10
2.3.2.3 Influence of percentage of solids in feed on mill hold-up	11
2.3.2.4 Effect of mill speed	11
2.3.3 Parameters influencing the ball mill discharge	11
2.3.3.1 Discharge grate	11
2.3.3.2 Pebble discharge	11
2.3.3.3 Mill hold-up	12
2.3.3.4 Pulp lifters	12
2.3.4 Influence of slurry pool volume on milling efficiency	12

2.3.4.1	Impact of slurry pool volume on net power draw	12
2.3.4.2	Effects on the specific energy consumption due to pool volume.....	13
2.3.4.3	Effects on the size reduction index due to the pool volume.....	13
2.3.4.4	Effects on grinding index due to the pool volume	13
2.3.4.5	Effects of slurry filling on load orientation.....	13
2.3.5	Impact angle variation due to slurry filling	14
2.3.5.1	Toe angle variation due to slurry filling.....	14
2.3.5.2	Shoulder angle variation due to slurry filling.....	14
2.3.5.3	Pool angle variation due to slurry filling.....	15
2.3.6	Impact forces	15
2.3.6.1	Variation of impact forces with speed.....	15
2.3.6.2	Impact forces variations with slurry filling	16
2.3.6.3	Impact forces variations with slurry concentration	16
2.3.7	Effect of net power draw	17
2.3.7.1	Variation of power draw with media charge filling	17
2.3.7.2	Variation of power draw with mill speed.....	18
2.3.7.3	Power draw variations with slurry filling.....	18
2.3.7.4	Power draw variations with slurry concentration.....	18
2.3.8	Residence time distribution	19
2.4	Effect of Ball Mill Design on Slurry Discharge.....	20
2.4.1	Pulp lifters	20
2.5	Wet Classification	22
2.6	Summary	24
2.7	Objectives of Present Research Study.....	24
2.8	Research Methodology.....	25
CHAPTER 3	27
3	EQUIPMENTS AND METHODS USED IN THIS RESEARCH WORK	27
3.1	Introduction	27
3.2	Collection of Iron Ore Samples.....	27
3.3	Chemical Analysis.....	28
3.1.1	Sample preparation for XRF scan	28

3.2 Particle Size Analysis	29
3.2.1 Quadrant divider.....	29
3.2.2 Sieve shaker.....	30
3.2.3 Particle size analyzer	30
3.3 Grindability Test.....	31
3.3.1 Bond Work Index	31
3.3.2 Laboratory ball mill.....	33
3.4 Charaterization Study on Iron Ore Samples.....	34
3.4.1 Optical Microscopy and QEMSCAN analysis	34
3.4.1.1 Preparation of iron ore sample for Optical Microscopy and QEMSCAN analysis	36
3.4.2 Liberation analysis	37
3.4.3 Scanning Electron Microscope.....	37
CHAPTER 4	39
4 DESIGN AND FABRICATION OF NEW BALL MILL HYDRO- SQUEEZE CLASSIFIER.....	39
4.1 Introduction	39
4.2 Experimental Setup	40
4.3 Design of Outlet Discharge Trunnion With Lifter Arrangement	52
4.3.1 Experimental procedure for newly designed ball mill outlet discharge trunnion with lifter arrangement.....	54
4.3.2 Particle size measurements for Case-1, Case-2 and Case-3	56
4.4 Preparation of Feed Sample for New Ball Mill Hydro-Squeeze Classifier.....	56
4.4.1 Operation of ball mill hydro-squeeze classifier	57
4.4.2 Product Particle size analysis of ball mill hydro-squeeze classifier.....	61
CHAPTER 5	63
5 RESULTS OF EXPERIMENTAL INVESTIGATIONS.....	63
5.1 Bond Work Index Determination Using Standard Ball Mill.....	63
5.1.1 Bond Work Index calculation for HSHA iron ore sample	63
5.1.2 Bond Work Index calculation for LSHA iron ore sample.....	66
5.1.3 Bond Work Index calculation for LSLA iron ore sample	69
5.2 Grindability Studies Using Laboratory Ball Mill.....	73

5.2.1 Effect of varying grinding time in laboratory ball mill on particle size distribution of HSHA	73
5.2.2 Effect of varying grinding time in laboratory ball mill for LSHA on particle size.....	75
5.2.3 Effect of varying grinding time in laboratory ball mill for LSLA on particle size.....	77
5.3 Characterization Analysis of HSHA, LSHA, and LSLA Iron Ore Samples.....	80
5.3.1 Mineralogical analysis of feed sample by optical microscopy.....	81
5.3.2 Mineralogical analysis of feed sample by QEMSCAN.....	82
5.3.3 Effect of retention time on the degree of hematite liberation in HSHA, LSHA, and LSLA	84
5.3.4 Comparing PSD, percentage of hematite liberation and total grinding time taken for HSHA, LSHA and LSLA iron ore samples in BBM and LBM	92
5.4 Characterization of Blend Iron Ore Samples	95
5.4.1 OM and QEMSCAN analysis of blend feed sample with respect to liberation and locking of hematite.....	95
5.4.2 Grinding of blend sample in the BBM and LBM.....	97
5.4.3 Particle size analyses in OM for blend Product sample grounded in LBM at different grinding time	98
5.4.4 Sink and float test for iron ore blend with varied grinding time	101
5.4.5 Liberation analysis of blend product samples ground in LBM for different grinding times	102
5.4.6 Variation of hematite liberation and PSD with respect to grinding time for iron ore blend product.....	104
5.5 Comparative Analysis of a Newly Designed Ball Mill and the Conventional Ball Mill Performance With Respect to Particle Size Distribution and Recirculating Load at the Discharge End.....	106
5.5.1 Case 1: Effect of mill speed on the product particle size distribution and recirculating load of the ball mill without lifters and the discharge end open	107
5.5.2 Case 2: Effect of mill speed on the particle size distribution of the product and the recirculating load of the ball mill with lifters and the cap open at the discharge.....	110

5.5.3	Case 3: Effect of mill speed on the particle size distribution and recirculating load in the ball mill with lifters and the cap closed at discharge.....	114
5.5.4	Comparison of Case 1, Case 2 and Case 3	117
5.6	Evaluation of a New Ball Mill Hydro-Squeeze Classifier for Particle Size Reduction and Classification.....	121
5.6.1	Effect of the solid slurry concentration and the mill discharge end opening time on the size of particles discharged.....	121
5.6.2	Particle size analysis of classified ground product in Chamber-1 and Chamber-2 after squeezing.....	127
5.6.3	Characterization analysis.....	137
5.6.4	Effect of internal pressure created on particle size classification efficiency	140
6	CONCLUSIONS AND RECOMMENDATIONS FOR FUTURE WORK ...	145
6.1	Conclusions	145
6.2	Recommendations for Future Work	146
	REFERENCES	149
	APPENDIX-I.....	163
	LIST OF PUBLICATIONS BASED ON Ph.D RESEARCH WORK	163
	PATENT BASED ON Ph.D RESEARCH WORK.....	165
	APPENDIX-II.....	167
I.	Fabrication Methods for New Ball Mill Hydro-Squeeze Classifier.....	167
	BIODATA.....	175

LIST OF FIGURES

Fig. No.	Description	Page No.
1.1	Square AG/SAG Mill with Grating.	2
2.1	Ball filling effect on mill power draw data (Soleymani et al. 2016)	17
2.2	Schematic representation of the methodology	26
3.1	Quadrant divider	29
3.2	Sieve shaker	30
3.3	Particle size analyzer.....	30
3.4	Standard test mill (Bonds Ball mill)	33
3.5	Laboratory ball mill	34
3.6	Optical Microscope.....	35
3.7	QEMSCAN	35
3.8	Mould	36
3.9	Grinding wheel equipment.....	37
4.1	Ball mill hydro-squeeze classifier.....	42
4.2	Three dimensional view of ball mill hydro-squeeze.....	42
4.3	Two dimensional view of rotary drum ball mill grinding shell	43
4.4	Fabricated grinding shell.....	43
4.5	Fabricated feeder arrangement.....	44
4.6	Two dimensional view of classifier section.....	44
4.7	Fabricated classifier section.....	45
4.8	Two dimensional view of classifier disc.....	45
4.9	Two dimensional view of classifier disc.....	46
4.10	Two dimensional view of slip-in cap.....	46
4.11	Fabricated slip-in cap.....	47

4.12 Two dimensional view of flange.....	47
4.13 Fabricated flange.....	48
4.14 Two dimensional view of guide plate.....	48
4.15 Fabricated guide plate.....	49
4.16 Two dimensional view of guide rod.....	49
4.17 Fabricated guide rod.....	50
4.18 Two dimensional view of in classifier closing plate.....	50
4.19 Fabricated classifier closing plate.....	51
4.20 Three dimensional view of screw rod.....	51
4.21 Screw rod	51
4.22 2D view of the mill discharge trunnion (after Nelson, 1980).....	53
4.23 2D view of the lifter arrangement (after Nelson, 1980).....	53
4.24 Ball mill with newly fabricated discharge end.....	54
4.25 Discharge end with provision for bolting.....	54
4.26 Discharge end closed and classifier disc at parking position.....	60
4.27 Discharge end open and classifier disc at parking position.....	60
4.28 Discharge end closed and classifier disc is moved towards discharge end.....	60
4.29 Discharge end closed and classifier disc is moving towards parking position....	61
5.1 Particle size analysis for HSHA iron ore feed sample.....	65
5.2 Particle size analyses for HSHA iron ore product sample.....	66
5.3 Particle size analysis for LSHA feed sample.....	68
5.4 Particle size analysis for LSHA iron ore product sample.....	69
5.5 Particle size analysis for LSLA iron ore feed sample.....	71
5.6 Particle size analysis for LSLA Product sample.....	72
5.7 Particle size analysis for HSHA Product sample.....	75

5.8 Particle size analyses for LSHA Product sample.....	77
5.9 Particle size analyses for LSLA Product sample	79
5.10 Optical microscope photo for feed samples of HSHA.....	81
5.11 Optical microscope photo for feed samples of LSHA	82
5.12 Optical microscope photo for feed samples of LSLA	82
5.13 QEMSCAN photos for feed samples of HSHA.....	83
5.14 QEMSCAN photos for feed samples of LSHA	84
5.15 QEMSCAN photos for feed samples of LSLA.....	84
5.16 Optical microscopy of HSHA sink sample of size -150 μm grounded for 16 min in BBM	85
5.17 Optical microscopy of LSHA sink sample of size -150 μm grounded for 13 min in BBM	86
5.18 Optical microscopy of LSLA sink sample of size -150 μm grounded for 12 min in BBM	86
5.19 Optical microscopy of HSHA sink sample of size -150 μm grounded for 14 min in LBM.....	87
5.20 Optical microscopy of LSHA sink sample of size -150 μm grounded for 11 min in LBM.....	87
5.21 Optical microscopy of LSLA sink sample of size -150 μm grounded for 10 min in LBM.....	88
5.22 Optical microscopy of HSHA sink sample of size -150 μm grounded for 12 min in LBM.....	88
5.23 Optical microscopy of LSHA sink sample of size -150 μm grounded for 9 min in LBM.....	89
5.24 Optical microscopy of LSLA sink sample of size -150 μm grounded for 8 min in LBM.....	89
5.25 Optical microscopy of HSHA sink sample of size -150 μm grounded for 10 min in LBM.....	90
5.26 Optical microscopy of LSHA sink sample of size -150 μm grounded for 7 min in LBM.....	91

5.27	Optical microscopy of LSLA sink sample of size -150 μm grounded for 6 min in LBM.....	91
5.28	PSD, percentage of hematite liberation and total grinding time taken for HSHA, LSHA and LSLA iron ore samples in BBM	93
5.29	PSD, percentage of hematite liberation and after reducing 2 min from total grinding time for HSHA, LSHA and LSLA iron ore samples in LBM	93
5.30	PSD, percentage of hematite liberation and after reducing 4 min from total grinding time for HSHA, LSHA and LSLA iron ore samples in LBM	94
5.31	PSD, percentage of hematite liberation and after reducing 6 min from total grinding time for HSHA, LSHA and LSLA iron ore samples in LBM	94
5.32	OM images of the iron ore feed blend	95
5.33	3-dimensional view of liberation and locking of minerals in blend feed samples	96
5.34	Mineralogical analysis and phases in the blend feed sample by QEMSCAN	96
5.35	Specific gravity classification analysis of blend feed sample by QEMSCAN	97
5.36	Particle size analysis for blend sample ground in the LBM	98
5.37	Particle size analyses in OM for blend Product sample grounded in LBM at 11 min grinding time.....	99
5.38	Particle size analyses in OM for blend Product sample grounded in LBM at 9 min grinding time.....	99
5.39	Particle size analyses in OM for blend Product sample grounded in LBM at 7 min grinding time.....	100
5.40	Float analysis of iron ore blend with varied grinding time	101
5.41	Sink analysis of iron ore blend with varied grinding time.....	102
5.42	Liberation analysis in OM of blend sink sample grounded in LBM at grinding time - (a)11 min, (b) 9 min, and (c)7 min.....	104
5.43	Variation of hematite liberation and PSD with respect to grinding time for iron ore blend product.....	105
5.44	Discharge end without lifters (discharge end open)	106
5.45	Discharge end with lifters (discharge end open).....	107
5.46	Discharge end with lifters (discharge end closed)	107

5.47 Particle size analysis of discharge product when mill operated at different critical speeds (CS) without lifter and discharge end open.....	108
5.48 Over size (+150 μ m), narrow size (-150 μ m/+10 μ m) and undersize particle size (-10 μ m) analysis of discharge product when mill operated at different critical speeds without lifter and discharge end open	109
5.49 Influence of mill speed on percentage of recirculating load when mill operated without lifter and discharge end open	110
5.50 Particle size analysis of discharge product when mill operated at different critical speeds (CS) with lifter and discharge end open.....	112
5.51 Over size (+150 μ m), narrow size (-150 μ m/+10 μ m) and undersize particle size (-10 μ m) analysis of discharge product when mill operated at different critical speeds with lifter and discharge end open	113
5.52 Influence of mill speed on percentage of recirculating load when mill operated with lifter and discharge end open	114
5.53 Particle size analysis of discharge product when mill operated at different critical speeds (CS) with lifter and discharge end closed	115
5.54 Over size (+150 μ m), narrow size (-150 μ m/+10 μ m) and undersize particle size (-10 μ m) analysis of discharge product when mill operated at different critical speeds with lifter and discharge end closed.....	116
5.55 Influence of mill speed on percentage of recirculating load when mill operated with lifter and discharge end closed.....	116
5.56 Particle size distribution comparison for mill without lifter (cap open), with lifter (cap open), and with lifter (cap close) at different critical parentage speed (a) 20 % of C.S, (b) 30 % of C.S, (c) 40 % of C.S, (d) 50% of C.S, (e) 60 % of C.S, (f) 70 % of C.S.....	118
5.57 Influence of mill speed on particle size fraction distribution with P ₈₀ passing percentage	119
5.58 Influence of mill speed on passing % of 150 μ m particle	119
5.59 Influence of mill speed on percentage of recirculating load to ball mill	120
5.60 Particle size analysis before squeezing in Chamber-1 –(a) for 55% solids, (b) for 60% solids, (c) for 65% solids, (d) for 70% solids, and (e) for 75% solids	124
5.61 P ₈₀ passing percentage at different slurry solids percentage before squeezing in Chamber-1	125

5.62	Weight percentage of +150 μm particles collected in Chamber-1 (before squeezing) at different slurry solid concentrations	126
5.63	Weight percentage of -150 μm particles collected in Chamber-1 (before squeezing) at different slurry solid concentrations	127
5.64	Particle size analysis of leftover product in Chamber-1 after squeezing in Chamber-1 – (a) for 55% solids, (b) for 60% solids, (c) for 65% solids, (d) for 70% solids, and (e) for 75% solids.....	130
5.65	P_{80} passing percentage at different slurry solid percentages after squeezing in Chamber-1	131
5.66	Weight percentage of -150 μm particles collected in Chamber-1 (after Squeezing) at different slurry solid concentrations	132
5.67	Particle size analysis of collected product in Chamber-2– (a) for 55% solids, (b) for 60% solids, (c) for 65% solids, (d) for 70% solids, and (e) for 75% solids	135
5.68	P_{80} passing percentage at different slurry solids percentages in Chamber-2 after squeezing in Chamber-1	136
5.69	Weight percentage of -150 μm particles collected in Chamber-2 (after squeezing) at different slurry solid concentrations	137
5.70	Optical microscope images (a) for iron ore feed (b) for iron ore sample collected in Chamber-1, and (c) for iron ore sample collected in Chamber-2..	138
5.71	SEM with EDS images (a) SEM image of the iron ore feed (b) EDS image of the iron ore feed (c) SEM image of the iron ore sample collected in Chamber-1 (d) EDS image of the iron ore sample collected in Chamber-1 (e) SEM image of the iron ore sample collected in Chamber-2 and (f) EDS image of the iron ore sample collected in Chamber-2.	139
5.72	Pressure created in Chamber-1 (after squeezing) at different slurry solid concentrations for varying the mill discharge end closing time	141
5.73	Squeezing efficiency of disc at different slurry solid concentrations	143

LIST OF TABLES

Table No.	Description	Page No.
3.1	Percentage variation of silica and alumina by weight in iron ore	28
3.2	Chemical composition of iron ores	28
4.1	Chemical and physical specification of iron ore sample	56
4.2	Experimental operating condition.....	56
4.3	Ball mill hydro-squeeze classifier operating conditions.....	59
5.1	BWI iterative process for HSHA	64
5.2	Sieve analysis of HSHA with respective to feed and product	65
5.3	BWI iterative process for LSHA to get the undersized fraction.....	67
5.4	Sieve analysis of LSHA with respective to feed and product.....	68
5.5	BWI iterative process for LSLA to get the undersized fraction	70
5.6	Sieve analysis of LSLA with respective to feed and product	71
5.7	Physical analysis of iron ore by using bond work index method	72
5.8	Sieve analysis of HSHA product after 14 (min) of grinding in LBM	74
5.9	Sieve analysis of HSHA product after 12 (min) of grinding in LBM	74
5.10	Sieve analysis of HSHA product after 10 (min) of grinding in LBM	74
5.11	Sieve analysis of LSHA product after 11 (min) of grinding in LBM.....	76
5.12	Sieve analysis of LSHA product after 9 (min) of grinding in LBM.....	76
5.13	Sieve analysis of LSHA product after 7 (min) of grinding in LBM.....	76
5.14	Sieve analysis of LSLA product after 10 (min) of grinding in LBM	78
5.15	Sieve analysis of LSLA product after 8 (min) of grinding in LBM	78
5.16	Sieve analysis of LSLA product after 6 (min) of grinding in LBM	79
5.17	Physical analysis of HSHA, LSHA and LSLA using Bond's Work Index Method	80
5.18	Physical analysis of HSHA, LSHA and LSLA using LBM	92

5.19 Physical properties of iron ore blend by using LBM.....	100
5.20 Weight percentage of narrow blend particle size fraction analysis of feed and product obtained in BBM and LBM	100
5.21 Sink and float analysis for iron ore blend	102
5.22 Effect of mill speed, with and without lifter arrangements at the discharge end of the mill on percentage passing of -150 μm particle, percentage of recirculating load to the ball mill and passing particle size fraction at P_{80}	121

CHAPTER 1

1 INTRODUCTION

This chapter deals with the brief introduction about ball mill, its operating characteristics, need for development of new equipment for producing desired particle size for pellet feed making along with research objectives and methodology.

1.1 General

Comminution is one of the most important process in the mining and mineral processing industry for the liberation of different concentrates and the gangue. The first stage of comminution in the mining industry is the blasting operation (both primary and secondary blasting) followed with crushing by making use of different types of crushers (Primary, secondary, tertiary crushers etc). After crushing, the next stage of comminution is the grinding operation.

In general, conventional grinding takes place in tumbling mills. Here, the ore is introduced into a horizontal mill where the cylindrical body of the mill is rotated by making use of motor, causing the mill charge (ore and grinding media) to tumble. Grinding is accomplished by impact, attrition and abrasion of the ore by the free motion of unconnected media such as steel rods, steel or ceramic balls, or coarse ore pebbles. Grinding is usually performed “wet” to provide a slurry feed to the concentration process.

The biggest consumers of energy in comminution (as much as 90%) are undoubtedly the grinding equipment, especially grinding mills (Abazarpour and Halali 2017). It has been reported that comminution consumes, on average, 36% of the energy utilized by the industry (Ballantyne et al. 2018). The total input energy in grinding mills will be absorbed by the machines and a small percentage of total input energy is converted into rock breakage. This implies that the existing grinding machines are inefficient.

A number of developments have taken place in the past in the area of grinding technology as well as design of different types of grinding mills (Chimwani et al.

2013). In mining industry, for all the downstream extraction/separation, liberation of valuable mineral as well as gangue from the ore is one of the important steps. Ball mills have been used for generating fine and ultrafine particles of ores in mineral industries due to their flexibility (Chimwani et al. 2013; Danha et al. 2015; Fuerstenau et al. 2004). A number of developments have taken place in the past regarding the grinding technology as well as design of different types of grinding mills.

The presently available ball mills have certain drawback especially in the design of its discharge end. The discharge ends are fitted with slotted grates acting as a diaphragm as shown in Fig.1.1. There is a chance of holds back of the smaller particles along with larger particles from discharging into the product stream. The size, spacing and design of the holes in the diaphragm are important as they affect the rate of throughput and product size (Gupta and Yan 2016). Three types of discharge ends are used, namely, mills with wide peripheral discharge, mills with scoop and mills with trunnion. All these discharge ends are not able to separate different size particles produced in the ball mill efficiently. It is also difficult to produce controlled size particles in the mill in this type of discharge end.

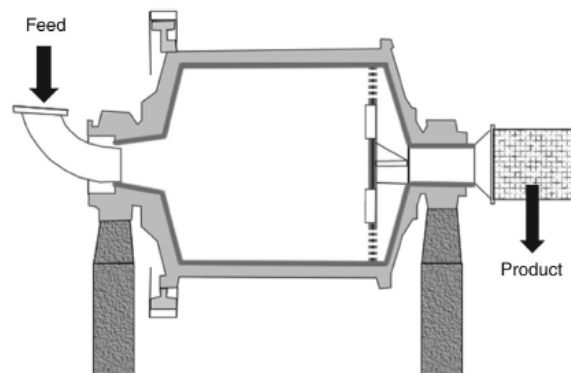


Fig. 1.1 Square AG/SAG Mill with Grating.

For sustainable development of mineral processing industry, it is very important to develop energy-efficient comminution circuits. Classification plays an important role in improving the energy efficiency of comminution circuits. The potential of classifiers in the comminution circuits is assessed based on the circulating load to the ball mill (Morrell 2008).

The conventional equipment utilised for wet classification is hydro-cyclone, screening machine, hydraulic, and centrifugal classifiers which are used for separating oversize particles from undersized particles. Among them, screens are commonly used classifiers compared with the other classifying devices (Markauskas and Kruggel-Emden 2019). Wet screen classifiers encounter high screen blinding, leading to an increased circulating load and a decreased throughput (Barkhuysen 2009; Jankovic et al. 2015; Shanmugam et al. 2019a; b, 2020, 2021).

Therefore, for obtaining proper and enhanced liberation of valuables and also for controlling particle size and getting particles of appropriate sizes as output for pellet feed making, there is a need to design a new type of ball mill to cater the desired particle size distribution for downstream process.

1.2 Organization of Thesis

CHAPTER 1

The background on the ball mill is given; brief note on ball mill performance and the operation principle are presented in this chapter.

CHAPTER 2

A comprehensive literature review has been carried out regarding the studies undertaken by previous researchers in the area of iron ore grinding in ball mill with respect to mill performance based on varying mill operation parameters and its effect on particle size distribution, liberation. Based on the literature review gap objectives and research methodology are presented in this chapter.

CHAPTER 3

Details of iron ore samples used, chemical analysis of iron ore sample and particle size analysis of iron ore samples are discussed in this chapter. The grindability tests by using Bond's Ball mill and laboratory ball mill are discussed.

CHAPTER 4

Laboratory studies by using newly designed ball mill discharge end and newly fabricated ball mill hydro-squeeze classifier are discussed in terms of size of the particles discharged from the mill and classification efficiency of classifier section are presented in this chapter.

CHAPTER 5

This chapter presents the detailed discussion on results and observations of the product particle size analysis obtained from Bonds ball mill and laboratory ball mill. The performance of newly designed ball mill discharge end and newly fabricated ball mill hydro-squeeze classifier are evaluated in this chapter with respect to size of the particles discharged from the mill and classifier separation efficiency.

CHAPTER 6

Conclusions drawn based on the investigations; recommendations and scope for the future study are presented in this chapter.

CHAPTER 2

2 LITERATURE REVIEW AND OBJECTIVES OF THE RESEARCH WORK

This chapter deals with a detailed literature study on characterization studies, ball mill design, ball mill operation parameters and classification devices.

2.1 General

Iron ore is commonly used in the steel making industry for producing different grades of steel, which are useful in motor, aerospace, medical equipment, and transportation fields. In India, the leading steel producing industry, JSW Steel Ltd. in Hospet, India, is facing acute shortage of high-grade iron ore, and hence the JSW plant is converting low-grade iron ore, which is available as fine particle size, to high- grade ore. These iron ore fines cannot be fed directly into the blast furnace because of higher gangue materials in their composition. Hence, it is required to process the iron ore before feeding it into the blast furnace.

Comminution has an extensive range of applications in the mineral industry. In the mineral processing plant, operations such as grinding, crushing and separation are carried out to liberate the appropriate minerals from the ore, so that they can be classified from the gangue minerals in the downstream process(Shanmugam et al. 2019b; a). Ball mills are commonly used to grind the ores for particle size reduction and to liberate valuable minerals from the ores. The grinding of ore is a highly energy-intensive process (Narayanan and Whiten 1988; Saeidi et al. 2013; Singh et al. 2018). In this process, the size of the particle obtained depends on the energy consumption of the ball mill. The major challenge encountered in the process of iron ore grinding is to maintain the desired product Particle size distribution (PSD) with sufficient liberation of valuable minerals. The demand for desired particle size with maximum liberation of valuables is increasing, particularly in the last phase of the grinding, for primary feed preparation for the making of pellets.

2.2 Characterization Studies

In the present scenario, characterization studies were carried out pertaining to ore liberation and associations of mineral phases, grain size, and textural features by using automated microscopic techniques (Donskoi et al. 2007; Lane et al. 2008; Sutherland and Gottlieb 1991). The mineralogical characterization is considered as a vital tool governing the process of grinding and liberation related productivity improvement. The study of microstructure and mineralogy plays a significant role in understanding mineral behavior at different stages of the grinding process (Dwarapudi et al. 2008).

Improvement of computerized microscopic systems has now made it possible to scan the mineral components of different types of ores (Devasahayam 2015). An ore can be characterized by QEMSCAN based on the presence of minerals and their association with respect to every single mineral (Hagni 2008; Hoal et al. 2009). The analysis rate of QEMSCAN is rapid to determine the mineralogy and individual ore particle size measurement. The QEMSCAN analysis data consists of minerals association, the grain size of the minerals, and the phase of the minerals.

Many types of liberation studies have been proposed beginning with Gaudin (Petrakis et al. 2017), but at present, no such process has been standardized for different types of rocks. In the literature, a vast amount of work has been reported on mineral liberation models by assuming random breakage of ore, which helps in simplifying the mathematical consideration (Ahmadi and Shahsavari 2009).

It is well-recognized in conventional grinding that PSD and effective liberation of valuable materials from the gangue, which occurs at different particle sizes, depends mainly on the properties of the ore being ground. The liberation properties of the valuables depend on its chemical and physical composition, which helps in the selection of the processing methods enabling effective utilization of the iron ore (Angadi et al. 2012; Rao et al. 2015; Rath et al. 2016; Srivastava et al. 2001). The size reduction and liberation of the particles is accomplished by the grinding process (Kotake et al. 2011). It is often hard to control the PSD in the end product. In mineral processing, the liberation of valuables assists as a link between the grinding and the

separation by creating particle structure information for the ground products (Chen et al. 2014). However, it has been documented that there is uneven breakage in ores, which leads to uneven liberation of minerals (Engmeermg 1990; Horst, W. E. 1998).

2.3 Assessing Ball Mill Response Based on Mill Performance

Ball mills are commonly used for size reduction of ores in processing plants. About 50% of the total energy is utilized for ore grinding in a concentrator plant (Yang et al. 2010; Yin et al. 2019). In general, grinding process is used to produce the desired particle size with minimum fine particle recirculating to the ball mill. This process plays a vital role in the recovery of valuable minerals (Hanumanthappa et al. 2020a; Harish et al. 2020). The maximum valuable liberation depends on the composition of the ores. However, ore hardness, feed particle size, and feed rate frequently change in the grinding circuit, which can intensely vary the mill capacity.

In case of pellet and sinter making, the pellet plant of JSW Steel Ltd. gets fines from different mines in Karnataka state. The physical and chemical composition of the iron ore varies for each mine site. So, it is challenging to produce the desired particle size with acceptable hematite liberation from the iron ore for pellet and sinter making (Dwarapudi et al. 2008; Hanumanthappa et al. 2020b).

Hardness and grindability are the major physical properties, which influence the fracture parameters of the materials (Harish et al. 2020; Kumar 2017). However, the performance of a grinding circuit is typically developed and designed based on PSD, rather than liberation. Hence, to determine the behaviour of different ores, raw ores are ground in a BBM (Bond's Ball Mill), which adopts the standard grinding procedures, which help in the grinding analysis. The ore physical grindability characteristics are identified based on the Bond Work Index (BWI) (Bond FC 1960; Gupta and Hussain 2017) to approximate the energy necessary for ore breakage, to compare different ore behaviours while grinding, and for designing new ball mill circuits. Bond's standard grinding procedure has attracted much attention in recent days due to its wide range of applications, and a lot of research has been done on Bond's work to optimize the grinding circuits (Jankovic et al. 2015; Mosher and

Tague 2001). Deniz et al. (Deniz et al. 2012) stated that Bond's work index is more effective than the sink- and- float method to determine the physical behaviour of the materials. Hacifazlıoğlu & Korkmaz (Hacifazlıoğlu and Korkmaz 2019) also used Bond's ball mill for particle size reduction from 780 to 455 μm and recorded that the time required by the Bond's ball mill to reduce the required size was 3 min.

From the literature, it is revealed that extensive research has been done explaining the overall performance of the ball mill when the mill is operated under different conditions. The overall performance of the ball mill depends on different factors viz., energy consumption, slurry filling, impact forces, net power draw, mill hold-up and discharge of mill.

2.3.1 Energy consumption

In the ball mill, energy consumption for a particular ore depends on bond work index in producing targeted product size. But in the real field, the actual power consumed by the mill is much more. This is due to over grinding of material inside the mill. The main parameters influencing for ball mill energy consumption are feed rate and speed of the mill.

2.3.1.1 Feed rate

In many cases it was noted that, with increasing feed rate in ball mill, the power consumption will also increase. In mill, retention time of the material mainly depends on the rate of feeding to the mill. If the feed rate to the mill is low and retention time in mill is high, then it will ultimately increase the ultrafines generation in the mill. To overcome this effect it is better to reduce the retention time of mill by increasing feed to the mill. Hence, with increased feed the discharge rate increases. Also, specific power consumption per ton production of the product will reduce. Based on the ultrafine generation, feed rate and power consumptions are correlated. By adequately controlling feed rate, the power consumption and ultrafines generation in a ball mill can be optimized.

2.3.1.2 Speed of the mill

Energy consumption by the mill depends upon the mill speed. At higher critical speed ball mill consumes high energy (Napier-Munn and Lynch 1992). The critical speed of the mill was calculated by using equation 1.

$$C_s = \frac{42.3}{\sqrt{D}} \text{ r/min} \quad (1)$$

Where,

C_s Critical speed of the mill

D Mill diameter in meters

However, in many cases, more effective grinding mills are operated at 80% critical speed. The rate of energy consumption is high at higher critical speed. To overcome these, many experimental trials have been carried out to optimize the speed of the mill. Whenever mills operated at 15- 17 r/min i.e., 60-70% critical speeds, the energy consumption of mill were reduced (Abouzeid et al. 1974).

2.3.2 Mill hold-up

In ball mills, grates are used for effective grinding and to remove slurry from mills. In many cases, this grate obstructs the flow of slurry inside the mill by forming a pool of slurry inside the mill. This results in filling up of the mill with excessive slurry and decreasing the efficiency of grinding.

The excessive slurry in the mill will reduce the further fine generation in the mill due to reducing density of charge or media in the mill. It also leads to reducing internal friction between media and charge (Napier-Munn et al. 1996). It was revealed that, mill holdup mainly influenced based on the grate hole size and its position. Mill holdup not only depends on the position and size of the hole, but it also depends on the density of the charge or media.

2.3.2.1 Variation of slurry hold-up based on time

At dynamic condition, slurry holdup cannot be measured accurately with respect to the time. The holdup may decrease or increase non-uniformly from one state to another steady state with respect to time and percentage of solids in the feed.

2.3.2.2 Effect of mill feed rate

Mill holdup and feed rate are linearly related to dry grinding conditions for open-end and constricted-end mills (Morrell and Stephenson 1996; Nasr-El-Din et al. 1992). At lower feed rate, slurry levels will be less than the lip of discharge end of the mill. Hence, discharge of solids from the mill will not take place. Discharge in the mill is due to gravity force generated at the top of the discharge end and movements of lifters in the mill.

Also, it has been recorded by several researchers that, the slurry hold-up consist of higher percentage of solids and hence, mean residence time of the solids is higher than the mean residence time of liquid (Powell et al. 2001; Rezaeizadeh et al. 2010; Rogers and Austin 1984; Shoji et al. 1982). The material mass holdup in the mill was calculated by using equation (2).

$$M_H = \left(\frac{L}{\psi_s v_{op}} \right) F + M_{HO} = c_1 L F + M_{HO} \quad (2)$$

Where,

M_H	Material mass holdup in kg
ψ_s	Fractional cross sectional area opened for discharge at mill
V_{op}	Mill opening velocity of material discharge in m/s
M_{HO}	Mill retained mass of the material at F=0 in kg
F	Mass feed rate in kg/s
L	Mill length in m
c_1	Constant expressing the discharge properties at the mill exit.

2.3.2.3 Influence of percentage of solids in feed on mill hold-up

Horst and Freeh (1972) carried out studies by varying percentage of solids in the feed with respect to slurry hold-up. The results revealed that, with the increasing feed percentage solid, slurry hold-up was exponential increasing as the percentage of solids in the mill increases frictional factors (Horst and Freeh 1972).

2.3.2.4 Effect of mill speed

In dry grinding, mill hold-up decreases with the increasing mill speed with respect to mill critical speed (Morrell and Stephenson 1996). In case of wet grinding, the mill holdup increases with increasing mill speed and it is low at 60% to 70% critical speed compared to 70% to 80% at constant feed rate (Nomura 2012). It was recorded that, at the higher critical speeds the large voids are formed which intern disturbs the tumbling charge (Shoji et al. 1980). Due to this effect, slurry inside the mill starts to fill in newly formed voids. Hence pool of slurry increase which in turn increases the mill holdup. Also, above 80% critical speed it was observed that there is sudden drop in mill holdup, this is due to free movement of charges inside the mill.

2.3.3 Parameters influencing the ball mill discharge

Pulp lifters and grate mainly controls discharge from the mills. Slurry discharge from the mill also depended on grinding media and mill design.

2.3.3.1 Discharge grate

The design of grate in a mill plays a very important role in the discharge of products from the mill. Design of grate depends upon the size of the product required. The discharge grates mainly consist of apertures with different size. It may be larger size apertures or smaller size apertures in the discharge grates. The configuration of grate mainly depends on open aperture area and its radial position.

2.3.3.2 Pebble discharge

Pebble ports are mainly used to minimize over grinding in the mill and slurry transport through the mill. In large open circuit, rate of discharge depends on a

number of apertures open in the pebble port. The mills with high number of the pulp lifters will increase discharge capacity with increase in pebble ports.

2.3.3.3 Mill hold-up

Latchireddi and Morrell, (1997) demonstrated that mill hold up increases with slurry pooling inside the mill. They also demonstrated that with increased feed flow inside the mill, mill hold up drastically increased (Latchireddi and Morrell 1997). Morrell and Stephenson 1996 studies revealed that the mill hold-up is a response variable for discharge from the mill (Morrell and Stephenson 1996).

2.3.3.4 Pulp lifters

Pulp lifter plays a very important role in removal of materials from the mills. The pulp lifters are used to maximize the discharge capacity of the mill. The discharge capacity of mill depends on kind of pulp lifter design profiles used in the mill.

2.3.4 Influence of slurry pool volume on milling efficiency

The discharge from the ball mill depends on mill hold-up and the rate of feed to the mill. In any case, overfilling the mill is not recommended. As, overfilling to the mill increases the formation of voids in the media which leads to formation of a slurry of pool in the lower region of media charge. It was reported that, mill with higher speed increases dynamic bed porosity (Sichalwe et al. 2011). Due to this, mills can hold-up more slurry with added residence time to a pulp outside the grinding zone.

2.3.4.1 Impact of slurry pool volume on net power draw

Moys and Smit (1998) accepted that the net power draw by mill decreases with presence of the pool. As slurry filling in the mill increases, power drawn by the mill also increases initially. The power drawn starts to decrease, once slurry of the pool is formed in the mill. The power drawn in dry condition is less than wet condition when its compared with mill operated at same parameters (Moys and Smit 1998). Also, with increasing slurry filling to the mill, slurry pool formation in the mill takes place. As slurry pool formation inside the mill increase more than unity, then the mill net power drawn by the mill drops (Mulenga and Moys 2014). The net power drawn will also

depend on the density of slurry. To justify these, laboratory experiments are carried out by taking two liquids (water and slurry) with different density (Bu et al. 2019). The results confirm that, the liquid which is having less density has consumed less net power than the liquid (water) which is having higher density (slurry). The net power drawn was maximum at threshold slurry filling at the mill critical speed below 75% (Bu et al. 2019).

2.3.4.2 Effects on the specific energy consumption due to pool volume

It was observed that, for any given grinding time the slurry pooling process is more energy efficient (Mulenga and Moys 2014). This is due to the presence of slurry pool ultimately reduces energy drawn by the mill. At high slurry filling, energy consumption will be low as the product particles size distribution is not varying much. In practical condition, it is difficult to find the effect of pool volume on the specific energy consumption.

2.3.4.3 Effects on the size reduction index due to the pool volume

The size reduction index does not play a very important role in the presence of pool volume in a mill. But it was observed that, with an increase in pool volume there is a slight reduction of the size reduction index (Mulenga and Moys 2014). However, with decrease in size reduction index it will not increase the overall mass of the solids in the mill.

2.3.4.4 Effects on grinding index due to the pool volume

A review on the effect of a pool of slurry on milling was reviewed by grinding index. In general, the material with the highest grinding index can achieve more fines. In case, if the mill is fed with less feed, the time taken to grind is slightly high compared to the mill fed with high feed. But in case of slurry filling, grinding index is high at smaller filling capacity. The lower slurry level in a mill accelerates fines production. In case of high production of fines in the mill, it is better to choose the high volume of charge and filling low volume of slurry (Mulenga et al. 2016).

2.3.4.5 Effects of slurry filling on load orientation

It is observed from the literature review that, insufficient number of experiments have been carried on the influence of slurry pool on load orientation. It was observed that load orientation depends on speed, but has negligible effect due to pool formation. The level of the liquid in the mill will not impinge on change of shoulder angle and impact angle(Chimwani et al. 2015).

2.3.5 Impact angle variation due to slurry filling

The slurry filling will not influence the impact angle θ , but it is influenced by speed of the mill. It has been observed that, the angle of impact will decrease by 2° with increase in 1% of critical speed (Soleymani, 2014). It was observed that the impact angle decreases slightly with the increasing content of mill only at higher speeds of the mill. Also, recorded that with the increased speed of the mill, shoulder angle will increase and balls release rate from mill shell also increases. The main drawback observed with increasing speed of mill is the distance traveled by the ball is very less. This is due to shorter flying paths of the balls. Due to decrease in impact angle, there are chances for improper landing of the balls, which damage the liners and reduce the grinding efficiency.

2.3.5.1 Toe angle variation due to slurry filling

Toe angles are weak at lower speeds of the mill and it is almost fixed for lower filling. It was observed that toe angle increased to a certain degree once slurry of the pool is formed. The increase of the toe angle is due to increasing of flotation force caused by pooling and flotation of balls in the pool. The movement of the toe was calculated by using equation 3.

$$\Delta s = R \Delta \theta t \quad (3)$$

where

R mill radius

2.3.5.2 Shoulder angle variation due to slurry filling

Shoulder angle depends on the speed of mill rather than the level of filling. In the mill with increased slurry level shoulder angle will remain constant. The results show that the increase or decrease in shoulder angle depends on the increase or decrease of centrifugal force. At higher speed, centrifugal forces lead balls to cataract with each other at a higher angle. Due to this effect shoulder angle will increase (Moys and Smit 1998).

2.3.5.3 Pool angle variation due to slurry filling

In any mill, pool formation takes place whenever slurry reaches a certain level in the mill. According to Soleymani et al. (2016) pool angle in the mill will not depend on the speed of the mill. They also recorded that with increasing slurry level in the mill liquid level in mill rises and pool angle will decrease. Katubilwa and Moys (2011) proposed power function which can be used to describe the pool angle results. The expression of the power function is given in equation 4.

$$\theta_{\text{pool}} = C \cdot U^k \quad (4)$$

where,

C, k fitting parameters

2.3.6 Impact forces

Whenever forces acting normal to the particles, breakage of particles takes place due to impact forces. This kind of fracture mechanism leads to cleavage in the particles [54]. In wet milling, impact forces depend on buoyancy force, the diameter of the balls, the mass of the balls, velocity with which balls hit pool slurry, density, drag coefficient and viscosity of fluid (Soleymani et al. 2016).

2.3.6.1 Variation of impact forces with speed

Location and amount of the impact forces are highly influenced inside the mill due to speed of the mill. The experimental results of Soleymani et al. (2016) revealed that at a lower level of slurry filling and about 30% of charge filling in the mill, impact forces will increase with increasing speed of the mill. They also recorded that with increasing critical speed from 65% to 85%, the maximum impact force has been

increased from 600N to 1700N and also impact frequency increased. It was also observed that the rate of collision in the mill increased with increasing speed of mill. Therefore its necessary to run the mill with optimal speed for producing required impact forces. By running the mill with appropriate speed its possible to increase grinding efficiency and prevent excessive wear in the mill. Mill speed is a very important parameter in the operation of Semi-Autogenous Grinding (SAG) and Autogenous Grinding (AG).

2.3.6.2 Impact forces variations with slurry filling

The energy generated between the ball and ore inside the mill is observed by the pool based on the level of pool formation. In mill with the increased level of liquid increases the pool formation which leads to decrease in impact forces.

The experimental study was carried by Soleymani et al. (2016) to record the impact forces generated on the liners, both dry and wet condition by using sensors. It was observed that at dry condition impact load were more on liners compared to wet milling. Impact load on liners in wet condition decreases due to the resistance offered by a pool of slurry in the mill. Impact forces will also depend on speed and slurry level filling. In lower speed, cascading motion will not reach slurry, due to this high impact forces will act on the slurry. At higher speed, cascading motion formation in the mill is larger and balls fall directly into pool of slurry. Also, at higher speeds of the mill impact forces will drop, due to balls land in the center of the pool subjected to damping inside the mill. This damping will prevent the transfer of energy from balls to the ore.

2.3.6.3 Impact forces variations with slurry concentration

Slurry concentration in the mill plays a very important role on impact forces. If solid percentage is low in the slurry, pool formation takes place, contact between balls and ores will be less and consumes large amount of balls. Due to this maximum mill volume will be filled with liquid which leads to reduction in efficiency of the mill. The slurry which is having high density and viscosity will reduces the grinding

efficiency. Slurry with high density and viscosity will be having high damping and increases resistance to the balls movements against impact. Grinding efficiency can be improved by reducing slurry viscosity. In the mill packing of material takes place, when slurry concentration is more. Also, if slurry concentration in the mill is more than 70%, coating of balls with slurry takes place which decreases impact forces and increases grinding time.

2.3.7 Effect of net power draw

In the ball mill, net power draw depends on many parameters like, media charge filling, mill speed, slurry filling and slurry concentration.

2.3.7.1 Variation of power draw with media charge filling

Controlled milling depends on the load filling condition, in terms of power consumption. The Fig.2.1 suggest that the mill draws more power to rotate and lift the whole load in the mill. Soleymani et al. (2016) reported that the power draw in dry condition was less than that of wet condition when mill operated with same initial conditions. They also recorded that, with increasing ball filling to the mill, power consumption has been increased for both wet and dry conditions.

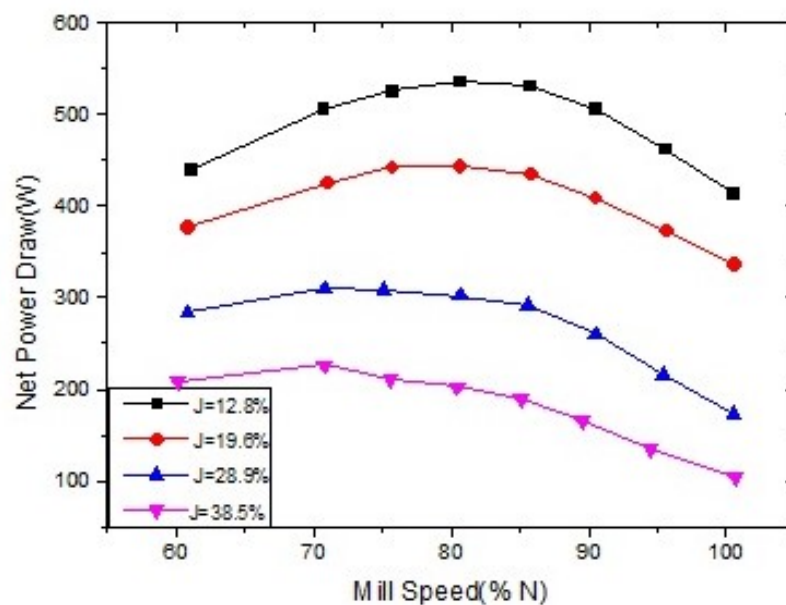


Fig. 2.1 Ball filling effect on mill power draw data (Soleymani et al. 2016)

2.3.7.2 Variation of power draw with mill speed

In general, power draw increases linearly with increase in speed of the mill. During mill operation at similar speeds, the power drawn in wet condition is more compared to the dry condition. Various mathematical models have been developed for relating power drawn with respect to increase or decrease of speed. With respect to mill speed, power draw is given by good co-relating mathematical relationship, i.e. power $\propto \phi_c^{0.979}$ and $R_2=0.98$ (Cleary 2001). The reason behind high power consumption at higher speeds is due to lifting of shoulder load, effective radius change and center of mass displacement.

2.3.7.3 Power draw variations with slurry filling

The power draw increases initially with irrespective to slurry filling and ball speed. At a certain level of slurry filling, pool formation takes place, at this stage power draw starts to reduce. At dry milling, power draw is slightly lower than a wet condition with similar operating conditions. The mill power draw in wet milling increases with increase in the slurry filling. This is due to slurry starts to fill in pores between the charges and also fills porosity between the solids. Mathematical expression for power draw and slurry filling is given in Equation 5 (Cleary 2001).

$$\text{Power}=f(U)=\begin{cases} A_1 + A_2U & \text{for } 0 \leq U \leq U^* \\ A_3U^{-b} & \text{for } U^* \leq U \leq 1.7 \end{cases} \quad (5)$$

where A_1 , A_2 , A_3 , and b are constants and depend on the mill speed, ball filling and ore properties.

U^* is the slurry filling before pool formation when net power draw is maximum.

2.3.7.4 Power draw variations with slurry concentration

Magnitude of power draw in mills depends on slurry concentration. Power draw by the mill increases with increasing slurry concentration initially. Further increasing slurry concentration to the mill increases slurry compact of materials, hence power draw by mill reduces. A mathematical expression was used to calculate the power

draw due to increase in slurry concentration is give in equation 6 (Nkwanyana and Loveday 2018).

$$\text{Power}=f(U)=\begin{cases} B_1 + B_2C & \text{for } 0.4 \leq C \leq C^* \\ B_3C^{-d} & \text{for } C^* \leq C \leq 0.8 \end{cases} \quad (6)$$

Where

B_1 , B_2 , B_3 , and d are constants and depend on the mill speed and slurry properties

C^* Slurry concentration for maximum net power draw

2.3.8 Residence time distribution

Along with different operating parameters of the mill and mineralogical characterization, the Residence Time Distribution (RTD) of the mill also plays a very important role in the design of the ball mill circuit. Numerous studies have focused on RTD measurement with respect to solid flow effect, solid transport alongside the mill axis, and variation of ball mill diameter on RTD in the ball mill (Cho and Austin 2002; Hassanzadeh and Hassanzadeh 2018; Mulenga and Chimwani 2013). The different types of RTD measurement methods used were attainable region technique, one-parameter RTD model, and radioactive tracer (Chimwani et al. 2015; Vinnett et al. 2018).

Cho and Austin (2002) examined the solid flow effect on RTD due to variation of operating variables in a dry ball mill. It was recorded that as the mill speed revolution increased, solid carrying along with the mill axis increased with decreasing RTD of the solids (Cho and Austin 2002). The optimal RTD of the ore was determined by Chimwani et al.2015 using the Attainable Region technique (AR). It was observed that with higher volume of charge filling in the mill and the mill operating at lower speed resulted in a highly significant effect on particle retention time inside the mill, which ultimately saved the energy consumption of the mill (Chimwani et al. 2015). Further, an open ball mill circuit was optimized for Mean Residence Time (MRT) by Mulenga and Chimwani. They calculated the ball mill MRT while keeping all the operating parameters constant and varied the diameter of the ball to 10, 20, 30, and 40 mm. It was seen that when the mill was operated with smaller ball diameter, it led to

an earlier production of fines, and with increased ball diameter, the production of fine particles required more time (Mulenga and Chimwani 2013). In a recent study, Gupta and Patel proposed a new RTD model called as one-parameter RTD model suitable for both ball and rod mill for predicting the RTDs of the mills accurately (Gupta and Patel 2015).

2.4 Effect of Ball Mill Design on Slurry Discharge

The slurry discharge from the ball mill not only depends on the ball mill operating condition and it also depends on design of ball mill (Kotake et al. 2011). The variation in PSD might be due to the ball mill design (Gao et al. 2017). The quantity of the particles discharge from the mill depends on type of lifters used in the mill and discharge end design of the mill.

2.4.1 Pulp lifters

Pulp lifters are used to transport slurry from the feed to the discharge end through grate holes in the mill. At the discharge end of the mill, based on the requirement, different types of lifter designs are used. Earlier, to lift the pulp, "pan pulp lifters" were used (Makokha and Moys 2007), however, their design prevented their usage especially during increasing pulp flow. In order to overcome this, pulp lifters with an advanced design were used at the peripheral or discharge end of the mill and were found to operate effectively with an increase in the pulp flow and have improved power utilisation (Makokha and Moys 2007).

The main drawback of lifters is that the slurry held up inside the mill is high as lifters are always in contact with the slurry; thus, the complete flowback of slurry to the mill cannot be avoided. This increasing backflow and formation of a pool of slurry ultimately affect the grinding efficiency of the mill (Latchireddi and Morrell 2003).

Mishra and Rajamani (1992 & 1994) used 2DMILL code to predict the effect of liners/lifters on the motion of the balls and the power drawn (Mishra and Rajamani 1994; Mishra and Rajamani 1992). Hlungwani et al. (2003) studied the effect of mill speed and lifter shape on power draw by using the Discrete Element Method (DEM) simulator Millsoft (2D), which can predict whether square lifters draw lesser power

than trapezoidal lifters when the mill operates at a normal operating speed of production mill (Hlungwani et al. 2003).

Latchireddi and Morrell (2003) stated that the lower discharge rates in grate-pulp lifter assemblies are due to the inherent drawbacks in both radial and curved pulp lifter, allowing a proportion of the slurry to flow back into the mill before being discharged. In this system of design, a minor part of the slurry flows back to the mill while the major part is discharged through the grate-pulp system (Latchireddi and Morrell 2003). Also, at higher mill speeds (typically > 80% of the critical speed) in addition to the flow back, a part of the slurry is carried over to the inside of the pulp lifter, which further reduces the discharge rate (Latchireddi and Morrell 2003). Furthermore, it has been demonstrated that the discharge rate, performance and effectiveness of mills are controlled by pulp lifters (Weerasekara and Powell 2014).

Djordjevic et al. (2004) adopted the DEM particle flow code (3D) to study the effect of lifter height and mill speed on power draw and found that as the mill speed increases, the mill with lower lifter height draws more power, but the mill with higher lifter height draws less power (Djordjevic et al. 2004). It was also recorded that when grinding smaller particles, the power consumed was high for a mill with different lifter heights compared to the one with similar lifter heights. Makokha and Moys (2007) used cone lifters at the discharge end of the mill and observed, improvement in the mill product discharge as compared to the mill operated without cone-lifters (Makokha and Moys 2007).

Mill speed significantly affects the behavior of a particle inside the mill when it rotates at different operating speeds. At a rotating rate of 75%–80% critical speed of the mill, particle behavior is highly consistent due to particle trajectory (Bian et al. 2017). The lifter design also plays a very important role in the inconsistent particle trajectory falling position. The particle movement towards the discharge end reduces when the height of the lifter is bigger. The number of lifters also influences the particle stream flow inside the mill. More lifters increase catatracting of particles

inside the mill, leading to an increasingly dense flow stream of particles (Bian et al. 2017).

Gutiérrez et al. (2018) used DEM to simulate the material transport of different lifter profiles in the mill and found that the material discharge flow is higher in the case of a mill with inclined and radial lifters compared to the one with straight and radial pulp lifters (Gutiérrez et al. 2018).

2.5 Wet Classification

Wet grinding is one of the methods used to reduce various size particles to fine scale particles (Kotake et al. 2004). In wet grinding, the slurry phase executes various key roles, viz., coarse particle dynamics modification, particle breakage, and transport of finer particles (Austin and Bagga 1981; Bu et al. 2020; Danha et al. 2015; Tangsathitkulchai 2002). Also, slurry solid concentration and the viscosity of the slurry influences optimum wet grinding (Mori et al. 2004; Yin et al. 2019). The percentage of water present in the slurry alters the behaviour of the balls and the coarse particles in the wet grinding process (Ulusoy and Igathinathane 2016). Further, the reduced particles are classified in the downstream process, i.e., wet and dry process. The wet classification process is generally used for particle classification of the iron ore slurry.

Hydrocyclone is the most commonly used classifiers in the grinding circuits for the classification of the particles from dispersed liquid in environmental, chemical and mineral processes (Vakamalla et al. 2017). Based on the review of previous researchers, a few major drawbacks in the existing hydrocyclone and other classifiers were identified. Hydro-cyclones are recognized as wet classifiers, which play a major role in solid-fluid classification based on size, shape, and density of the particles (Wang et al. 2018).

Even a minor change in a geometric shape parameter of hydro-cyclone will have a major effect on the classification performance (He et al. 2020; Tue Nenu and Yoshida 2009). Generally, due to basic operational constraints of the hydrocyclone, the size

distribution of the hydrocyclone product has a broad range. This results in over grinding and excess ultra-fine generation from the recirculated portion and undesired over size fractions in the final overflow product. The recirculation of the underflow product increases the load on the mill and is a function of the ore type/ore blends resulting in requirements of change in media and mill operation set points reflecting on the mill throughput/efficiency (Eswaraiah et al. 2012). However, quantifying the effect of the ball mill and the hydrocyclone as individual is difficult because the parameters of the ball mill and the hydrocyclone are interrelated.

The classification efficiency of the hydrocyclone varies with varying operating parameters of the ball mill. Due to this variation, the output from the hydrocyclone may have more coarse or fine particles in the underflow and overflow, thus affecting the circulating loads. This in turn reduces the grinding efficiency of the ball mill (Kumar et al. 2009). A major drawback of the hydrocyclone is that it can produce neither moderately clean underflow nor overflow. Also, a rope type discharge occurs when the hydrocyclone is operated at optimal control condition causing major loss in classification efficiency with variation in pulp rheology (Yianatos et al. 2002).

Fish-hook is one of the physical phenomena observed in hydro-cyclones (Kraipech et al. 2002, 2005; Majumder et al. 2003, 2007). However, the fish-hook phenomenon occurs in the periphery layer flow, which pushes the fine particles to the underflow stream (Frachon and Cilliers 1999). The fish-hook also produces low quantities of particles, which reduces the classification sharpness and increases the cost in downstream processing (Dueck et al. 2014; Roldán-Villasana et al. 1993). The fish-hook effect reduces the performance of the hydrocyclone, and several studies regarding the fish-hook phenomena are reported (Kraipech et al. 2005; Roldán-Villasana et al. 1993).

A few fine size classification technologies such as screening, hydraulic, and centrifugal were developed. Among them, screens are commonly used classifiers compared with the hydrocyclone and other classifying devices (Markauskas and Kruggel-Emden 2019). Continuous wet fine screening encounters many issues such as

high screen panel consumption, low capacity, and blinding leading to increase in circulating load and decrease in throughput (Barkhuysen 2009; Jankovic et al. 2015; Shanmugam et al. 2019a; b).

2.6 Summary

However, from the literature survey, it was observed that PSD and size-by-size liberation in the fine grinding phase is not clear with a variation of grinding time (Chapman et al. 2011; Gilvarry and Bergstrom 1961; Solomon et al. 2011; Vizcarra et al. 2010). Hence, liberation of minerals from ores is still uncertain and conflicting, and this may be associated with the mineralogical textures of dissimilar ores. Furthermore, the difference in the relation between PSD and hematite liberation in the product size has not been specified clearly in earlier works. Also, in previous studies, size reduction was done in the ball mill and the reduced particles were classified in different classifier devices with few limitations in the classification efficiency. However, a single unit with size reduction and classification was not completely explored. In view of the knowledge gap, the objective of the present study is to evaluate a newly developed ball mill hydro-squeeze classifier for restricting the recirculation of very fine materials to the grinding mill by efficient separation of the desired fine particles from oversize particles and to provide desired particle sizes to pellet making.

2.7 Objectives of Present Research Study

The main objectives of the research work are as follows:

1. To study the mineralogical characterization of iron ores to identify the operating window through matrix mapping for ball mill comminution process.
2. To develop new process to bridge the gaps to improve the ball mill efficiency and built-in flexibility for selective size output.
3. To demonstrate the new concept through lab scale equipment design development, bench scale tests and results.

2.8 Research Methodology

Following is the methodology followed for achieving the above objectives of the research and a schematic diagram of the same is shown in Fig. 2.2.

1. Literature review on different types and designs of ball mill will be carried out in detail to understand the new technology used in the ball milling operation.
2. Review on different operating parameters of ball mill to understand its performance will be carried out in detail through online journals, thesis and in case required visiting other reputed research and academic institutions.
3. Three different types of ore samples are collected from mines located in Bellary, Chitradurga and Tumkur districts of Karnataka State.
4. The collected ore samples are in the form of fines and lumps with different sizes. Size reduction was carried out by selecting suitable crushing equipment. The size of the ore samples was reduced below 3mm using crushing equipment.
5. After size reduction sieving was carried out to remove over size particles.
6. For three iron ore samples and for its blend sample chemical analysis, characterization studies, dry grinding studies and liberation analysis was carried out to understand the nature of ore.
7. Ball mill hydro-squeeze was designed and fabricated (as described earlier) to enhance the performance of ball mill equipment in terms of separation of different particle size for pellet feed making.
8. A new type of lifter was designed and fabricated to enhance the performance of ball mill equipment in terms of discharging of ground product from mill section to classification section.
9. The experiment was conducted by using newly designed Ball mill hydro-squeeze for iron ore.
10. The result obtained was analyzed for efficiency of produced participle size separation in stationary cylinder in ball mill hydro-squeeze.

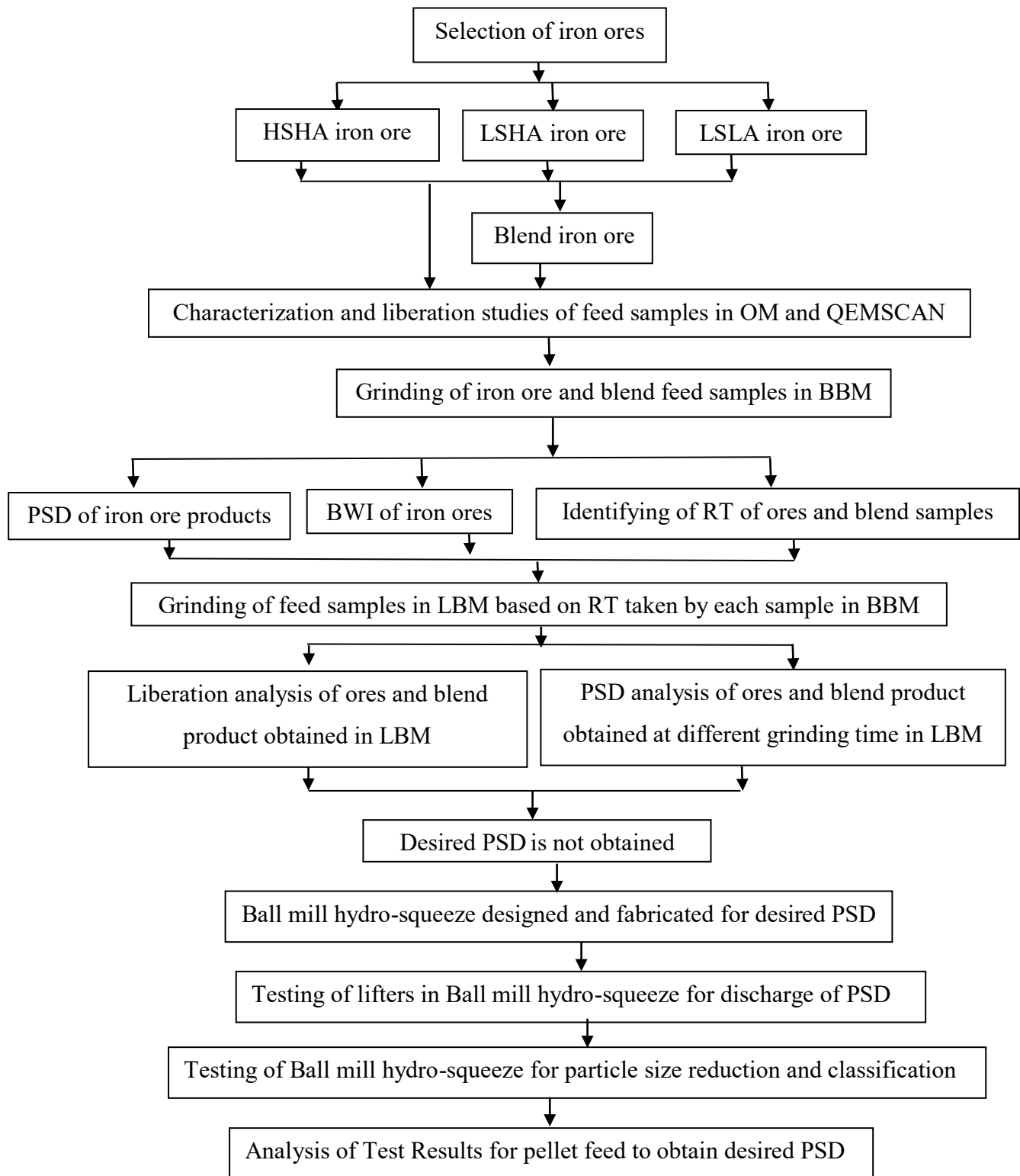


Fig. 2.2 Schematic representation of the methodology

CHAPTER 3

3 EQUIPMENTS AND METHODS USED IN THIS RESEARCH WORK

3.1 Introduction

Materials used in the present research study and their characterization are discussed in this chapter. The specimen preparation for characterization study and details of the procedure adopted to determine the Bond Work Index (BWI) of iron ores, particle size distribution before and after grinding of iron ores and liberation analysis of each iron ore are discussed in this chapter.

Three types of iron ore mine samples were considered in the present study i.e., viz., High Silica High Alumina (HSHA), Low Silica High Alumina (LSHA), and Low Silica Low Alumina (LSLA). Blend was prepared by blending three types of iron ores with different percentages of HSHA, LSHA, and LSLA. The grinding process for all the iron ores is carried out individually in Bond's Ball Mill (BBM) and the total retention time taken by each iron ore sample is calculated. The present investigation focuses on utilizing the calculated retention time of the iron ore as a standard grinding reference time to the Laboratory Ball Mill (LBM) for optimizing the grinding time of each ore.

3.2 Collection of Iron Ore Samples

In the present study, iron ore of three different chemical compositions was selected from Karnataka region. These samples are typical raw materials used in JSW Steel, Ballari Pellet Plant, to produce pellets. The selected iron ores are mainly classified into three groups based on the percentage of silica and alumina present in each sample, as shown in Table 3.1. The selected iron ores are blended in terms of percentage as shown in Table 3.2.

Table 3.1 Percentage variation of silica and alumina by weight in iron ore

Sl. No.	Type of ore	Silica% by wt. in Iron ore	Alumina% by wt. in Iron ore
1	HSHA Iron ore	>4.5%	>3.5
2	LSHA Iron ore	<4.5%	>3.5
3	LSLA Iron ore	<4.5%	<3.5

Table 3.2 Chemical composition of iron ores

Sl. No.	Type of ore	Fe T%	SiO ₂ %	Al ₂ O ₃ %	LOI%
1	HSHA Iron ore	60.61	5.63	4.45	2.6
2	LSHA Iron ore	60.95	4.29	4.59	3.09
3	LSLA Iron ore	59	3.72	3.42	5.55
4	Iron ore blend	59.746	4.082	3.874	4.517

3.3 Chemical Analysis

The X-ray fluorescence (XRF) technique was used to find the iron ores chemical composition. Since there is no any other technique which gives quantitative as well as qualitative reading for chemical analysis of iron ore sample. In the existing X-ray fluorescence technique sample is exposed to polychromatic radiation, where the accurate elemental composition of ores can't be identified. But in XRF technique, each element in the ore excited to release their specific X-ray with high intensity curve. These curves can easily identify for each element in the ore based on the intensity of the peak of the curve. Hence XRF technique was used to find the chemical composition of iron ores

3.1.1 Sample preparation for XRF scan

For XRF scan iron ore samples are powdered and pressed. The iron ore sample of 10 gm is mixed with binder by using -300 mesh. The mixed sample is then pressed into a boric acid cup to obtain a pellet of required diameter. The prepared sample is placed

in to XRF equipment and initial settings are made to find the elements present in the ore. The chemical composition of the selected iron ore samples and its blend is shown in Table 3.2.

3.2 Particle Size Analysis

In the crushing machine, all the iron ore and blend samples were crushed to -3mm and analyzed for desired P_{80} passing ($-150\ \mu\text{m}$). For all iron ore samples, particle size analysis was carried out before and after grinding. The particle size measurement was carried by using mechanical vibratory sieve shaker and HELOS; a parallel beam laser diffraction set-up. Before particle size analysis, sampling for all iron ore sample are carried by using cone and quartering method.

3.2.1 Quadrant divider

Sampling of any ore is done by using quadrant divider. Sampling is a process of taking representative sample from a given large quantity of sample and is done by various techniques. The coning and quartering technique was adopted to carry out the sampling process as shown in Fig. 3.1. Coning & quartering technique is basically a sample reduction technique as its successive iterations reduces the sample to half of its previous value (quantity) each time. This method is convenient for any quantity of material. Steps involved in this method are making pile of material (conical in shape), settled at its natural angle of repose. The cone has to be radially symmetrical. Then with the help of a spatula, it is flattened into a circular disc and subsequently quartered using the Quadrant Divider. Quarter of opposite quadrants is taken and remaining material is discarded. This process is repeated till the desired sample quantity is achieved.



Fig. 3.1 Quadrant divider

3.2.2 Sieve shaker

Sieve analysis was carried out with the help of Ro-Tap reciprocating mechanical sieve shaker to determine the percentage of different grain sizes contained within a sample. The sieve shaker used in the present investigation is shown in Fig. 3.2.



Fig. 3.2 Sieve shaker

3.2.3 Particle size analyzer

The Particle Size analyser used in the present investigation is HELOS laser diffraction series together with the unequaled dry dispersing system RODOS as shown in the Fig. 3.3. The analyzer has a range of 0.1 μm up to 8,750 μm of particle size to measure either in dry or suspended condition. The Particle size analyzer works on the principle of laser diffraction in parallel beam using forward scattering only (Low Angle Laser Light Scattering (LALLS)). This setup guaranties both the high reliability of measurements and the good comparability of the measuring instruments.



Fig. 3.3 Particle size analyzer

3.3 Grindability Test

There are many tests for determining grindability. The most commonly used test is the Bond's Ball Mill (BBM). It enables the installation of a plant scale ball mill (Rodríguez et al. 2016). The Bond Work Index test is used to measure the energy required for the desired particle size reduction and for designing new circuits for comminution (Rodríguez et al. 2016). The Bond's Work Index is commonly agreed as a grindability factor for ores in order to relate different materials' composition (Ahmadi and Shahsavari 2009). Several works are discussed and strength the Bond test with respect to grindability factor (Aguado et al. 2006; Coello Velázquez et al. 2008; Jankovic et al. 2015; Magdalinovic et al. 2012; Morrell 2004; Mosher and Tague 2001; Tavares et al. 2012). The Bond's test analysis specifies that one of the vital parameters for computing work indices is PSD (Mosher and Tague 2001). In this sense, the standard Bond's test procedure is used to analyze PSD in terms of F_{80} and P_{80} parameters.

3.3.1 Bond Work Index

In the laboratory, work index of HSHA, LSHA, LSLA, and blend iron ore samples is determined in a standard test mill (Bonds Ball mill) under standard conditions. The grindability test determines the hardness of the ore and the work index obtained is important in the design of a grinding circuit. The work index is used while determining the size of the mill and grinding power required for producing the required ore throughput in a ball mill. The BBM is a standard ball mill having length and diameter of 300 mm X 300 mm with smooth liner as shown in Fig. 3.4. A rotating drum is attached to a gearbox and has adjustable speed nob. The number of steel balls and the weight of the balls are selected according to Bond's standard procedure (Bond FC 1960).

A bench test was developed for dry grinding to determine the Bond Work Index and to know the PSD and hematite liberation in all the six iron ore product samples obtained from the BBM. For each iron ore sample, 700cc of feed was weighed and added into the BBM. The BBM was set for 100 revolutions in the first iteration. The product from the mill was withdrawn after completion of 100 revolutions. The

product was then screened and analyzed. Oversized fractions were added back into the mill (as it is a closed-circuit operation). The amount of fresh feed added to the mill is equal to the amount of undersized fractions produced in the first iteration. The number of revolutions for the second iteration is determined based on Bond's standard test procedure (Bond FC 1960). The experiments were continued for a minimum of five consecutive iterations until the net grams per revolution became constant.

A new method was adopted to measure the total retention time taken by each ore in the BBM. The retention time of the ore in the mill is measured based on the total number of revolutions taken by each ore to produce 250% of circulating load. The number of revolutions for each trail is set to the BBM based on Bond's procedure. For each trial, the set number of revolutions are recorded and represented as $R_1, R_2, R_3, R_4, \dots, R_n$. The total number of revolutions taken by each ore sample in the BBM is calculated using Equation 7.

$$R = R_1 + R_2 + R_3 + R_4 + \dots + R_{n-1} + R_n \quad (7)$$

The total retention time taken by the BBM for each iron ore sample is given by Equation (8).

$$T = \frac{\text{Total number of revolution taken by BBM to produce 250\% circulating load for each iron ore sample}}{\text{number of revolutions per minute}} \quad (8)$$

The standard equation used to determine the work index is given in Equation (9).

$$BWI = \frac{48.95}{A^{0.23} \times G_{bp}^{0.82} \left(\frac{10}{\sqrt{P_{80}}} - \frac{10}{\sqrt{F_{80}}} \right)} \text{ kWh/t} \quad (9)$$

Where, F_{80} is 80% passing particle size of the feed in μm , P_{80} is 80% passing particle size of the final grinding cycle product in μm , A is the mesh size of the test in m , and G_{bp} is the grindability of the undersized product produced per mill revolution (g/rev).



Fig. 3.4 Standard test mill (Bonds Ball mill)

3.3.2 Laboratory ball mill

Grinding of samples is carried out in laboratory ball mill (LBM). The test mill has an internal diameter of 500 mm and it is 1000 mm long as shown in the Fig. 3.5. A ball mill is a type of grinder used to grind and blend materials for use in mineral dressing processes, paints, pyrotechnics, ceramics and selective laser sintering. It works on the principle of impact and attrition, i.e., size reduction is done by impact as the balls drop from near top of the shell.

The same feed samples of HSHA, LSHA, LSLA and blend samples used in the BBM are used as feed for the LBM. In LBM, the experiments were conducted based on the total retention time taken by HSHA, LSHA, LSLA, and blend iron ore samples in the BBM. The LBM experiments were performed based on trial and error method, i.e., by reducing the total retention time obtained from BBM by 2 min, 4 min, and 6 min for the HSHA, LSHA, LSLA, and blend samples, respectively.

For all the samples, the speed of the mill, feed to the mill, and media (balls) were kept constant. The only parameter, which varied in the LBM, was the grinding time. The grinding time of LBM in each case was changed by reducing two minutes from the total retention time taken to produce 250% circulating load in the BBM. After the completion of each experiment in the LBM, particle size analysis was

carried out to identify the P_{80} passing percentage particle size fraction and percentage of liberation. The operations were repeated in the LBM for the HSHA, LSHA, LSLA, and blend samples until the P_{80} passing particle size fraction of $150\ \mu\text{m}$ was achieved.



Fig. 3.5 Laboratory ball mill

3.4 Characterization Study on Iron Ore Samples

Characterization is commonly used technique in mineral processing to identify mineral phases, interface, surrounding environment and flow parameters. Iron ore characterization is most important since it helps to select suitable processes based on the ore formation. Bulk chemical analysis is insufficient to identify the individual elements present in the ores. But characterization study can identify the minerals chemistry, minerals structure, quantification of phases, occurrence of elements and elemental association. Also more complex amorphous phase, structural disorder, strain and crystallite size can also be identified through characterization study (Kumar 2017). For the HSHA, LSHA, LSLA, and blend iron ores different types of characterization analysis are carried out i.e. optical microscopy analysis, QEMSCAN analysis, and sink float analysis.

3.4.1 Optical Microscopy and QEMSCAN analysis

The micrographs and degree of hematite liberation from the iron ore feed samples were analyzed and compared using the optical microscope (model Leica DMLP) and the QEMSCAN (Quanta FEG 650). Optical microscope consists of a system of lenses which uses visible light for magnification of images of small objects as shown in Fig. 3.6. Optical microscope is generally used to find mineralogy of the rocks, minerals and man-made materials.

QEMSCAN is a device which is used to know petrology and mineralogy by means of quantitative analysis as shown in Fig. 3.7. It is mainly used to scan rocks, minerals and moulded samples to know their nature of occurrences at different conditions. The abbreviation for QEMSCAN is Quantitative Evaluation of Minerals by SCANNing electron microscopy.



Fig. 3.6 Optical Microscope



Fig. 3.7 QEMSCAN

3.4.1.1 Preparation of iron ore sample for Optical Microscopy and QEMSCAN analysis

For the characterization study, both feed and product samples of HSHA, LSHA, LSLA, and blend iron ores were used. For both the feed and product samples moulds were prepared as shown in Fig. 3.8. For preparing of mould 10gm of iron ore samples is added to 9gm of resin and 15gm of hardener. Then the mixture is thoroughly mixed and poured in to mould. Later mould is placed in vacuum chamber to dry with compressed pressure. After 24 hours the mould is removed from vacuum chamber. The dried mould is polished on grinding wheel equipment. The mounting and polishing of a sample is typically done on grinding wheel equipment as shown in Fig. 3.9. To obtain a metal sample possessing the proper conditions for the purpose of viewing its microstructure, grinding wheel equipment is used. It mainly consists of grinding wheel where the speed of grinding wheel can be controlled based on the required surface finish of the sample. The grinding wheel has a provision to change the different abrasive sandpapers during smoothing and polishing of sample. Also grinding wheel equipment consists of a jet of water which is made to fall on grinding disc continuously to prevent excess of deformation of sample during grinding. After grinding process, the samples are examined in optical microscopy and QEMSCAN.



Fig. 3.8 Mould



Fig. 3.9 Grinding wheel equipment

3.4.2 Liberation analysis

For liberation analysis, the sink and float study was conducted using the di-iodo-methane organic liquid (3.3 g/cm^3). The sink and float test was conducted to identify the degree of hematite liberation in the iron ore blend feed and for iron ore products obtained at different grinding times in the BBM and the LBM. A specimen was prepared from the iron ore blend feed and ground product for the liberation study. The degree of liberation in the iron ore sample was determined by using equations 10 and 11.

$$T\% = \frac{\text{Total area of valuable minerals}}{\text{Total area of particles}} * 100 \quad (10)$$

The following Equation 11 ratio expresses the apparent degree of liberation of the sample of particles represented in a section of the sample.

$$L\% = \frac{\text{Total area of valuable minerals}}{\text{Total area of mineralized particles}} * 100 \quad (11)$$

3.4.3 Scanning Electron Microscope

A Scanning Electron Microscope (SEM) is a type of electron microscope that produces images of a sample by scanning the surface with a focused beam of electrons. The electrons interact with atoms in the sample, producing various signals that contain information about the surface topography and composition of the sample. The surface morphology and particle size of iron ore were examined by SEM and

Energy-dispersive X-ray spectroscopy (EDS) by using Hitachi-Japan with magnification 40 to 300000x.

CHAPTER 4

4 DESIGN AND FABRICATION OF NEW BALL MILL HYDRO-SQUEEZE CLASSIFIER

In this chapter new ball mill hydro-squeeze classifier design, fabrication and experimental strategies are presented. The experimental design framework is structured for newly developed ball mill hydro-squeeze classifier according to the key objectives. Each objective is talked separately.

4.1 Introduction

For sustainable development of the mineral processing industry, it is vital to develop energy-efficient comminution circuits. Classification plays a crucial role in improving the energy efficiency of comminution circuits. The classifier potential in the comminution circuits is assessed based on the particle size classification efficiency and circulating load to the ball mill. So, attempted have mad to obtained high classification efficiency with minimum recirculating load to the mill by combining the grinding and screening process in the newly developed hydro squeeze ball mill.

It is also found from the literature that the wet grinding and wet classification are carried out separately for particle size reduction and classification. So, new machine was developed for exploring the possibility of combining the process of wet grinding and wet classification in a single unit. Also keen on developing a unit that integrates grinding and classification processes. In the new machine, wet grinding and classification are carried simultaneously in the ball mill section and classification section. The classification section has the flexibility to classify the particles to the desired size and recirculate the entire coarser particles from the classifier section to the mill section. The classification section will also restrict the flow of the coarser particle to the downstream process completely.

4.2 Experimental Setup

A ball mill hydro-squeeze classifier is designed and fabricated for removing narrow size particles from the mill as shown in Fig. 4.1. The three dimensional view of new laboratory ball mill with classifier set-up, shown in Fig. 4.2, was specially designed for conducting experiments in the laboratory. The grinding chamber has a length and diameter of 1900 mm and 962mm, respectively as shown in Fig. 4.3 and 4.4. The feed end of the rotating drum has an opening of 0.3 m to feed the sample. An external feeding stand with feeder in the opening is provided at the feed end of the rotating drum as shown in Fig. 4.5. The rotating mill is filled with three steel balls of sizes 25 mm, 40 mm and 50 mm with 45%, 40% and 15% weight percentage, respectively. For collecting the ground product, the discharge end of the mill is connected to the classifier section, as shown in Fig. 4.6 and 4.7. For providing continuous feed to the mill, a pump set-up is used to pump the slurry from the feed sump to the rotating mill. The rotating drum is driven by a motor with variable speed. The rated power of the motor was 3.7 kW and the rated speed 1450 rpm. A gearbox was used to decrease the speed of the motor. The reduction ratio of the gearbox was found to be 1:7; thus, the speed of the motor was reduced to 200 rpm. The motor speed was controlled using a potentiometer.

The mill classification section is fixed to the frame and is called the stationary section. The ball mill discharge end is retrofitted into the stationary section, as depicted in Fig.4.1. The classifier mainly consists of a pressure gauge, two outlet valves, and a squeezing mechanism.

The pressure gauge was used to measure the classifier section pressure during the squeezing process, as shown in Fig.4.1. Two outlet valves were provided in the classifier section to collect separated oversize and undersize particles. The squeezing mechanism consists of a squeezing disc, closing cap, guide rod, screw rod, and guide plate. The classifier section was divided into two chambers based on the position of the classifier disc. Figures 4.8 and 4.9 shows the classifying disc used to separate oversize and undersize particles from milled discharge slurry product. The dimension of the classifying disc was selected based on the internal diameter of the squeezing section. Teflon material was used to avoid excess weight, and it also helps in easy disc movement in the classifier section without any resistance. The classifier disc is

provided with a groove for rubber sealing, which prevents the transfer of particles from Chamber-1 to Chamber-2. The classifier disc is provided with a one-third opening to fit the screen. The disc is fitted with a 150 μm screen for separating oversize particles from undersize particles. Figures 4.10 and 4.11 shows a closing cap connected to the rod, and the other end of the rod is connected to the flange. This newly designed closing cap rod system in the ball mill hydro-squeeze classifier helps to control the inlet flow of the ground material from the grinding section to the classifier section based on the product particle size requirement. It also helps to block the material backflow into the ball mill during the squeezing of slurry in the classifier section. The closing cap diameter is 5 mm larger than the mill discharge end diameter. The larger diameter of the closing cap helps close the mouth of the mill discharge end inside the classification section. The closing cap rod is placed inside the classifier disc pipe, where the cap rod and disc pipe are independently operated. One end of the classifier disc pipe consists of a flange that is placed into the guide plate, as shown in Figs.4.12 and 4.13.

The purpose of the guide-plate is to guide the screw rod, support the guide rod, and convert the screw rod rotation to the classifier disc linear movement inside the classifier section as shown in Figs 4.14 and 4.15. The guide rod dimensions are selected based on the length between the mill discharge end and the classifier disc parking position inside the classifier section, as shown in Figs.4.16 and 4.17. One end of the screw rod is connected to the classifier closing plate as shown in Figs.4.18 and 4.19, and the other end is connected to the electric hand drill device for the rotating screw rod as shown in Figs.4.20 and 4.21. The electric hand drill device with a reversible motor is used for forward and backward the classifier disc movement inside the classification section. The classifier disc speed inside the classification section is controlled using the speed control knob in an electric hand drill. The screw rod end was machined for 15mm*15mm to connect the screw rod to the hand drill based on the electric hand drill chuck size dimension. The guide plate moves forward when the screw rod rotates in a clockwise direction, and it moves backward when the screw rod rotates in an anticlockwise direction. The screw rod can rotate either clockwise or anticlockwise by using a reversible motor in a hand drill.

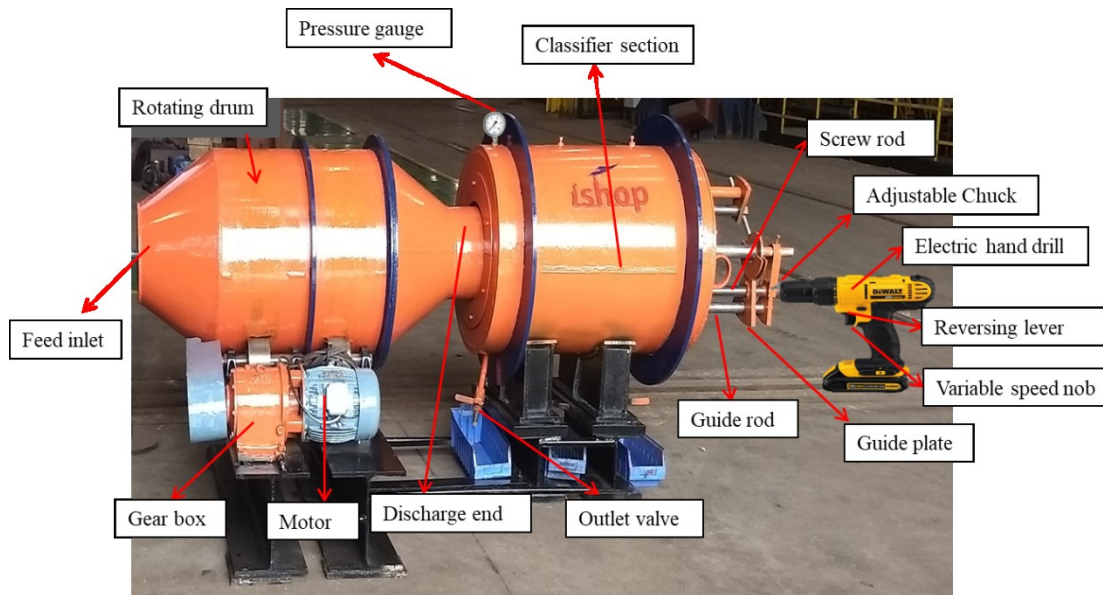


Fig. 4.1 Ball mill hydro-squeeze classifier

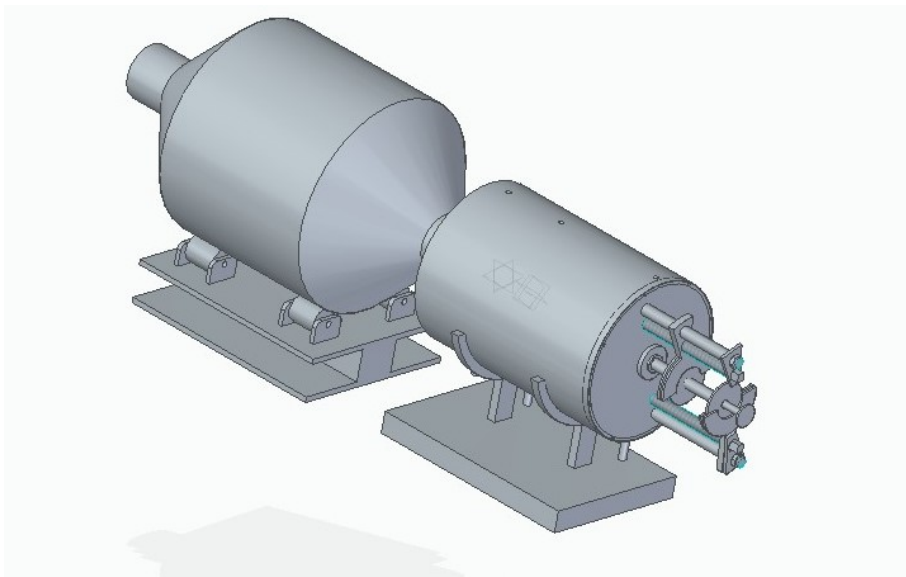


Fig. 4.2 Three dimensional view of ball mill hydro-squeeze

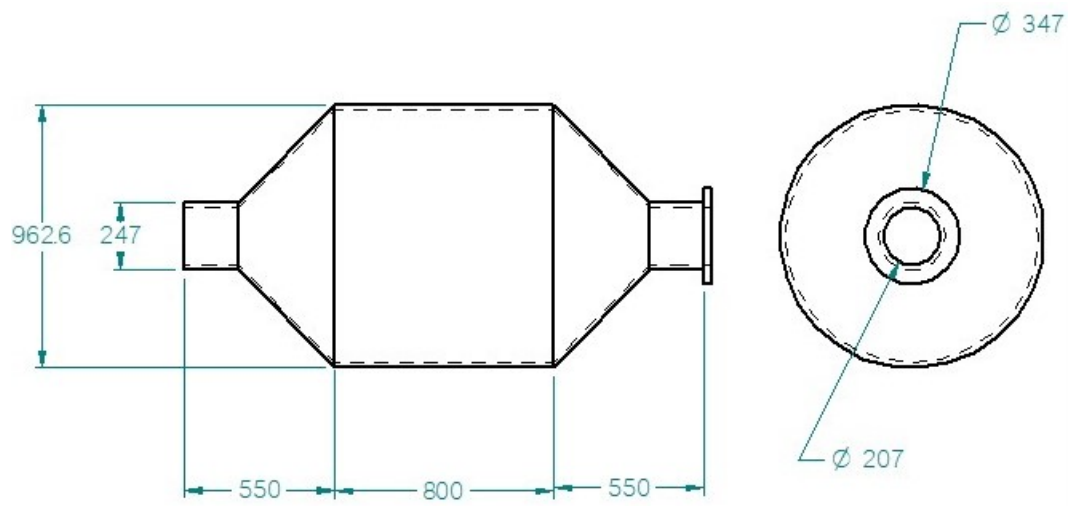


Fig. 4.3 Two dimensional view of rotary drum ball mill grinding shell



Fig. 4.4 Fabricated grinding shell



Fig. 4.5 Fabricated feeder arrangement

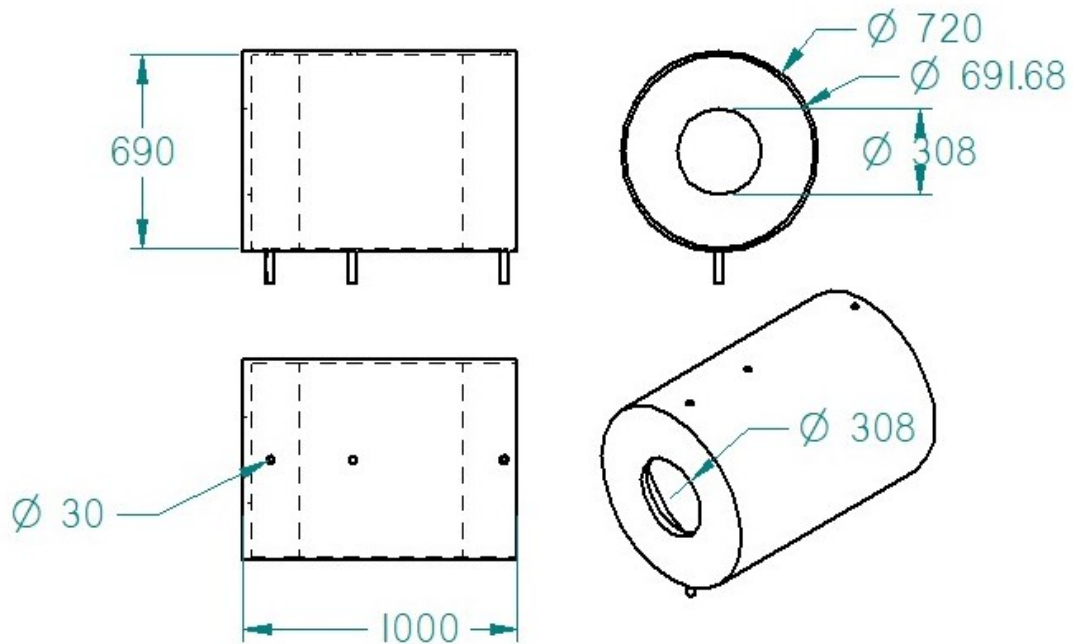


Fig. 4.6 Two dimensional view of classifier section



Fig. 4.7 Fabricated classifier section

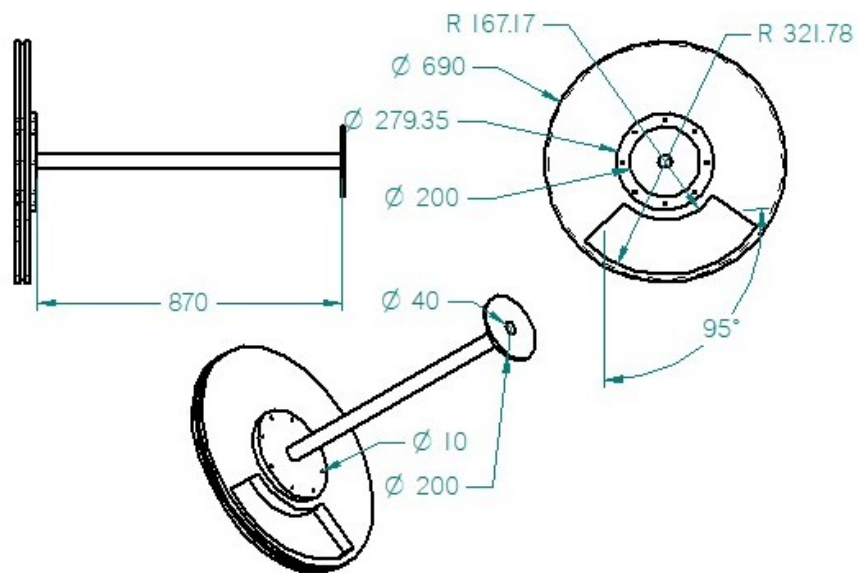


Fig. 4.8 Two dimensional view of classifier disc



Fig. 4.9 Two dimensional view of classifier disc

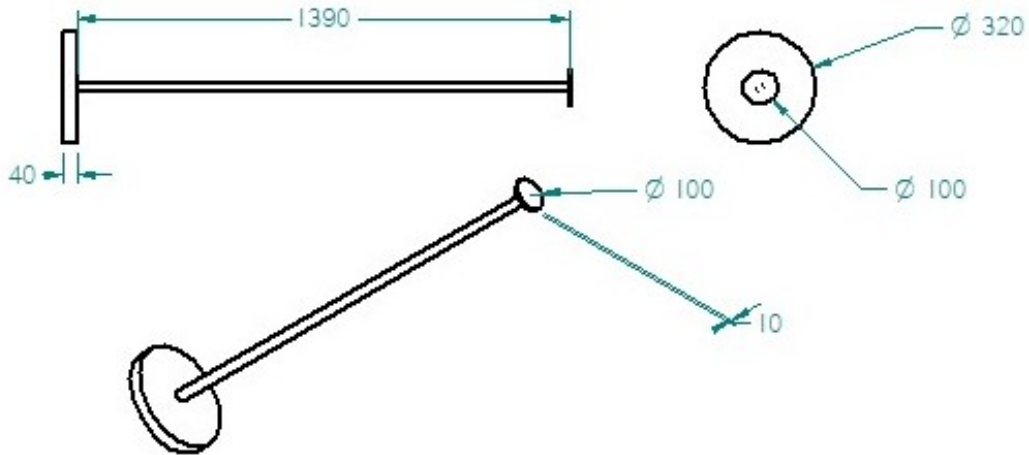


Fig. 4.10 Two dimensional view of slip-in cap

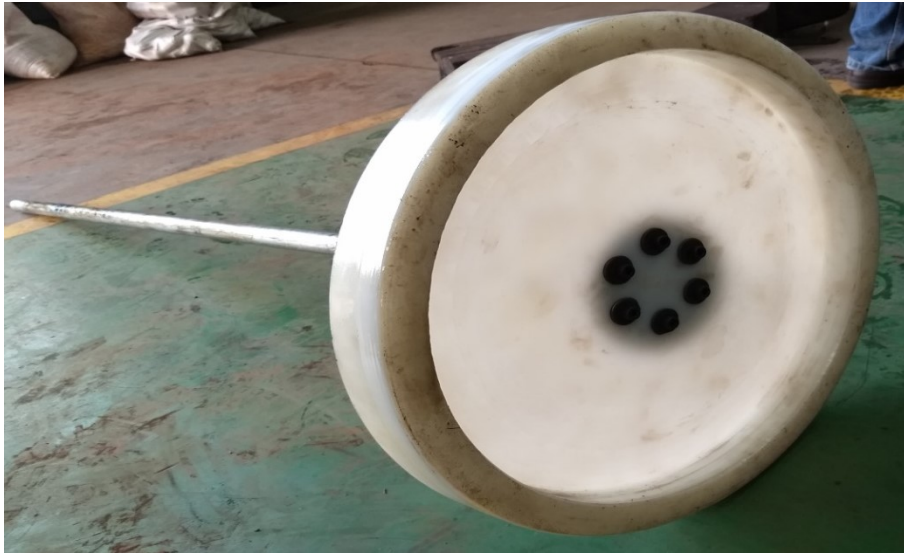


Fig. 4.11 Fabricated slip-in cap

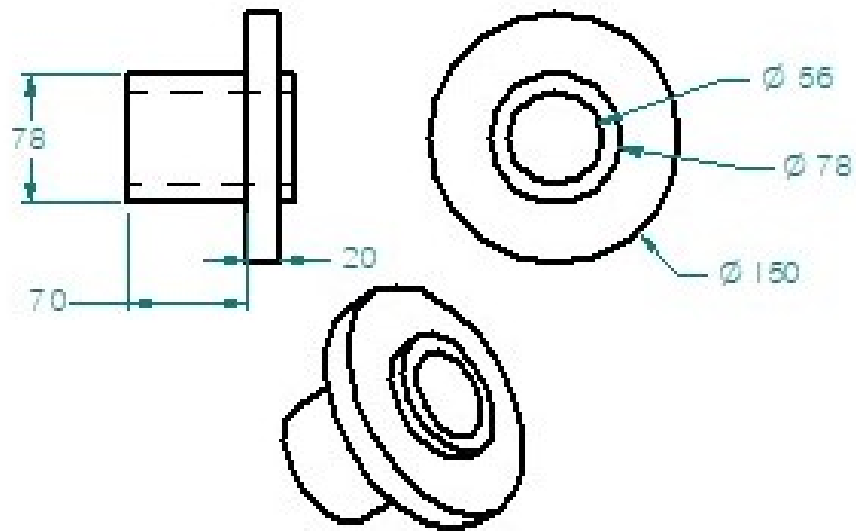


Fig. 4.12 Two dimensional view of flange



Fig. 4.13 Fabricated flange

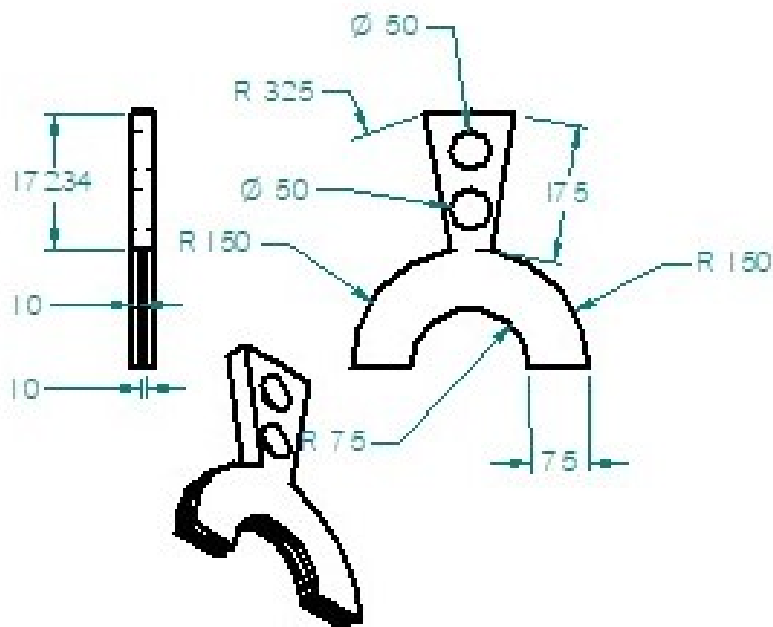


Fig. 4.14 Two dimensional view of guide plate



Fig. 4.15 Fabricated guide plate

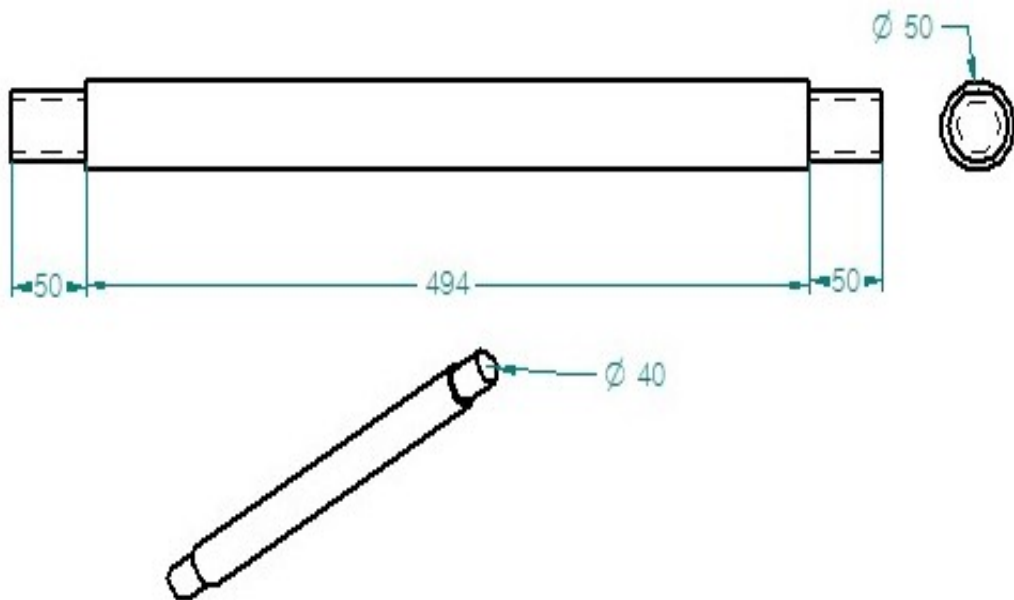


Fig. 4.16 Two dimensional view of guide rod



Fig. 4.17 Fabricated guide rod

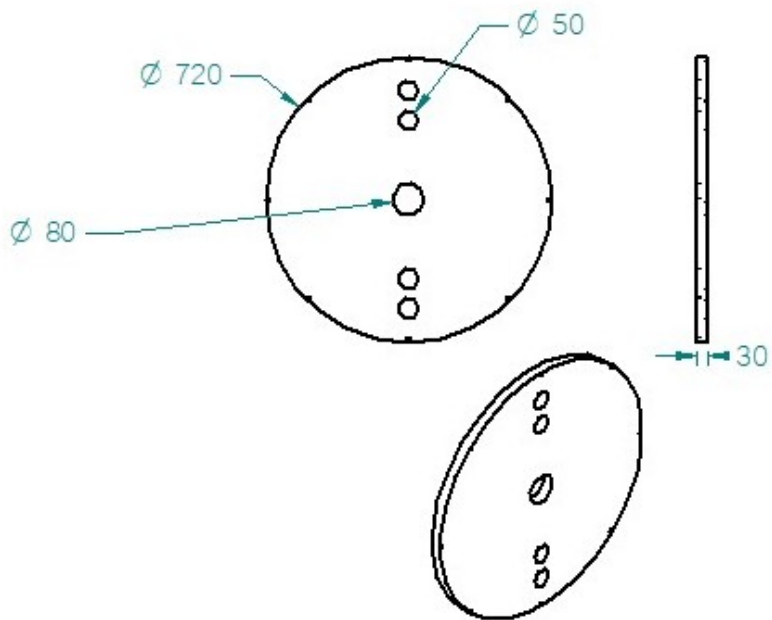


Fig. 4.18 Two dimensional view of in classifier closing plate



Fig. 4.19 Fabricated classifier closing plate

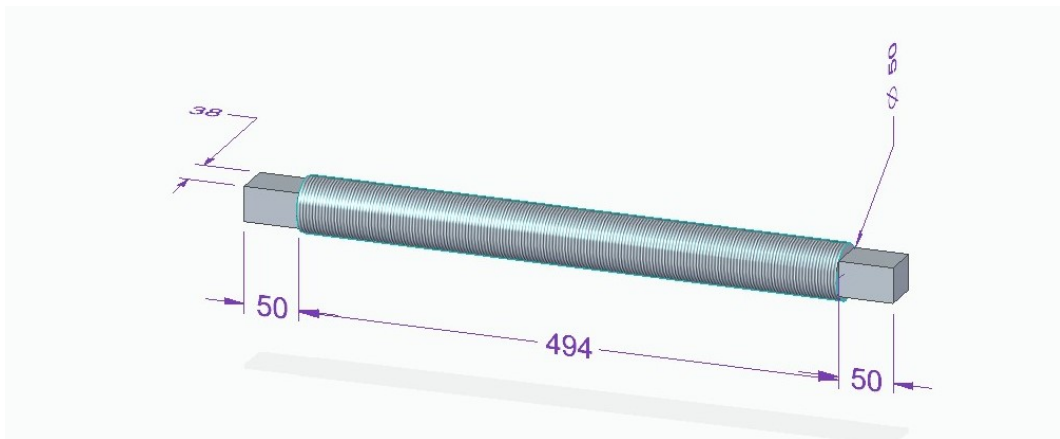


Fig. 4.20 Three dimensional view of screw rod

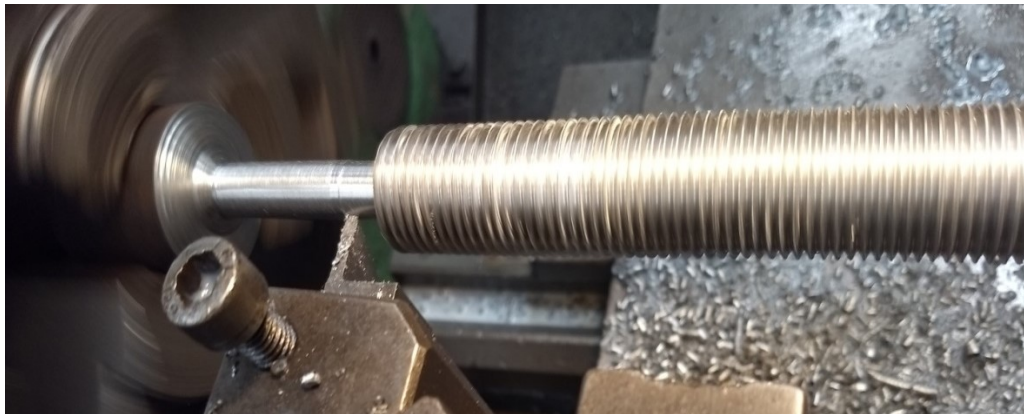


Fig. 4.21 Screw rod

4.3 Design of Outlet Discharge Trunnion With Lifter Arrangement

In the present work, in order to improve the grinding equipment's performance, a special type of discharge end overflow trunnion was designed for fitting or removing lifters, as shown in Figs.4.22 and 4.23 (Nelson, 1980). The ball mill was differentiated into two parts (Figs.4.24), the first part known as the grinding section and the second as the discharge section. Both parts are fabricated in such a way that they can easily be fitted by using bolts and nuts, as shown in Figs.4.25.

In this system, the slurry flows through the inlet feed trunnion due to the gradient between the inlet and outlet openings of the rotating drum. The inlet feed trunnion section is steeped with a higher angular position of 15° to 20° to the horizontal compared to discharge end overflow trunnion. The steeped angle at the inlet restricts backward flow and maintains better settling and enhanced initial acceleration to the material flow in the pulp. As shown in Figs.4.24, reverse double helixes in the discharge-end trunnion liner retains a major portion of the balls (grinding media) in the mill and discharges the pulp to the next section through the extended section of the discharge-end overflow trunnion.

Figure 4.23 shows the lifter design with different orientation of lifter plates, which were installed at the discharge end of the experimental ball mill. A lifter plate mainly consists of primary, secondary and tertiary plates which are fixed and inclined at 30° , 35° and 30° respectively to the diaphragm plate. A total of six lifters were installed at the discharge end of the experimental ball mill. The lifter plates were made of rubber but they can also be made of other materials, such as PVC, steel, etc. The lifters were fitted at the discharge end of the ball mill using rivets. This shorter length of the lifter plates on the diaphragm acts as a separation zone from which fine particles are raised. Coarse particles and balls which enter the separation zone due to the tumbling action and gradient, and flow between the inlet and outlet of the mill are not carried by the lifter blades. This is because the lifter plates are inclined towards the mill section and of shorter length. The coarse particles and the balls are rolled back to the mill section.

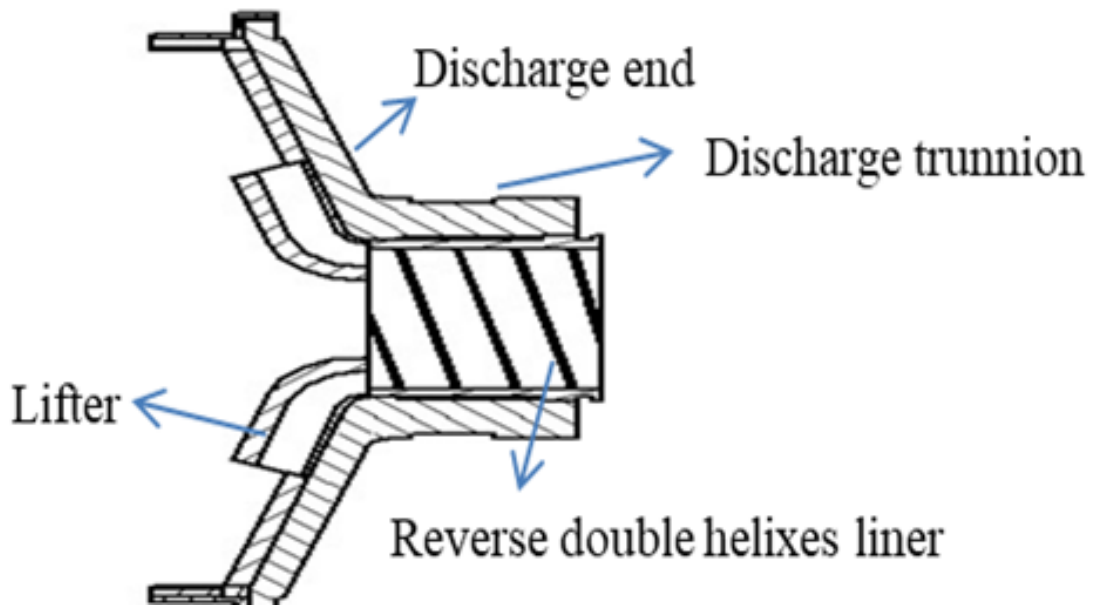


Fig. 4.22 2D view of the mill discharge trunnion (after Nelson, 1980)

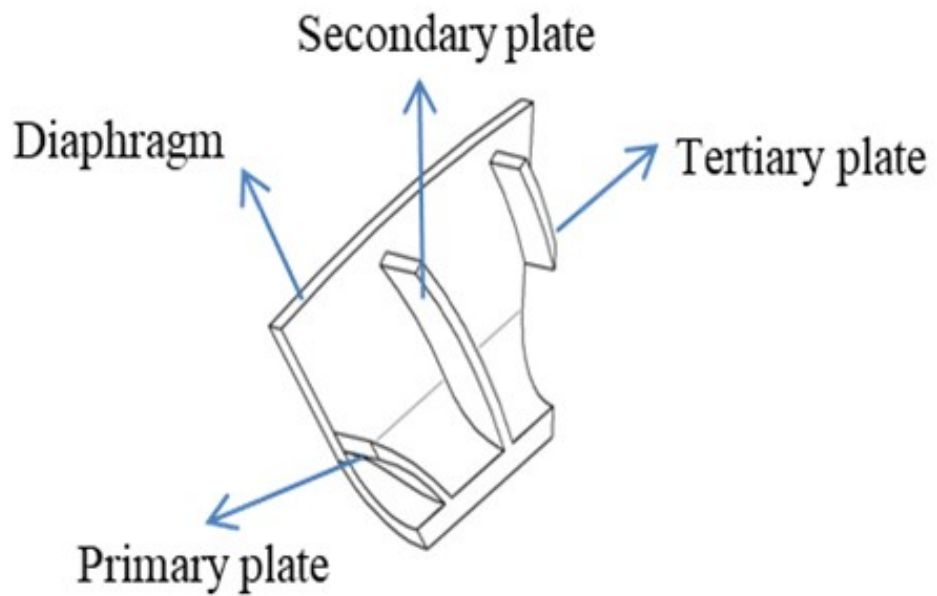


Fig. 4.23 2D view of the lifter arrangement (after Nelson, 1980)

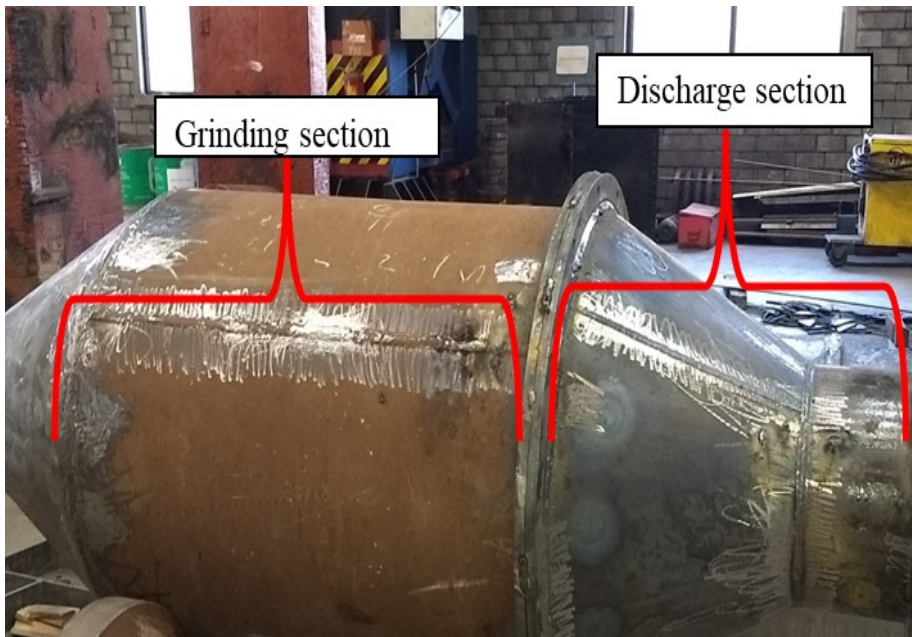


Fig. 4.24 Ball mill with newly fabricated discharge end

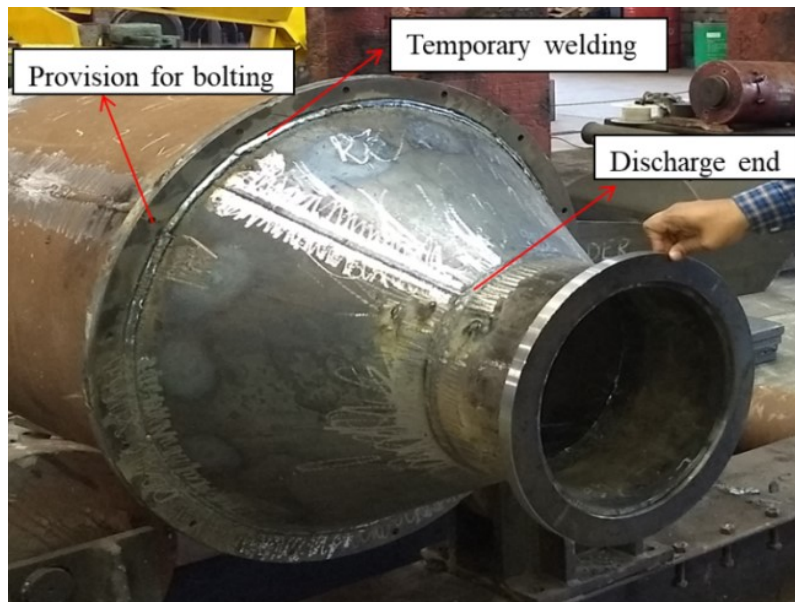


Fig. 4.25 Discharge end with provision for bolting

4.3.1 Experimental procedure for newly designed ball mill outlet discharge trunnion with lifter arrangement

Before starting the experiment, the chemical and physical composition of the selected iron ore sample was determined, as shown in Table 4.1. In the present study, the experiments were carried out at different discharge end operating conditions, as

shown in Table 4.2. The discharge end was kept open for all the experiments in Case 1 and Case 2, as shown in Table 4.2. In Case 3, for all the experiments, the discharge end was kept open for 30 sec, during which the discharge particles were collected into the classifier unit. In Case 3, the discharge-end time was kept constant for all the experiments. After 30 sec, the mill discharge end was closed for another 30 sec by using a cap, during which the particles collected in the classification unit were removed and analysed. In Case 3, the discharge-end time was kept constant for all the experiments.

Initially, the mill discharge end is kept open by using an open-and-close mechanism at the discharge end. The mill is started by switching on the power button. The mill volume was maintained with 40% of charge throughout the experiment (Gupta & Yan, 2016). A rotating speed of 35.3 rpm, which corresponds to 100% of the mill's critical speed, was calculated using Equation 12. The mill speed was varied from 20% to 70% of the critical speed of the mill with an interval of 10% mill critical speed, as shown in Table 4.2. Once the mill starts to rotate, it is fed with -3 mm particles size of iron ore slurry having a slurry density of 2.1 kg/m³. For each critical speed, the mill was operated for 20 min. For the first 10 min of each critical speed, the mill was allowed to stabilise. During the stabilisation of the mill, the classifier section outlet valve of chamber one was kept open in order to remove the product discharged from the mill during the initial 10 min of grinding. After 10min, the classification outlet valve was closed for another 10 min to collect the discharged product from the mill; once the mill reached a stable condition. The collected samples were then removed from chamber one of the classifier section through the outlet valve and dried in the oven. After drying, a sample was collected for particle size analysis using a parallel beam laser diffraction set-up.

$$V_c = \frac{42.3}{\sqrt{D-d}} rev/min \quad (12)$$

where,

V_c = critical speed of the mill (in rpm);

D = the inner diameter of the mill (in meters); and

d = the size of the grinding balls (in meters).

Table 4.1 Chemical and physical specification of iron ore sample

Type of ore	Chemical Specification %				Grinding Specification	
Iron ore	Fe T	SiO ₂	Al ₂ O ₃	LOI	F ₈₀ (mm)	BWI(kWh/t)
	60.42	5.58	4.03	3.17	1.65	8.42

Table 4.2 Experimental operating condition

Constant Parameters	Varied Parameter	Different Operating Conditions		
		Case-1	Case-2	Case-3
Feed rate, Charge and Slurry density	Percentage of Critical speed (%) (20,30,40,50,60 &70)	without lifters (cap open)	with lifters (cap open)	with lifters (cap closed)

4.3.2 Particle size measurements for Case-1, Case-2 and Case-3

The particle size measurement for the feed sample was conducted using a mechanical vibratory sieve shaker. The product particle size analysis was conducted using HELOS; a parallel beam laser diffraction set-up, which offers a powerful technology. The equipment set-up is presented in Fig. 3.3.

The discharge product from the mill was dried in the oven. After drying, the samples were subjected to the parallel beam laser-diffraction set-up for particle size measurement. The particle size analysis obtained from the parallel beam laser-diffraction set-up is in terms of the cumulative passing particle size fraction. Based on the particle size analysis data, the size above +150 μm was considered as a recirculating load to the mill, the particle size range in -150 μm /+10 μm was considered as desired the size particles and particle size below -10 μm was considered as fine particles. This classification was done based on the different particle size range requirement for pellet feed. Pellet making requires feed particles to contain about 60 - 70% of 150 - 10 μm , less than 30% for particles smaller than 10 μm and no particles above 150 μm (Umadevi et al., 2013).

4.4 Preparation of Feed Sample for New Ball Mill Hydro-Squeeze Classifier

Iron ore samples were used as feed to the ball mill. The samples were crushed in a jaw crusher to reduce the lump size to -3 mm size particles. The crushed samples were then screened using sieve shakers to remove oversize particles. The feed particle size

was analyzed before feeding into the ball mill. The screened particles were used to prepare different iron ore feeds of varying slurry solid concentration of 55%, 60%, 65%, 70%, and 75%. The different percentages of solid slurry concentration were prepared based on the grinding performance of the ball mill. The slurry below 55% solid concentration was not considered, as the diluted slurry could cause a pool of slurry at the bottom of the mill shell, which might reduce the grinding capacity of the mill (Tangsathikulchai and Austin 1989). The slurry solids concentration above 75% would be very viscous, leading to a high cushioning effect resulting in low grinding efficiency (Tangsathikulchai and Austin 1989). Hence, the slurry with a solid concentration below 55% and above 75% was not considered. Therefore solid slurry concentration to the mill was varied from 55% to 75% with an interval of 5%.

4.4.1 Operation of ball mill hydro-squeeze classifier

For each varied slurry solid concentration (55% to 75% solids), mill discharge end open time was varied from 30 s to 150 s with an interval of 30 s mill discharge end open time. For all varying conditions, the mill discharge end closing time was kept constant for 120 s as represented in Table 4.3. During discharge end closing time, slurry discharged from ball mill to the classifier section was squeezed to separate oversized particles from undersized particles. In the meantime, the separated particles are removed from the classifier section.

The newly designed ball mill hydro-squeeze classifier was operated in two cases. In case-1, the ball mill hydro-squeeze classifier was operated to know the size of particles discharged from the ball mill to the classifier section. In case-2, a ball mill with a classifier disc was operated inside the classifier section to know the classifier disc classification efficiency. In case-1, initially, the discharge end of the mill and outlet valves of the hydro-squeeze classifier chambers were kept open, and the mill was continuously fed with iron ore slurry by using a slurry pump system. The mill volume was maintained with 40% of the charge and operated for about 10 min at 60% mill critical speed. The classifier disc in the classifier section was parked at its parking position, about 400 mm distance from the mill discharge end, as shown in Fig.4.26. Once the mill reached stable condition, the mill discharge end was closed for 120 s using the closing cap. The outlet valve of Chamber-1 and Chamber-2 were

kept open to remove the slurry discharged from the mill. After closing the mill discharge end for 120 s, the closing cap was retracted to open the mill discharge end, as shown in Fig.4.27. As the mill discharge end opens, slurry starts to flow from the mill discharge end to Chamber-1 of the classifier section. The discharge end of the mill was kept open for 30 s. After 30 s, the mill discharge end was closed for another 120 s using the closing cap. In this duration, the slurry was removed from the outlet valves of Chamber-1 and 2. The slurry collected from Chamber-1 and 2 were mixed and dried. The dried samples were used to determine the particle size discharged from the ball mill section to the classifier section. Dried product samples were analyzed for P_{80} particle size passing percentage, the weight percentage of oversize particles (+150 μm), and the weight percentage of undersize particles (-150 μm) discharged from the ball mill section to the classifier section. The experiment was repeated by varying the discharge end opening time and the slurry solids concentration to the mill.

In Case-2, both ball mill and classifier disc was operated all together to determine the classification efficiency of the newly designed ball mill hydro-squeeze classifier. In this case, the grinding operation parameters, discharge end opening time, discharge end closing time, and slurry solid concentration were maintained the same as in Case-1. Initially, the mill discharge end was closed using a closing cap, the outlet valve of Chamber-1 was closed, the outlet valve of Chamber-2 was kept open, and the classifier disc was placed at the parking position, as shown in Fig.4.26. The mill was continuously fed with iron ore slurry, and the discharge end of the mill was closed for 120 s using the closing cap. After 120 s, the closing cap was retracted to open the mill discharge end, as shown in Fig.4.27. The slurry starts to flow from the discharge end of the mill to Chamber-1 of the classifier section. The discharge end of the mill was kept open for a set time. Soon after completion of the mill opening time, the mill discharge end was closed for 120 s using the closing cap, as shown in Fig.26. In this duration, the classifier disc was moved inside the classifier section by switching on an electric hand drill. The slurry collected in Chamber-1 was squeezed by moving the classifier disc from its parking position to the mill discharge end, as shown in Fig.4.28. As the classification disc reaches the mill discharge end, the electric hand drill automatically gets switched off. Further, the classifier disc was moved back from

the mill discharge end to the classifier disc parking position by switching to reverse mode in an electric hand drill. Meantime, the outlet valve of Chamber-1 was opened to remove the leftover slurry in Chamber-1, as shown in Fig.4.29. Since the outlet valve of Chamber-2 was opened, the slurry entering into Chamber-2 is continuously removed. Simultaneously, after removing slurry from Chamber-1 and 2, the outlet valve of Chamber-1 was closed before the opening of the discharge end of the mill, as shown in Fig.4.26. The entire squeezing process, along with the removal of the classified particles in Chamber-1 and 2, was completed within 120 s of mill discharge end closing time. The slurry collected from the outlet valves of Chamber-1 & 2 after squeezing was dried separately in the oven after each trial. The dried samples from Chamber-1 and 2 were separately analyzed to calculate classifier disc separation efficiency. Analyses were carried to find P₈₀ particle size passing percentage, the weight percentage of oversize particles (+150 μm), and undersize particles (-150 μm) collected from Chamber-1 and 2 during the different operating condition. The process was repeated for various slurry solid concentrations at varying discharge end opening times of the mill, as given in Table 4.3. The efficiency of the classifier disc was calculated as follows:

$$\eta = \frac{\text{Wt.\% of } -150 \mu\text{m particles collected in chamber-2 after squeezing}}{\text{Wt.\% of } -150 \mu\text{m particles collected in chamber-1 before squeezing}} * 100 \quad (13)$$

Where, η= efficiency of classifier disc

Table 4.3 Ball mill hydro-squeeze classifier operating conditions

Constant operating parameters	Slurry solid concentration (%)	Mill discharge end open time (s)
Feed rate, Charge, Mill speed and Mill discharge end close time	55,60,65,70 and 75	30,60,90,120 and 150

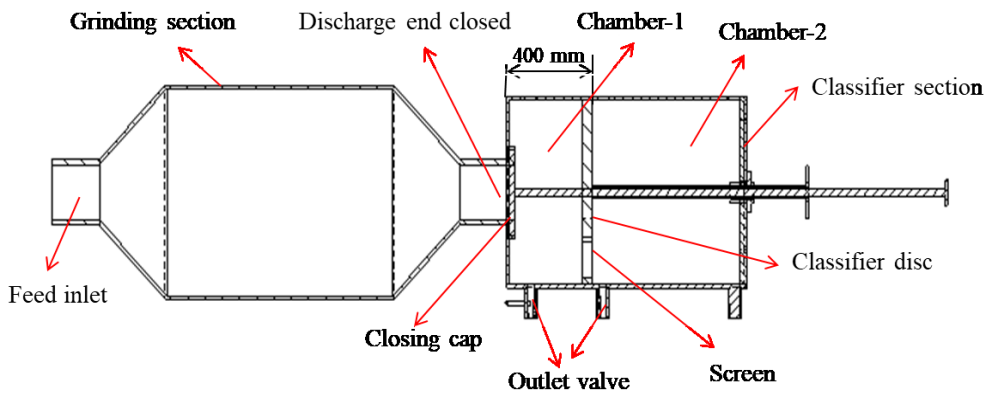


Fig. 4.26 Discharge end closed and classifier disc at parking position

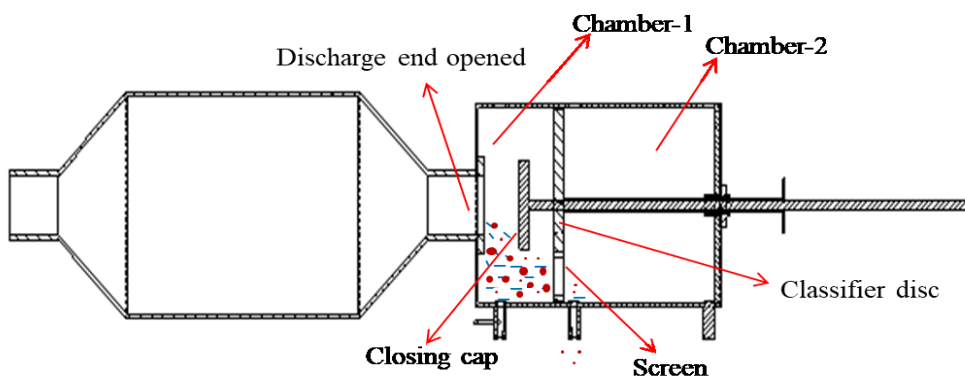


Fig. 4.27 Discharge end open and classifier disc at parking position

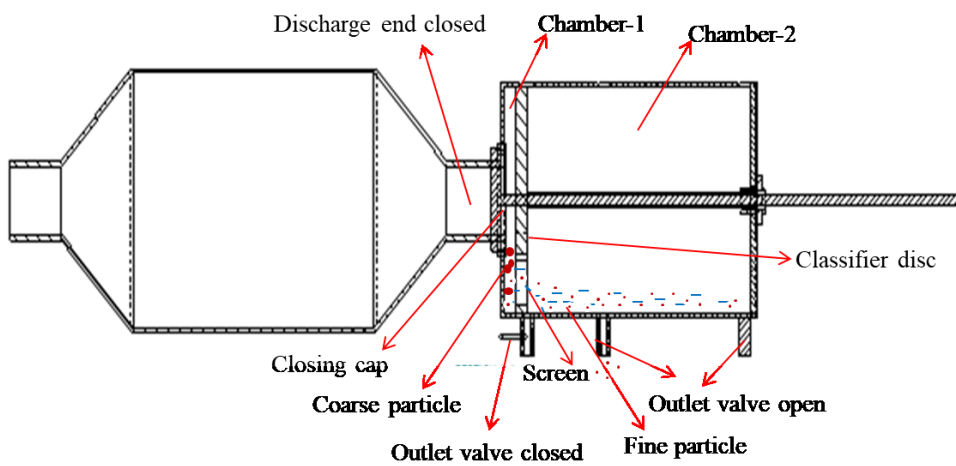


Fig. 4.28 Discharge end closed and classifier disc is moved towards discharge end

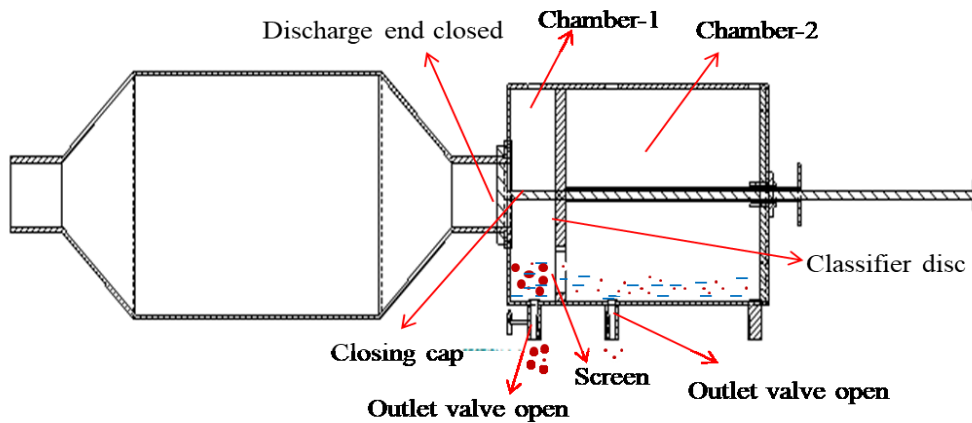


Fig. 4.29 Discharge end closed and classifier disc is moving towards parking position

4.4.2 Product Particle size analysis of ball mill hydro-squeeze classifier

Analysis were carried to find P_{80} particle size passing percentage, the weight percentage of oversize particles (+150 μm), and undersize particles (-150 μm) collected from Chamber-1 and 2 for different operating conditions. Optical image acquisition model Leica DMLP was used to find different mineral phases for feed and samples collected in Chamber-1 and 2 after the classification. An optical microscope with image analyser software (Carl Zeiss AxioVision SE64) was also used to find the feed particle size and product particle size collected in Chamber-1 and 2 after the classification. The surface morphology and particle size of iron ore were examined by Scanning Electron Microscope (SEM) and Energy-dispersive X-ray spectroscopy (EDS) by using Hitachi-Japan with magnification 40 to 300000x.

CHAPTER 5

5 RESULTS OF EXPERIMENTAL INVESTIGATIONS

In this chapter, the results of experimental investigations to determine the iron ores Bond Work Index and its optimum grinding time to obtain desired particale size are discussed. Also, the new ball mill hydro-squeez classifier performance is evulated for various operating conditions are discussed in this chapter.

5.1 Bond Work Index Determination Using Standard Ball Mill

The grinding studies were conducted based on Bond's standard procedure to determine Bond's Work Index and retention time using the BBM. The effect of retention time on PSD and the liberation of hematite from the iron ore for all the samples were analyzed. Bond Work Index, time taken to produce 250% circulating load and particle size distribution of iron ores are determined and the results obtained are analysed. To obtain Bond Work Index for HSHA, LSHA, LSLA, and blend iron ore samples Standard ball mill was used. The Bond Work Index of each over is calculated by using Equation 9.

5.1.1 Bond Work Index calculation for HSHA iron ore sample

The required under size fraction which is used to calculate BWI for HSHA iron ore sample is obtained by iterative process as shown in Table 5.1.

Required size below which particles are categorized as undersize particles	=75 μ m
Weight of 700cc feed	=1600gm
Weight % of undersize fraction in the feed (700cc)	=10%
Circulating load of the mill	=250%
Weight of undersize fraction to be produced in an iteration	=457.14gm

Table 5.1 BWI iterative process for HSHA

Sl. No	No. of Revolutions	Return feed (gm)	Fresh feed (gm)	Undersize in the feed (gm)	Undersize produced (gm)	Net under size produced (gm)	Grams per revolution (Gbp)	Next Revolution	Circulating load (%)
1	100	0	1600	160	430	270	2.9	147	219
2	147	1170	430	43	420	377	1.78	165	285
3	165	1180	420	42	425	383	1.67	184	270
4	184	1175	425	42	430	387.5	1.59	187	266
5	187	1170	430	43	445	402	1.589	203	255
6	203	1150	445	44	457	412.5	1.57	217	250
7	217	1143	457	45.7	374	328.3			

Note:

The total number of revolution required to produce 250% circulating load = 1204
 Total time taken to produce 250% circulating load = 16 min
 Average grams per revolution produced = 1.68 Gbp
 From the Fig 5.1 the size through which 80% of the feed passes = 2500 μm
 From the Fig 5.2 the size through which 80% of the product passes = 70 μm
 Bond Work Index for HSHA = 12.8 KWh/mt

Table 5.2 shows the HSHA iron ore sample particle sieve analysis of feed and product respectively. The 80% passing feed and product size is 2400 μm and 60 μm as shown in Figs 5.1 and 5.2. The calculated BWI of HSHA iron ore sample is 14 KWh/mt. The total time taken by HSHA iron ore sample in standard ball mill to produce 250% circulating load is 16 min.

Table 5.2 Sieve analysis of HSHA with respective to feed and product

Sieve analysis of the feed				Sieve analysis of final undersize fraction (product)			
screen size (μm)	wt retained (gm)	%retained	%passing	screen size (μm)	wt retained (gm)	%retained	%passing
3150	0	0	100	75	0	0	100
2000	172	34.4	65.6	63	78	16.2	83.8
1000	100	20	45.6	53	89	18.5	65.4
500	67	13.4	32.2	45	102	21.2	44.2
210	61	12.2	20	25	124	25.7	18.5
75	41	8.2	11.8	0	89	18.5	0.0
0	50	10	0				

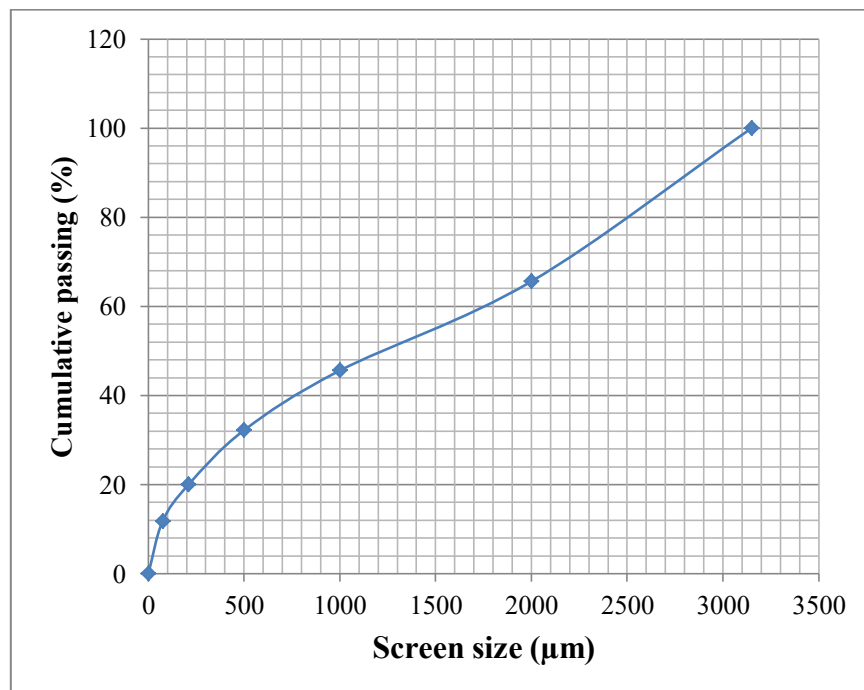


Fig. 5.1 Particle size analysis for HSHA iron ore feed sample

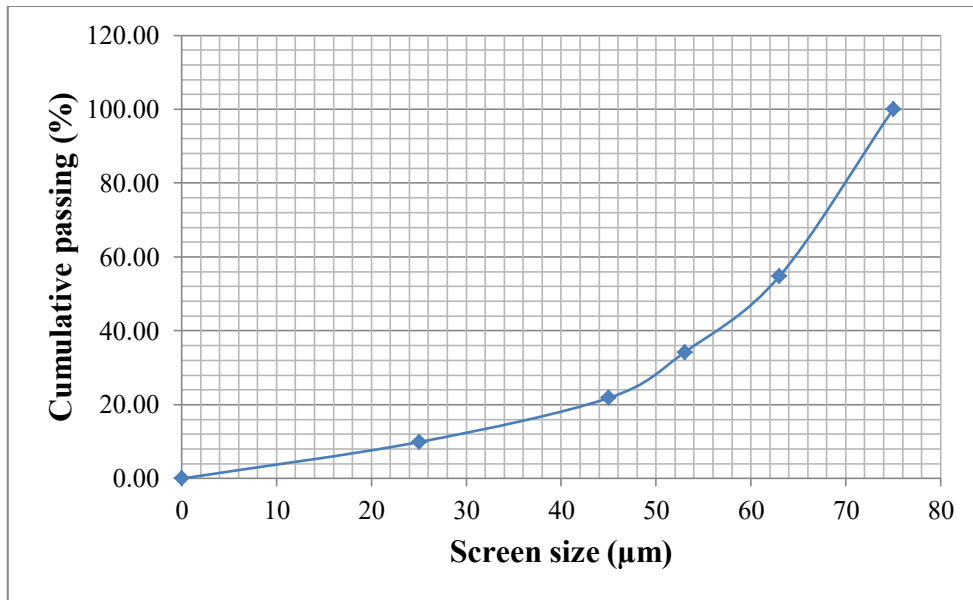


Fig. 5.2 Particle size analyses for HSHA iron ore product sample

5.1.2 Bond Work Index calculation for LSHA iron ore sample

The required under size fraction which is used to calculate BWI for LSHA iron ore sample is obtained by iterative process as shown in Table 5.3.

Required size below which particles are categorized as undersize particles	=75 μm
Weight of 700cc feed	=1500gm
Weight % of undersize fraction in the feed (700cc)	=12%
Circulating load of the mill	=250%
Weight of undersize fraction to be produced in an iteration	=428.14gm

Table 5.3 BWI iterative process for LSHA to get the undersized fraction

Sl. No	No. of Revolutions	Return feed (gm)	Fresh feed (gm)	Undersize in the feed (gm)	Undersize produced (gm)	Net under size produced (gm)	Grams per revolution (Gbp)	Next Revolution	Circulating load (%)
1	100	0.0	1500	180.0	470.0	290.0	2.9	123	219
2	123	1030	470	56.4	390.0	333.6	1.7	155	285
3	155	1110	390	46.8	405.0	358.2	1.6	182	270
4	182	1095	405	48.6	410.0	361.4	1.5	200	266
5	200	1090	410	49.2	428.0	378.8	1.5	237	250
6	237	1072	428	51.4	457.0	405.6			

The total number of revolution required to produce 250% circulating load = 997
 Total time taken to produce 250% circulating load = 13 min
 Average grams per revolution produced = 1.68 Gbp
 From the Fig.5.3, the size through which 80% of the feed passes = 2350 μm
 From the Fig.5.4, the size through which 80% of the product passes = 60 μm
 Bond Work Index for LSHA = 10.2 KWh/mt

Table 5.4 shows the LSHA iron ore sample particle sieve analysis of feed and product respectively. From Figs 5.3 and 5.4, 80% passing feed and product size is 2500 μm and 55 μm respectively. The calculated BWI of LSHA iron ore sample is 11 KWh/mt. The total time taken by LSHA iron ore sample in standard ball mill to produce 250% circulating load is 13 min.

Table 5.4 Sieve analysis of LSHA with respective to feed and product

Sieve analysis of the feed				Sieve analysis of final undersize fraction (product)			
screen size (μm)	wt retained (gm)	%retained	%passing	screen size (μm)	wt retained (gm)	%retained	%passing
3150	0	0	100	75	0	0	100
2000	142	28.4	71.6	63	38	7.9	92.1
1000	85	17	54.6	53	77	16.0	76.1
500	68	13.6	41	45	72	14.9	61.2
210	84	16.8	24.2	25	160	33.2	28.0
75	61	12.2	12	0	135	28.0	0.0
0	60	12	0				

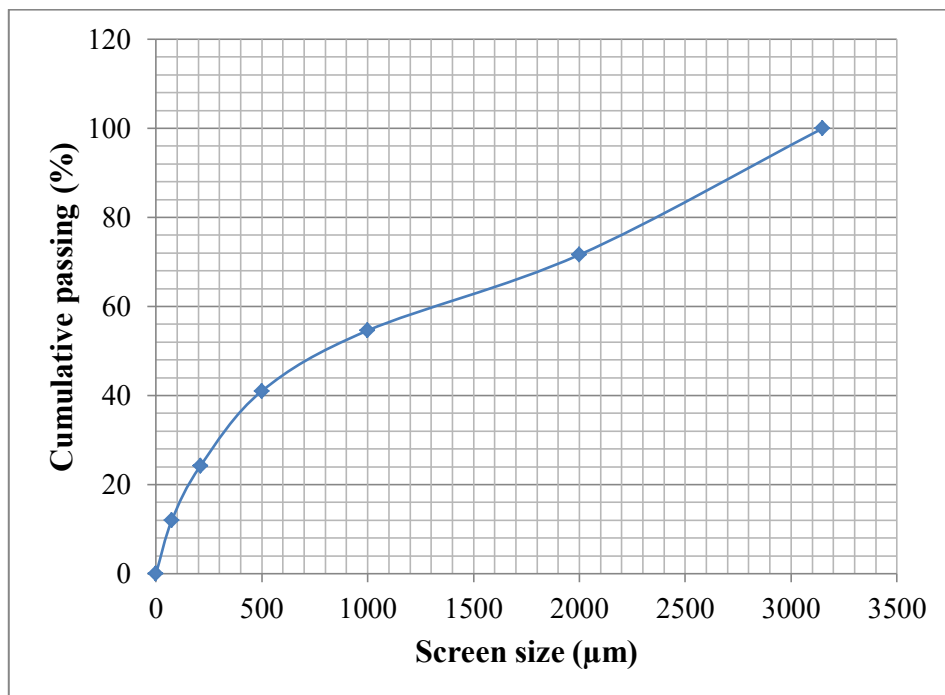


Fig. 5.3 Particle size analysis for LSHA feed sample

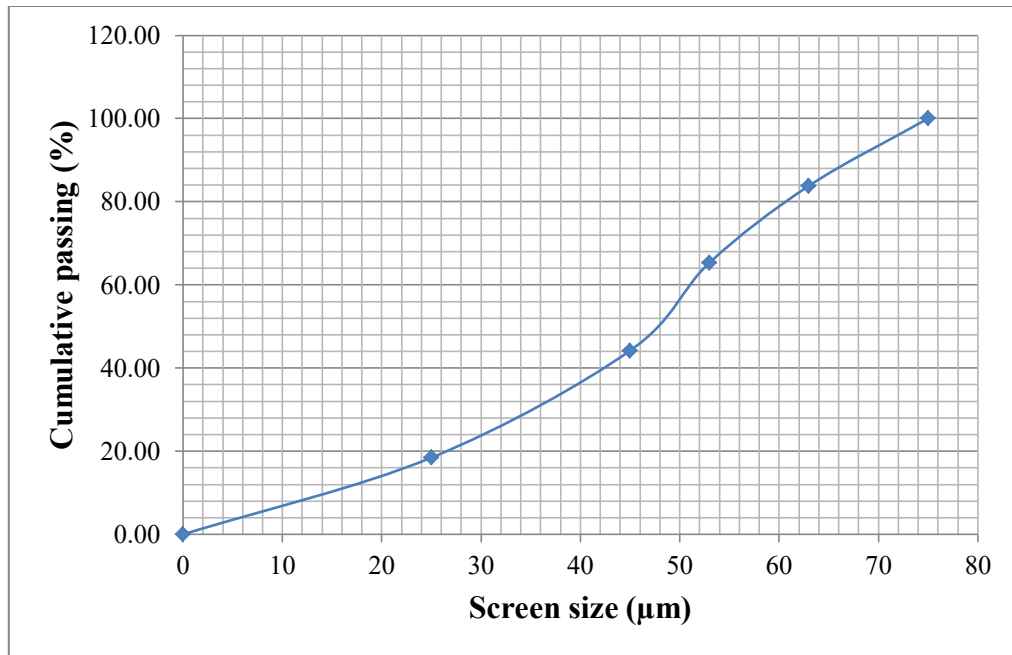


Fig. 5.4 Particle size analysis for LSHA iron ore product sample

5.1.3 Bond Work Index calculation for LSLA iron ore sample

The required under size fraction which is used to calculate BWI for LSLA iron ore sample is obtained by iterative process as shown in Table 5.5.

Required size below which particles are categorized as undersize particles	=75 μm
Weight of 700cc feed	=1390gm
Weight % of undersize fraction in the feed (700cc)	=16%
Circulating load of the mill	=250%
Weight of undersize fraction to be produced in an iteration	=397.14gm

Table 5.5 BWI iterative process for LSLA to get the undersized fraction

Sl. No	No. of Revolutions	Return feed (gm)	Fresh feed (gm)	Undersize in the feed (gm)	Undersize produced (gm)	Net under size produced (gm)	Grams per revolution (Gbp)	Next Revolution	Circulating load (%)
1	100	0.0	1390	222.4	450.0	227.6	2.276	187	209
2	187	940.0	450	72.0	371.0	299.0	1.599	211	275
3	211	1019.0	371	59.4	389.0	329.6	1.560	215	257
4	215	1001.0	389	62.2	397.0	334.8	1.559	214	250
5	214	993.0	397	63.5	428.0	364.5			

The total number of revolution required to produce 250% circulating load = 927
 Total time taken to produce 250% circulating load = 12 min
 Average grams per revolution produced =1.5 Gbp
 From the Fig. 5.5, the size through which 80% of the feed passes =2700 μm
 From the Fig. 5.6, the size through which 80% of the product passes =52 μm
 Bond Work Index for LSLA =8.5KWh/mt

Table 5.6 shows the LSLA iron ore sample particle sieve analysis of feed and product respectively. From Figs 5.5 and 5.6, 80% passing feed and product size is 2700 μm and 53 μm respectively. The calculated BWI for LSLA iron ore sample is 8 KWh/mt. The total time taken by LSHA iron ore sample in standard ball mill to produce 250% circulating load is 12 min.

Table 5.6 Sieve analysis of LSLA with respective to feed and product

Sieve analysis of the feed				Sieve analysis of final undersize fraction (product)			
screen size (μm)	wt retained (gm)	%retained	%passing	screen size (μm)	wt retained (gm)	%retained	%passing
3150	0	0	100	75	0.0	0.00	100.00
2000	240	48.00	52.00	63	50.0	10.37	89.63
1000	95	19.00	33.00	53	49.0	10.17	79.46
500	58	11.60	21.40	45	92.0	19.09	60.37
210	44	8.80	12.60	25	179	37.14	23.24
75	13	2.60	10.00	0	112	23.24	0.00

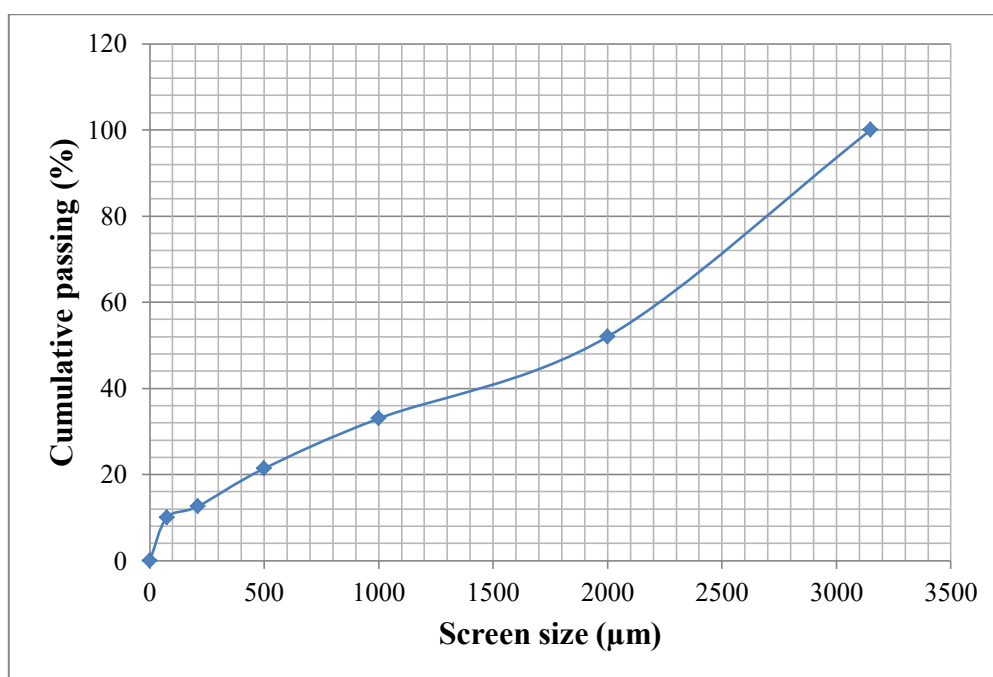


Fig. 5.5 Particle size analysis for LSLA iron ore feed sample

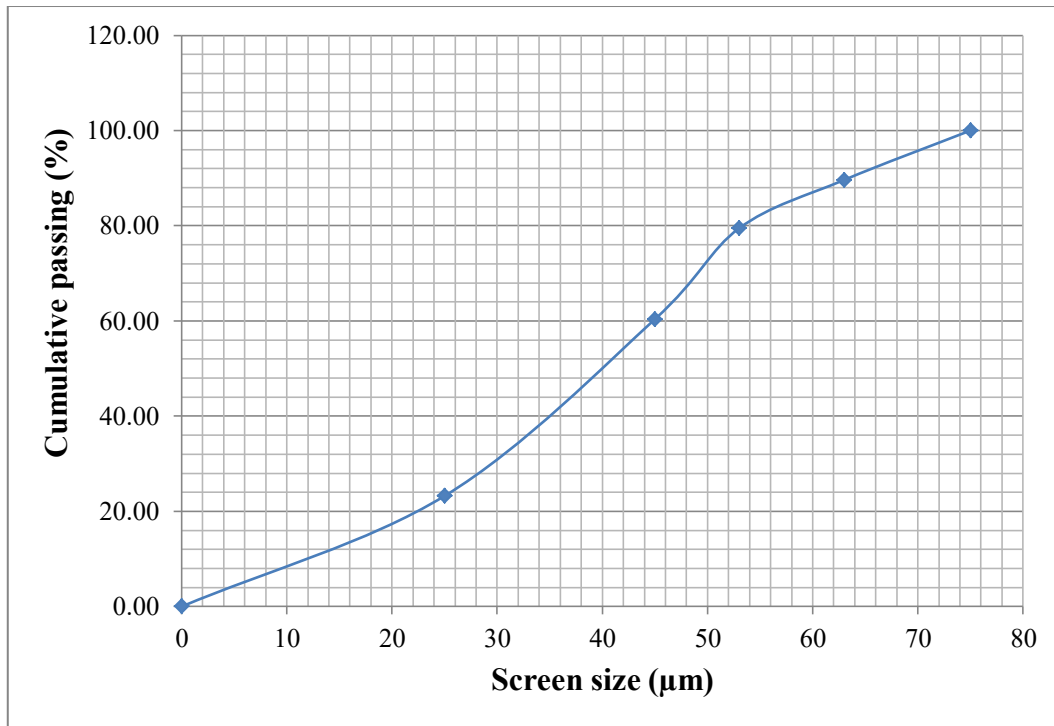


Fig. 5.6 Particle size analysis for LSLA Product sample

Table 5.7 Physical analysis of iron ore by using bond work index method

Sl. No.	Type of ore	F ₈₀ (μm)	P ₈₀ by BBM (μm)	BWI KWh/mt	Time for 250% CL(min)
1	HSHA	2500	70	12.8	16
2	LSHA	2350	60	10.2	13
3	LSLA	2700	52	8.5	12

Table 5.7 shows the BWI for all the samples and HSHA has maximum work index of 12.8 KWh/mt. Also, Table 5.7 shows the total retention time taken by iron ore samples to produce 250% circulating load in the BBM. The total retention time taken to produce 250% circulating load for HSHA is maximum when compared to all other samples. Further, the particle size analysis of ground samples reveal that the particle size fraction passing at P₈₀ in all the samples which is about 100% by weight (<150 μm) are finer size fractions. The product size fraction produced during grinding is undesirable to use in new hydro-squeeze ball mill for classification. Hence, to obtain

desire product particle size, all the iron ore samples are grounded in the laboratory ball mill with references to the BBM total retention time taken to produce 250% circulating load.

5.2 Grindability Studies Using Laboratory Ball Mill

The grinding studies in the LBM for all the iron ore samples were carried out based on the BBM total retention time taken for each representative sample to obtaining 80% passing of the desired particle size fraction of 150 μm . This study was conducted with an acceptable range of hematite liberation, and the results are analyzed and discussed in the following sections.

5.2.1 Effect of varying grinding time in laboratory ball mill on particle size distribution of HSHA

The HSHA feed sample used in BBM was also ground in the LBM. From Table 5.7, the total retention time taken for HSHA from BBM was 16 min. For HSHA the P80 passing percentage was 70 μm . But the desired passing percentage of 150 μm for a confined retention time was not achieved in the case of BBM. Hence, the BBM grinding behavior of HSHA was used in the LBM by considering retention times of 16 min. The HSHA iron ore feed sample used in the BBM was also ground in the LBM by reducing 2 min, 4 min and 6 min from the total retention time of 16 m. By trial and error method the grinding time of 14 min, 12 min, and 10 min was considered for HSHA. The sieve analysis of HSHA product at different grinding time is as shown in Table 5.8, 5.9 and 5.10. From the Fig. 5.7, P80 passing % was 96 μm , 130 μm , and 168 μm respectively. Finally the desired narrow particle size range for HSHA iron ore sample was achieved at 10 min with 80% passing product size of 168 μm .

Table 5.8 Sieve analysis of HSHA product after 14 (min) of grinding in LBM

Screen size (μm)	Wt. retained (gm)	%Retained	%Passing
180	0	0	100
150	40	9.7	90.3
75	73	17.7	72.6
45	140	33.9	38.7
25	90	21.8	16.9
0	70	16.9	0

Table 5.9 Sieve analysis of HSHA product after 12 (min) of grinding in LBM

Screen size (μm)	Wt. retained (gm)	%Retained	%Passing
180	0	0	100
150	73	14.6	85.4
75	85	17	68.4
45	79	15.8	52.6
25	134	26.8	25.8
0	129	25.8	0

Table 5.10 Sieve analysis of HSHA product after 10 (min) of grinding in LBM

Screen size (μm)	Wt. retained(gm)	%Retained	%Passing
180	0	0	100
150	136	27.2	72.8
75	96	19.2	53.6
45	79	15.8	37.8
25	90	18	19.8
0	99	19.8	0

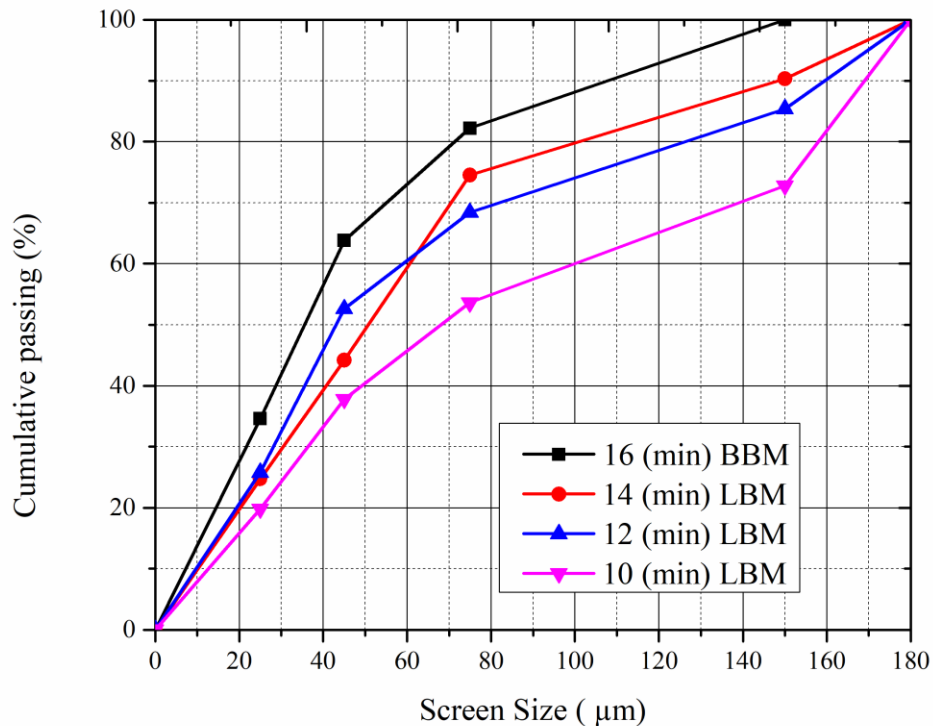


Fig. 5.7 Particle size analysis for HSHA Product sample

5.2.2 Effect of varying grinding time in laboratory ball mill for LSHA on particle size

The LSHA feed sample used in BBM was also ground in the LBM. From Table 5.7, the total retention time taken for LSHA from BBM was 13 min. For HSHA the P_{80} passing percentage was 60 µm. But the desired passing percentage of 150 µm for a confined retention time was not achieved in the case of BBM. Hence, the BBM grinding behavior of LSHA was used in the LBM by considering retention times of 13 min. The LSHA iron ore feed sample used in the BBM was also ground in the LBM by reducing 2 min, 4 min and 6 min from the total retention time of 13 min. By trial and error method the grinding time of 11 min, 9 min, and 7 min was considered for LSHA. The sieve analysis of LSHA product at different grinding time is as shown in Table 5.11, 5.12 and 5.13. From the Fig. 5.8, P_{80} passing % was 87 µm, 119 µm, and 152 µm respectively. Finally the desired narrow particle size range for LSHA iron ore sample was achieved at 7 min with 80% passing product size of 152 µm.

Table 5.11 Sieve analysis of LSHA product after 11 (min) of grinding in LBM

Screen size (μm)	Wt. retained(gm)	%Retained	%Passing
180	0	0	100
150	40	8.2	91.8
75	74	15.2	76.6
45	100	20.5	56.1
25	150	30.8	25.3
0	123	25.3	0

Table 5.12 Sieve analysis of LSHA product after 9 (min) of grinding in LBM

Screen size (μm)	Wt. retained (gm)	%Retained	%Passing
180	0	0	100
150	59	12.1	87.9
75	89	18.3	69.6
45	95	19.5	50.1
25	130	26.7	23.4
0	114	23.4	0

Table 5.13 Sieve analysis of LSHA product after 7 (min) of grinding in LBM

Screen size (μm)	Wt. retained (gm)	%Retained	%Passing
180	0	0	100
150	102	20.6	79.4
75	115	23.3	56.1
45	89	18	38.1
25	99	20	18
0	89	18	0

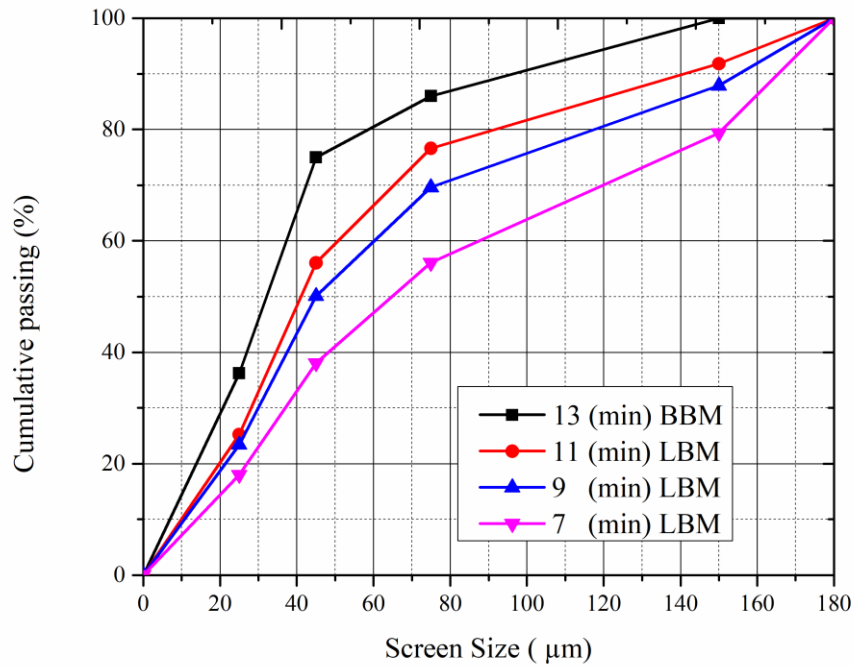


Fig. 5.8 Particle size analyses for LSHA Product sample

5.2.3 Effect of varying grinding time in laboratory ball mill for LSLA on particle size

The LSLA feed sample used in standard ball mill was also ground in the LBM by reducing 2min, 4min and 6 min from the 12 min total time taken to produce 250% circulating load during grinding as shown in Fig.5.9. The sieve analysis of LSLA product at different grinding time is as shown in Table 5.14, 5.15 and 5.16. The 80% passing product size achieved was 75 µm and 100 µm at grinding time 10 min and 8 min respectively. Finally the desired narrow particle size range with 80% passing product size of 140 µm was achieved at 6 min.

The LSLA feed sample used in BBM was also ground in the LBM .From Table 5.7, the total retention time taken for LSLA from BBM was 12 min. For LSLA the P_{80} passing percentage was 52 µm. But the desired passing percentage of 150 µm for a confined retention time was not achieved in the case of BBM. Hence, the BBM grinding behavior of LSLA was used in the LBM by considering retention times of 12 min. The LSLA iron ore feed sample used in the BBM was also ground in the LBM

by reducing 2 min, 4 min and 6 min from the total retention time of 12 m. By trial and error method the grinding time of 10 min, 8 min, and 6 min was considered for LSLA. The sieve analysis of LSLA product at different grinding time is as shown in Table 5.14, 5.15 and 5.16. From the Fig. 5.9, P₈₀ passing % was 75 µm, 100 µm, and 140 µm respectively. Finally the desired narrow particle size range for LSLA iron ore sample was achieved at 6 min with 80% passing product size of 140 µm.

Table 5.14 Sieve analysis of LSLA product after 10 (min) of grinding in LBM

Screen size (µm)	Wt. retained (gm)	%Retained	%Passing
180	0	0	100
150	102	20.6	79.4
75	115	23.3	56.1
45	89	18	38.1
25	99	20	18
0	89	18	0

Table 5.15 Sieve analysis of LSLA product after 8 (min) of grinding in LBM

Screen size (µm)	Wt. retained (gm)	%Retained	%Passing
180	0	0	100
150	59	11.9	88.1
75	65	13.2	74.9
45	100	20.2	54.7
25	126	25.5	29.1
0	144	29.1	0

Table 5.16 Sieve analysis of LSLA product after 6 (min) of grinding in LBM

Screen size (μm)	Wt. retained (gm)	%Retained	%Passing
180	0	0	100
150	78	16.4	83.6
75	89	18.7	64.9
45	93	19.5	45.4
25	111	23.3	22.1
0	105	22.1	0

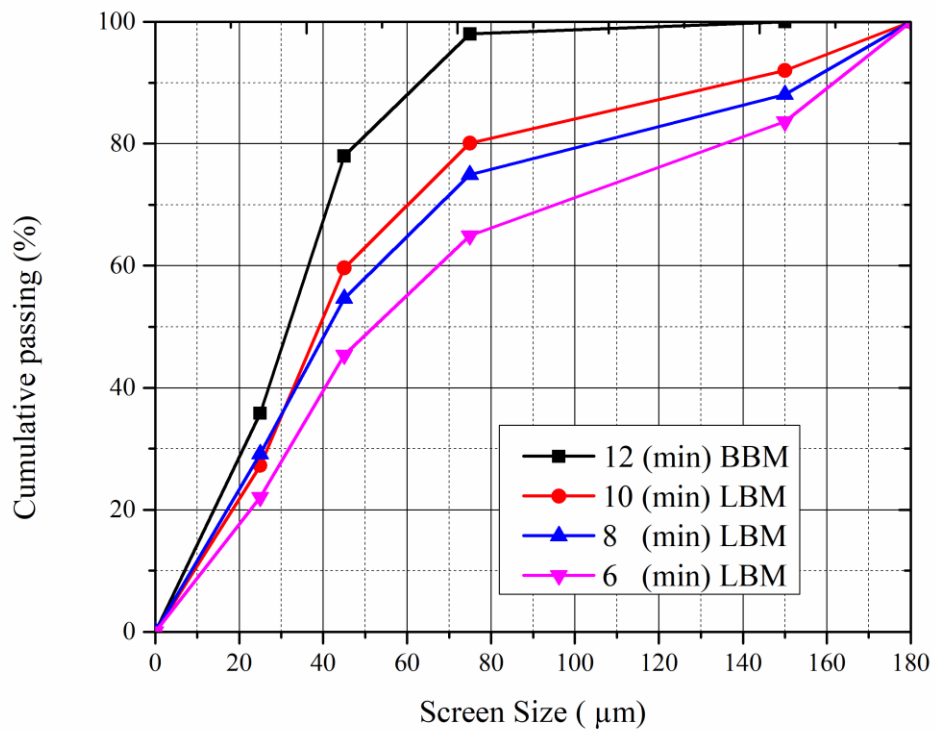


Fig. 5.9 Particle size analyses for LSLA Product sample

Table 5.17 Physical analysis of HSHA, LSHA and LSLA using Bond's Work Index Method

Sl. No.	Type of ore	F ₈₀ (μm)	P ₈₀ by BBM (μm)	BWI KWh/mt	Time for 250% Circulating load(min)	Percentage of Hematite Liberated
1	HSHA	2500	72	12.8	16	85
2	LSHA	2400	60	10.2	13	87
3	LSLA	2700	48	8.5	12	93

When compared with grinding parameters, it can be found that the higher the weight percentage of silica and alumina (SiO_2 is $>4.5\%$ and $\text{Al}_2\text{O}_3 > 3.5\%$), higher is the P₈₀ passing size of the grinding product (and therefore, the harder it is to grind). Also, lower the weight percentage of the silica and alumina (SiO_2 is $<4.5\%$ and $\text{Al}_2\text{O}_3 < 3.5\%$), lower is the P₈₀ passing size of the grinding product. This indicates that the presence of alumina and silica in the iron ore affects the grinding parameters of the ore. It is also clear that to obtain the desired percentage of P₈₀ passing particle size in HSHA takes high grinding time compared with LSHA and LSLA, since the percentage of alumina and silica percent in HSHA is high compared with LSHA and LSLA.

On comparing, the total retention time taken by each ore in the BBM is higher than the required grinding time of the ore to produce the desired PSD. The desired P₈₀ is obtained after reducing 6 min from the retention time taken by each ore in the BBM. This method of controlling the retention time of the ore may save energy consumption by the mills. Finally, the optimum desired P₈₀ passing (150 μm) percentage for HSHA, LSHA, and LSLA was 168 μm , 152 μm , and 140 μm , respectively, and is shown in Figures 5.7, 5.8, and 5.9 respectively.

5.3 Characterization Analysis of HSHA, LSHA, and LSLA Iron Ore Samples

The association of different phases present in the iron ore feed and product was quantified through optical microscopy and QEMSCAN, and the quantified mineral phases of samples are detailed analysed.

5.3.1 Mineralogical analysis of feed sample by optical microscopy

Figures 5.10, 5.11, and 5.12 illustrate the mineralogical analysis of the feed samples of HSHA, LSHA, and LSLA using an optical microscope. The analysis derived through optical microscopy was measured with a discontinuous method. Figure 5.10 and 5.11 represent HSHA and LSHA samples with a significant portion of hematite, and it are majorly distributed in spheroid form. In addition to this, some finer tubular structures of hematite are also observed in the optical microscopy. However, a major portion of HSHA is composed of Fe Ox-Al silicate interphase and goethite. The LSLA sample consists of major portions of hematite, and it is well-distributed in tubular and spheroid form, whereas LSHA samples include a minor part of limonite and kaolinite as shown in Fig.5.12. The gangue minerals in both LSHA and HSHA are majorly distributed in quartz form and other gangue mineral such as kaolinite and alumina are distributed separately from the quartz.

Where,

G-Goethite, H-Hematite, K-Kaolinite, A- Fe Ox-Al Silicate interface, Q-Quartz,
and L-limonite

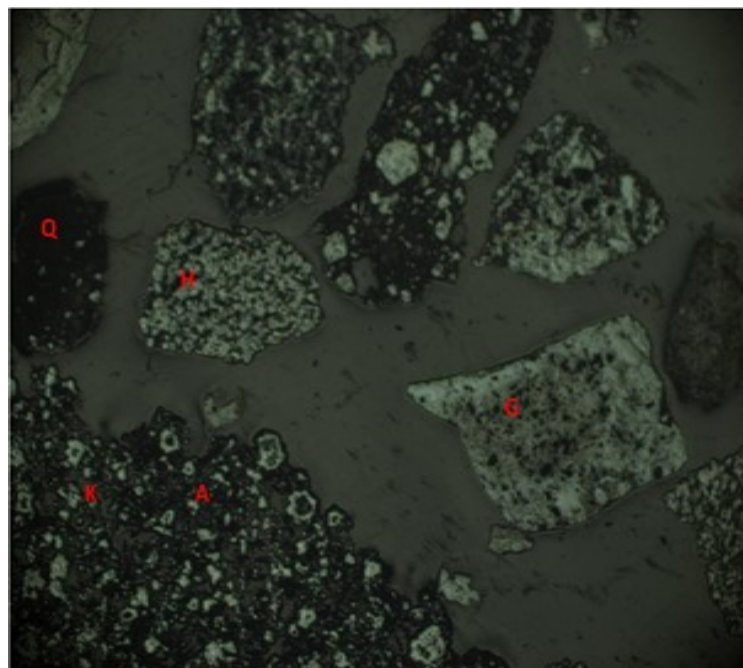


Fig. 5.10 Optical microscope photo for feed samples of HSHA

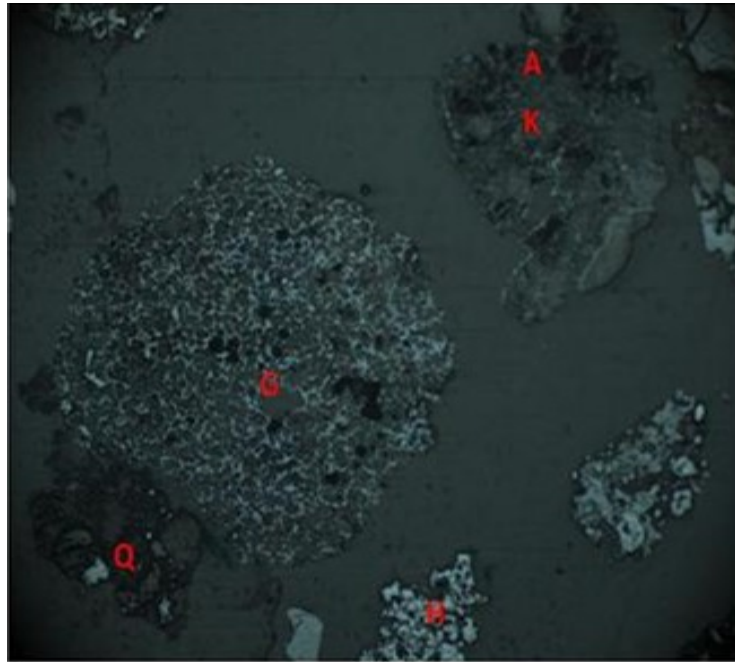


Fig. 5.11 Optical microscope photo for feed samples of LSHA

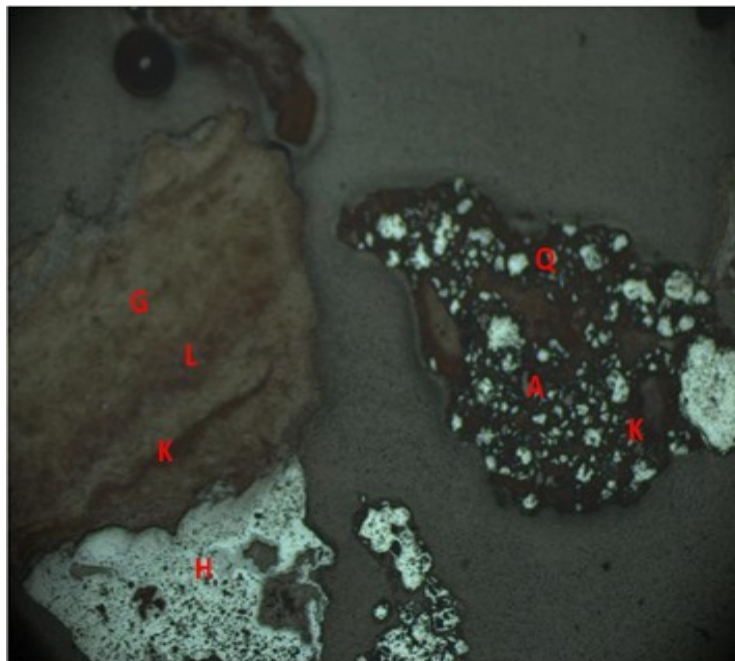


Fig. 5.12 Optical microscope photo for feed samples of LSLA

5.3.2 Mineralogical analysis of feed sample by QEMSCAN

Figures 5.13, 5.14, and 5.15 shows the mineralogical analysis of the feed samples of HSHA, LSHA, and LSLA using the QEMSCAN Quanta FEG 650. The

report obtained from the QEMSCAN was three major selections of field image, Bulk Mineral Analysis (BMA), and Particle Mineral Analysis (PMA). In the samples, HSHA and LSHA of Figures 5.13 and 5.14, respectively, the major quantified phase is hematite. From Fig. 5.15, in the LSLA sample, most of the quartz is present in bulk phase, which can be liberated easily by controlled grinding. In the samples of HSHA and LSHA, the quartz phase has a high proportion of hematite in composite form, and hence, the removal of gangue material from the hematite will require intensive grinding.

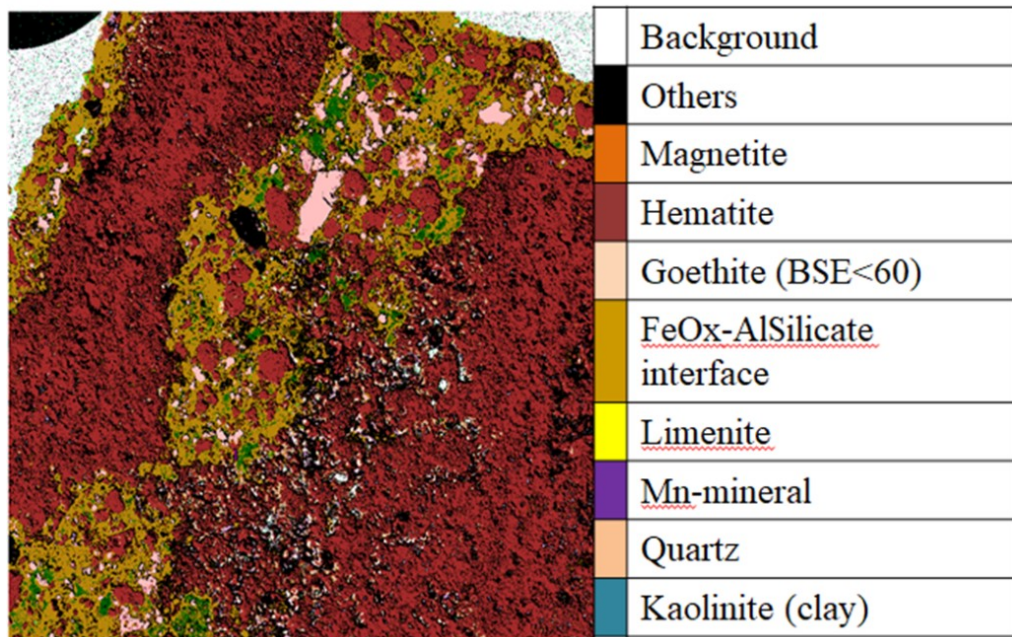


Fig. 5.13 QEMSCAN photos for feed samples of HSHA

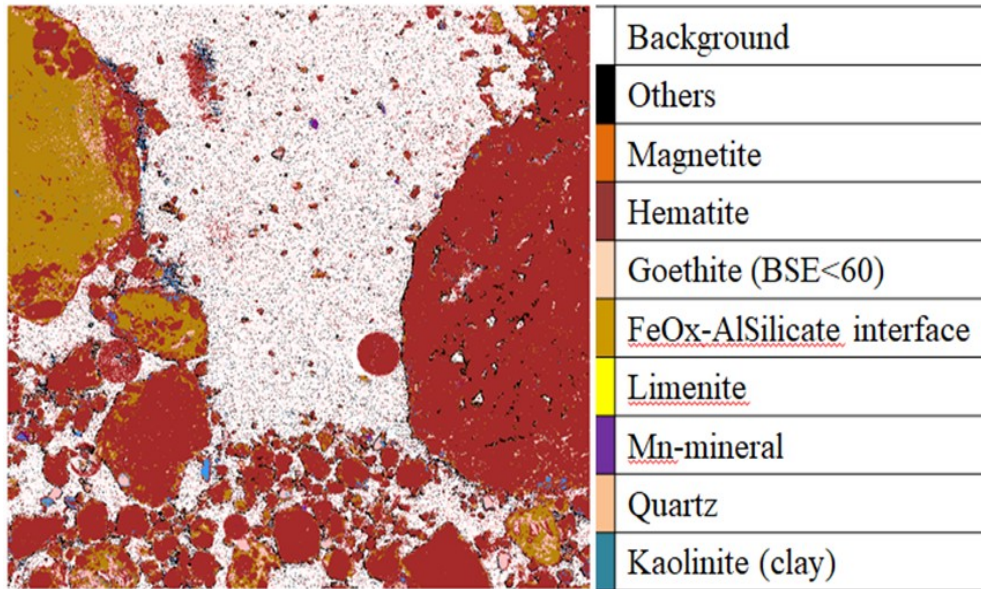


Fig. 5.14 QEMSCAN photos for feed samples of LSHA

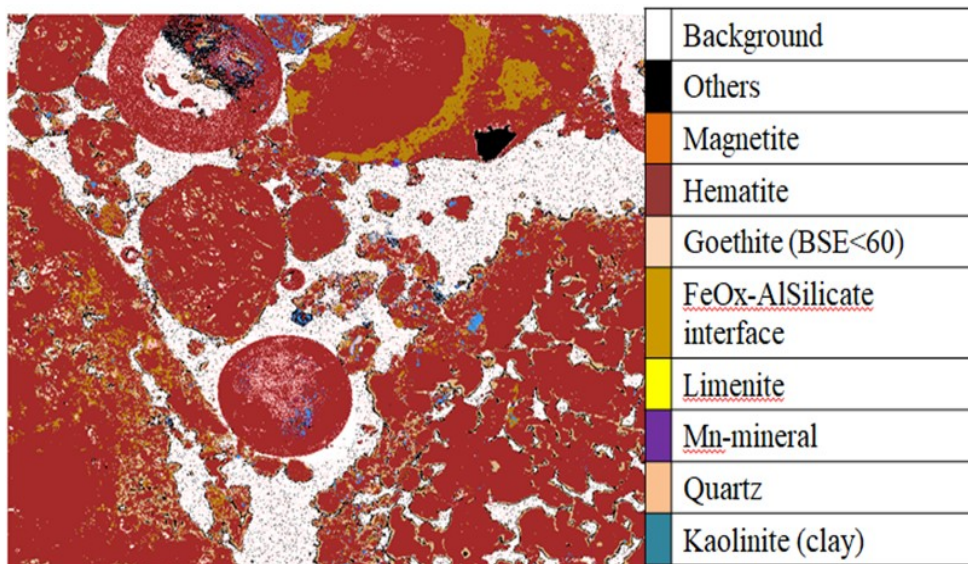


Fig. 5.15 QEMSCAN photos for feed samples of LSLA

5.3.3 Effect of retention time on the degree of hematite liberation in HSHA, LSHA, and LSLA

Figures, 5.16, 5.17, and 5.18 represent the optical microscope images of the liberated hematite of HSHA (retention time of 16 min), LSHA (retention time of 13 min), and LSLA (retention time of 12 min) obtained in the BBM. From Fig. 5.16, hematite liberation is high compared with LSHA and LSLA, as shown in Figs 5.17 and 5.18. This is because most of the hematite particles are in a liberated state in the feed

samples and most of the quartz present in bulk phase, which can be liberated easily from the locked hematite as shown in Figure 5.12 and 5.15. But in the case of HSHA and LSHA, the hematite particles were locked in quartz as finer tubular structures in feed samples and required intensive grinding to be liberated as shown in Figs 5.10, 5.11, 5.13, and 5.14. Hence, the liberation of hematite in the LSLA product sample is higher than the HSHA and LSHA product samples.

The optical microscope analysis suggested that for HSHA, LSHA, and LSLA, the hematite liberation was 85%, 87%, and 93%, respectively, as shown in Table 5.17. However, the liberation of hematite in all the cases was well within the acceptable range (>75%) and the P_{80} passing of all the three samples was very fine (72 μm , 60 μm , and 48 μm). The grinding results indicated that the desired P_{80} passing of 150 μm particles was not achieved for all the three types of the iron ore samples. Hence, all the three iron ore samples were further ground in the LBM based on the BBM retention time.

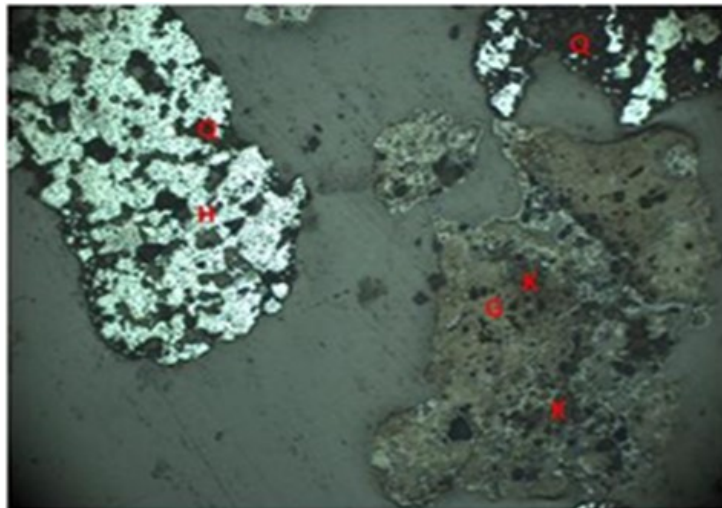


Fig. 5.16 Optical microscopy of HSHA sink sample of size -150 μm grounded for 16 min in BBM

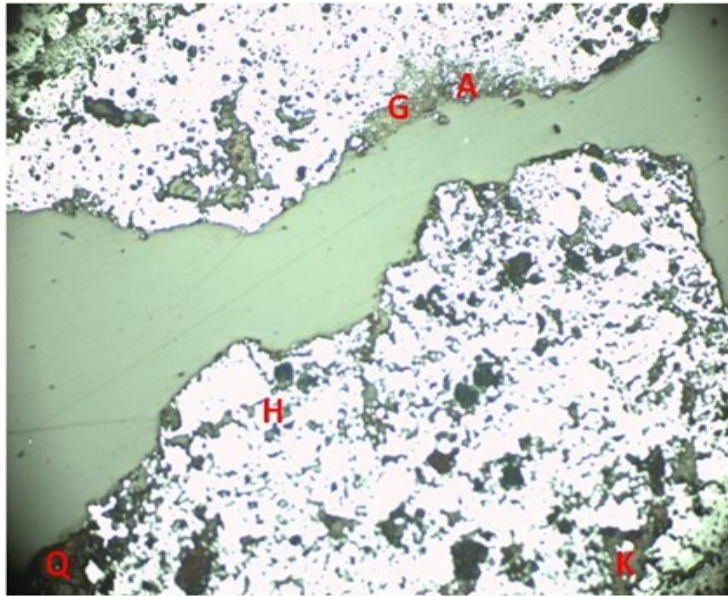


Fig. 5.17 Optical microscopy of LSHA sink sample of size $-150\ \mu\text{m}$ grounded for 13 min in BBM

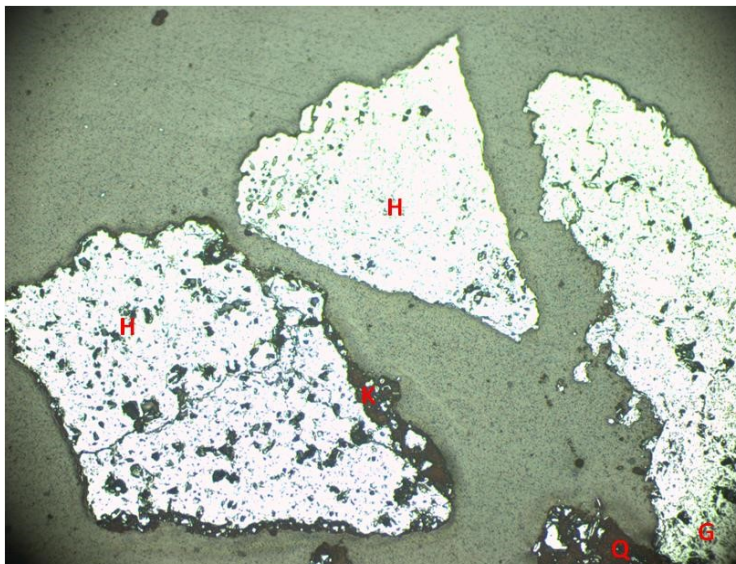


Fig. 5.18 Optical microscopy of LSLA sink sample of size $-150\ \mu\text{m}$ grounded for 12 min in BBM

Figures 5.19, 5.20, and 5.21 indicate that the optical microscope images of the liberated hematite of HSHA is 82% at 14 min, of LSHA is 84% at 11 min, and of LSLA is 90% at 10 min, respectively, using the LBM. The hematite liberation in all the cases was well within the acceptable range (hematite liberation $>75\%$). The P_{80}

passing for all three iron ore samples was 96 μm at 14 min, 87 μm at 11 min, and 75 μm at 10 min. Hence, the retention time of the LBM was further reduced to obtain the desirable P_{80} passing of 150 μm particles.

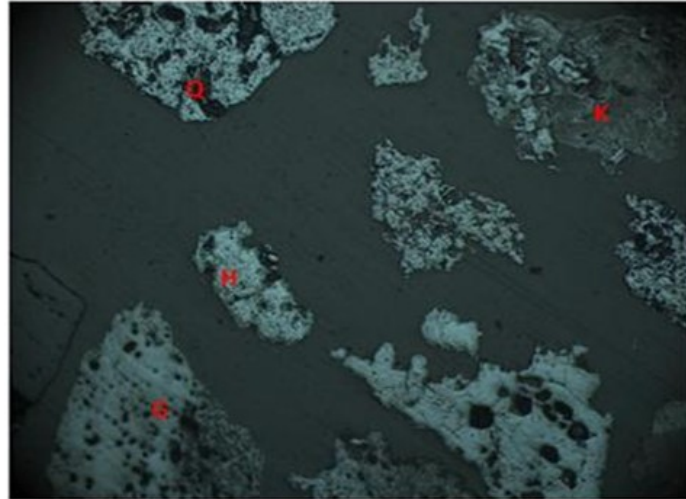


Fig.5.19 Optical microscopy of HSHA sink sample of size -150 μm grounded for 14 min in LBM

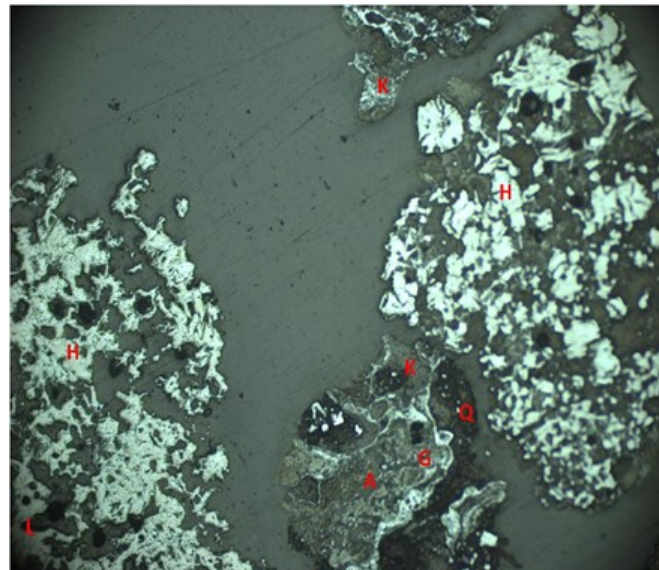


Fig.5.20 Optical microscopy of LSHA sink sample of size -150 μm grounded for 11 min in LBM

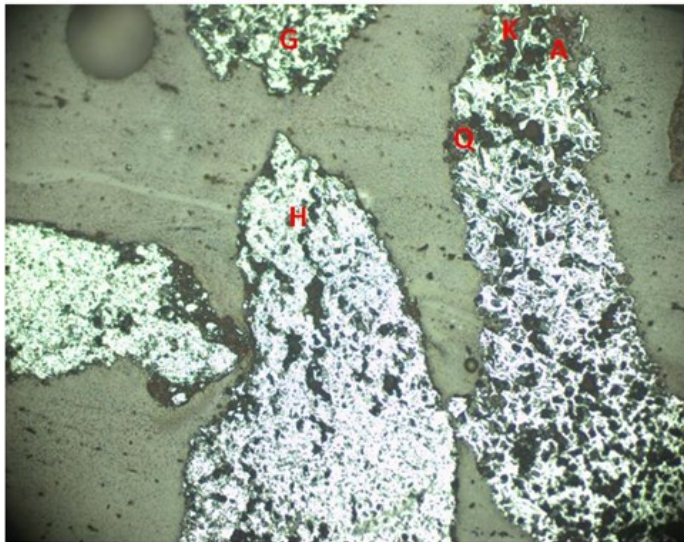


Fig.5.21 Optical microscopy of LSLA sink sample of size -150 μm grounded for 10 min in LBM

Figures 5.22, 5.23 and 5.24 indicate that the optical microscope images of the liberated hematite of HSHA is 79% at 12 min, of LSHA is 81.5% at 9 min, and of LSLA is 87% at 8 min, respectively, using the LBM. The hematite liberation in all the cases was well within the acceptable range (hematite liberation $>75\%$). The P_{80} passing for all the three iron ore samples was 130 μm at 12 min, 119 μm at 9 min, and 100 μm at 8 min. Hence, the retention time of the LBM was further reduced to obtain the desirable P_{80} passing of 150 μm particles.

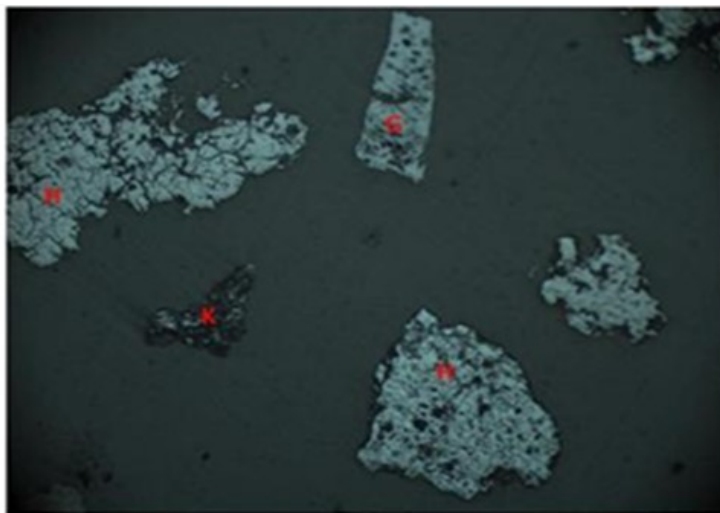


Fig. 5.22 Optical microscopy of HSHA sink sample of size -150 μm grounded for 12 min in LBM

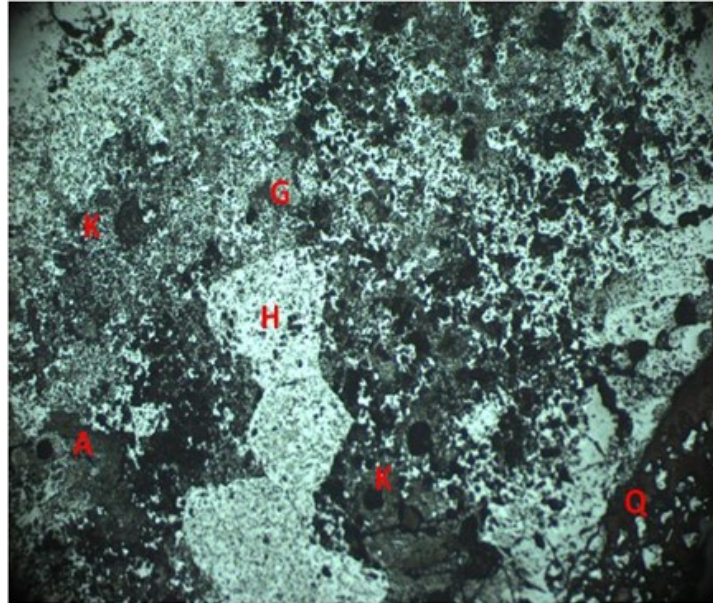


Fig. 5.23 Optical microscopy of LSHA sink sample of size $-150\ \mu\text{m}$ grounded for 9 min in LBM

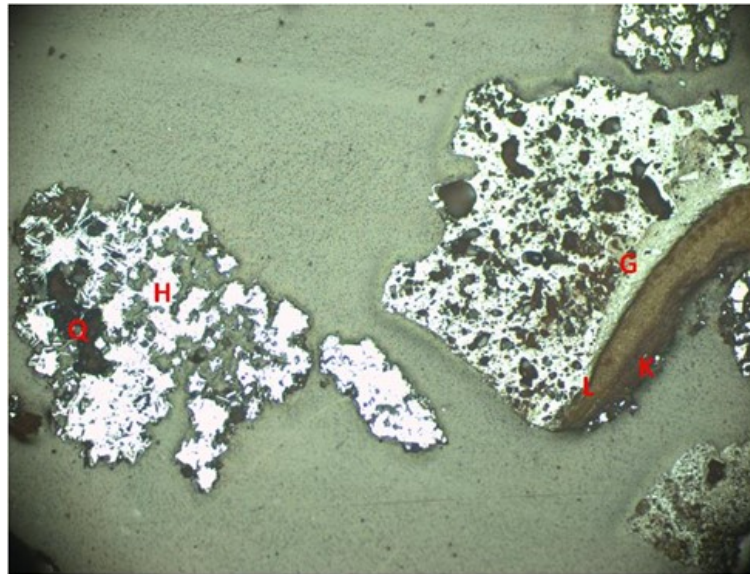


Fig. 5.24 Optical microscopy of LSLA sink sample of size $-150\ \mu\text{m}$ grounded for 8 min in LBM

Figures 5.25, 5.26, and 5.27 indicate that the optical microscope images of the liberated hematite of HSHA is 78% at 10 min, of LSHA is 80% at 7 min, and of LSLA is 85% at 6 min, respectively, using the LBM. The hematite liberation in all the cases was well within the acceptable range (hematite liberation $>75\%$). The P_{80}

passing for all three iron ore samples was within the desired P_{80} passing of $150\ \mu\text{m}$ particles.

On the other hand, Table 5.18 shows the influence of varying the grinding time on hematite liberation for HSHA, LSHA, and LSLA when ground in the LBM. The percentage of hematite liberated in all the three samples was less when ground for shorter duration. This may be due to the insufficiency of energy transmitted from the ball to the particles to crack the boundaries between the quartz and the oxidized iron minerals during the short period of grinding leading to the generation of a large number of “complex- type” locked-particles without hematite liberation (Hanumanthappa et al. 2020a). Due to this, mineral liberation, during short period grinding, is also very less. Also, with increasing milling time, the cracks between the quartz and the oxidized iron boundaries increase and propagate and gets fractured to liberate the hematite from the locked quartz. Hence, hematite liberation is higher with longer grinding period.

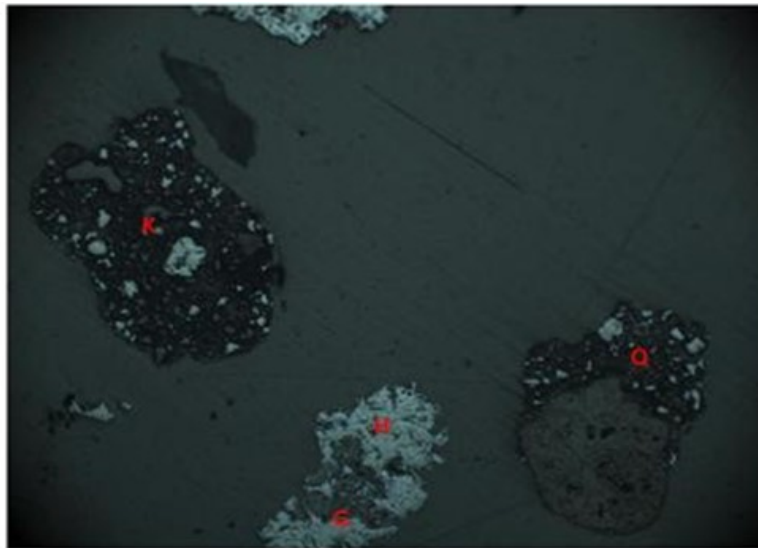


Fig. 5.25 Optical microscopy of HSHA sink sample of size $-150\ \mu\text{m}$ grounded for 10 min in LBM

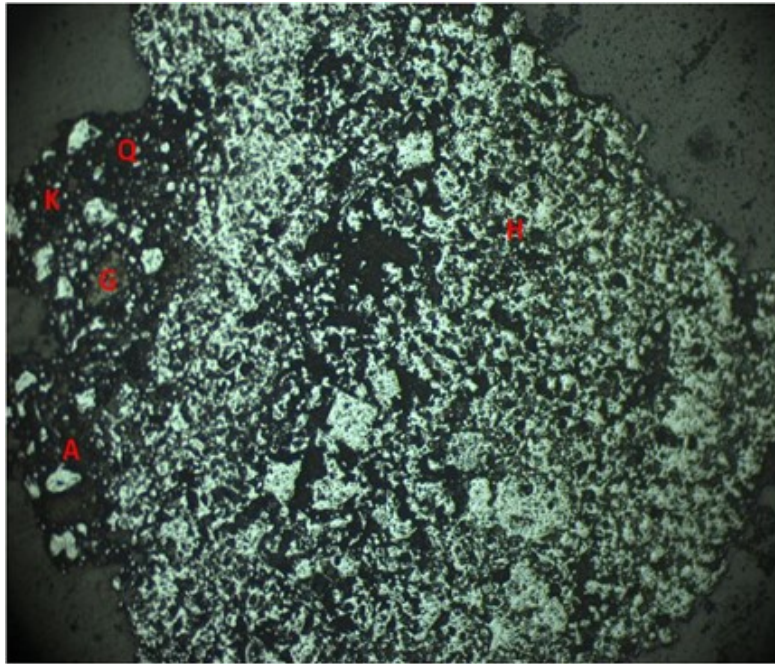


Fig. 5.26 Optical microscopy of LSHA sink sample of size $-150\ \mu\text{m}$ grounded for 7 min in LBM

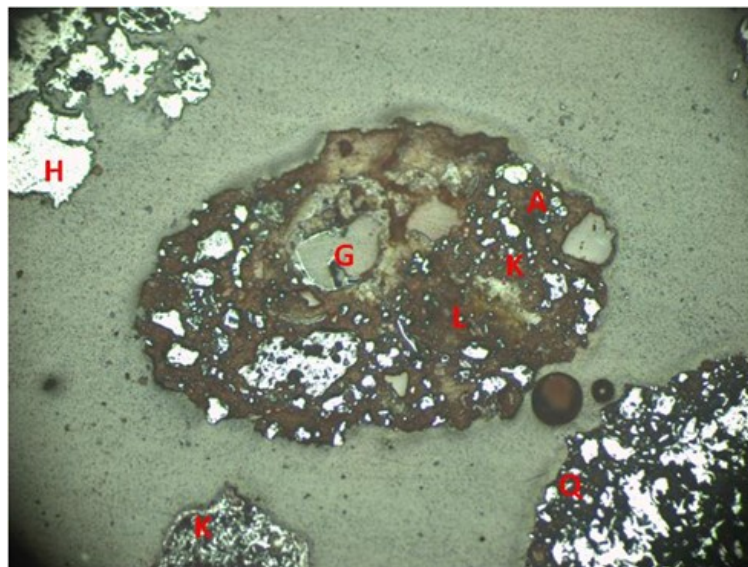


Fig. 5.27 Optical microscopy of LSLA sink sample of size $-150\ \mu\text{m}$ grounded for 6 min in LBM

Table 5.18 Physical analysis of HSHA, LSHA and LSLA using LBM

Sl. No.	Type of ore	F ₈₀ (μm)	P ₈₀ by LBM (μm)	Reduced grinding time in LBM (min)	Percentage of Hematite liberated
1	HSHA	2500	96	14	82
			130	12	79
			168	10	78
2	LSHA	2400	87	11	84
			119	9	81.5
			152	7	80
3	LSLA	2700	75	10	90
			100	8	87
			140	6	85

5.3.4 Comparing PSD, percentage of hematite liberation and total grinding time taken for HSHA, LSHA and LSLA iron ore samples in BBM and LBM

Figures 5.28 to 5.31 shows the PSD, percentage of hematite liberation, and total grinding time taken for HSHA, LSHA, and LSLA iron ore samples using BBM and LBM. The P₈₀ passing percentage for HSHA is higher compared with LSHA and LSLA. This is because the percentage of SiO₂ and Al₂O₃ is higher in the HSHA feed sample, which leads to higher grinding time compared with LSHA and LSLA. It can be observed that with increased grinding time, the P₈₀ passing percentage for all the three samples decreases, but the hematite liberation in all the three samples increases. This indicates that the grinding time is directly proportional to hematite liberation, and it is inversely proportional to the P₈₀ passing percentage.

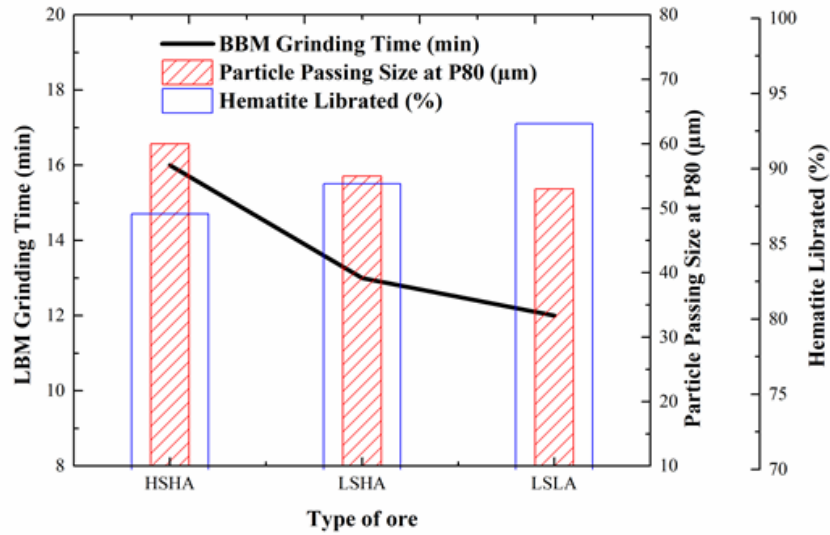


Fig.5.28 PSD, percentage of hematite liberation and total grinding time taken for HSHA, LSHA and LSLA iron ore samples in BBM

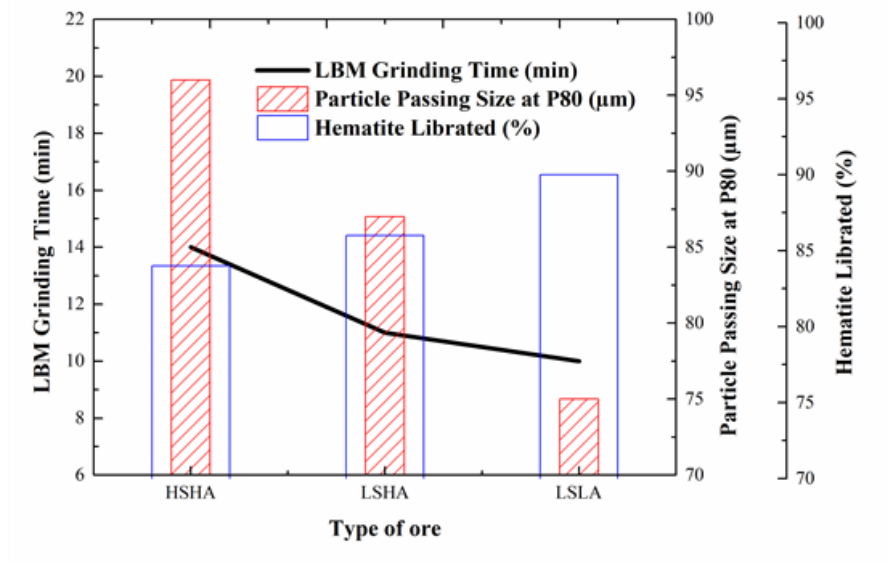


Fig. 5.29 PSD, percentage of hematite liberation and after reducing 2 min from total grinding time for HSHA, LSHA and LSLA iron ore samples in LBM

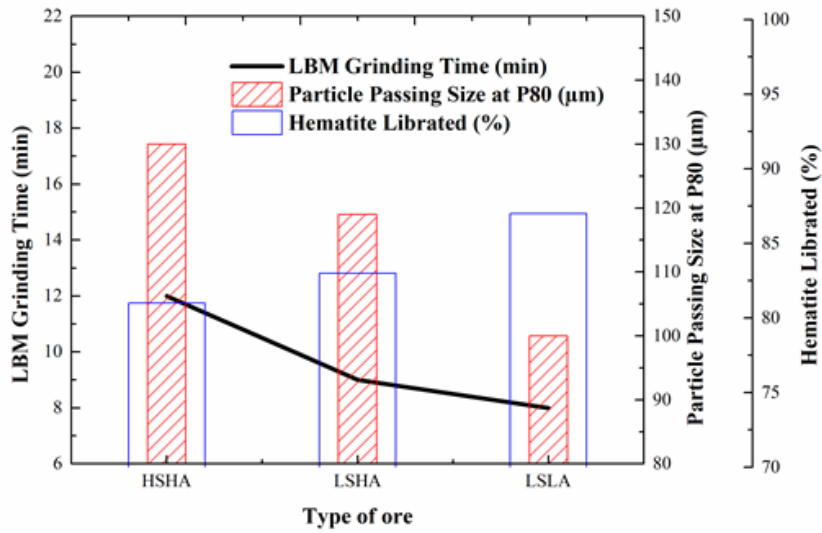


Fig. 5.30 PSD, percentage of hematite liberation and after reducing 4 min from total grinding time for HSHA, LSHA and LSLA iron ore samples in LBM

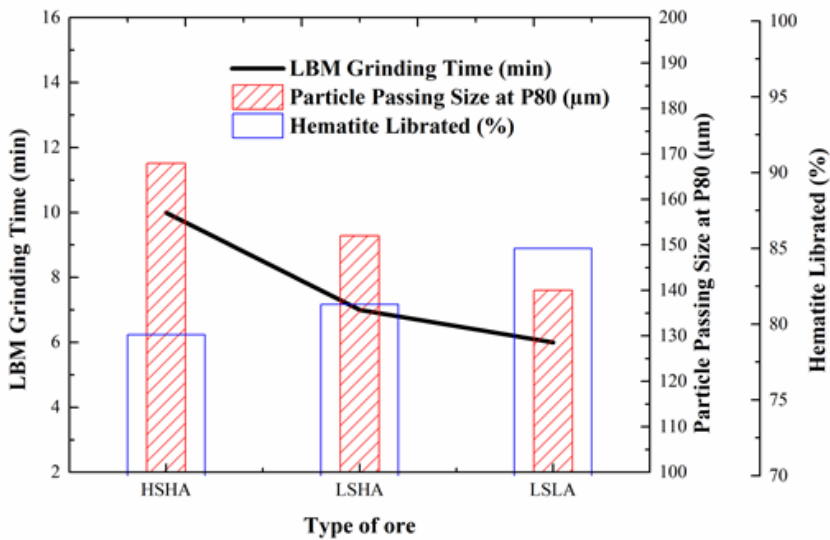


Fig. 5.31 PSD, percentage of hematite liberation and after reducing 6 min from total grinding time for HSHA, LSHA and LSLA iron ore samples in LBM

The present work was used to find the total grinding retention time of each ore in the mill. Based on the total retention time of each ore, the optimum grinding time for each ore was identified to obtain the desired P_{80} passing particle size with acceptable hematite liberation. The results obtained after considering the standard reference retention time to the LBM were improved with respect to the desired P_{80} passing

percentage of 150 μm and hematite liberation. Finally, the optimum grinding time required to achieve the desired P_{80} passing percentage of 150 μm with acceptable hematite liberation percentage (75%) for HSHA, LSHA, and LSLA was 10 min, 7 min, and 6 min, respectively. The new method followed in the present work to obtain the desired P_{80} passing percentage and hematite liberation from different types of iron ore can be implemented in a pellet plant to produce desire products for pellet feed making.

5.4 Characterization of Blend Iron Ore Samples

The association of different phases present in the iron ore blend feed and product was quantified through optical microscopy and QEMSCAN, and the quantified mineral phases of sample are detailed analysed.

5.4.1 OM and QEMSCAN analysis of blend feed sample with respect to liberation and locking of hematite

Figure 5.32 illustrates the mineralogical aspects of the iron ore feed blend. The percentage of sample LSLA was 50% of the total blends composition, where sample LSLA consists of hematite as the major iron-bearing mineral. Based on the blending percentage, it was clearly observed in blend that hematite is the major iron-bearing mineral. The blend also consists traces of goethite and limonite. Quartz is the major gangue bearing mineral in the blend, and most of the quartz is present in the bulk phase and can be easily liberated with controlled grinding.

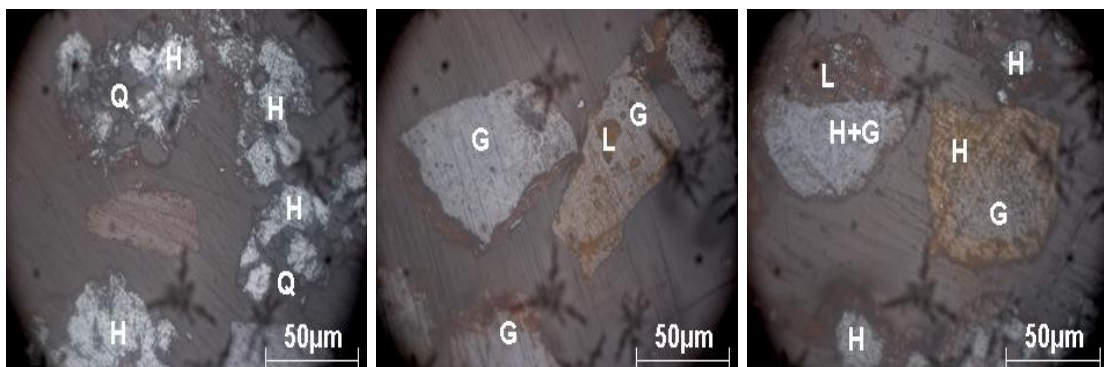


Fig. 5.32 OM images of the iron ore feed blend

The association of different phases present in the iron ore feed blend was quantified through QEMSCAN. Figures 5.33 and 5.34 illustrate the liberation and locking of

hematite in the blend feed sample in which the quartz phase is mainly associated with the FeOx-Alsilicate interphase, hematite, limonite, and kaolinite. The hematite phase does not have any association with the phase FeOx-Alsilicate interphase, but it has clear association with quartz and kaolinite as shown in Fig. 5.35. For the liberation of hematite from the iron ore feed blend sample, it was required to grind the sample for breaking the lock between the hematite and the quartz.

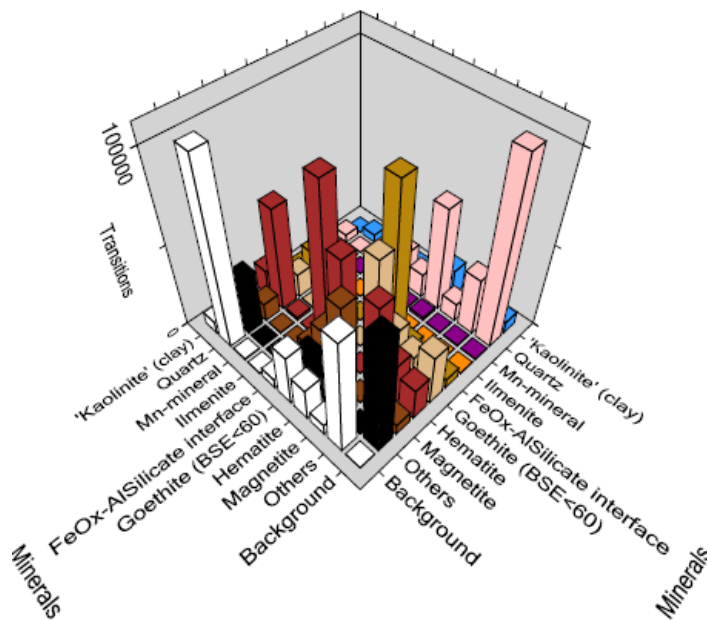


Fig. 5.33 3-dimensional view of liberation and locking of minerals in blend feed samples

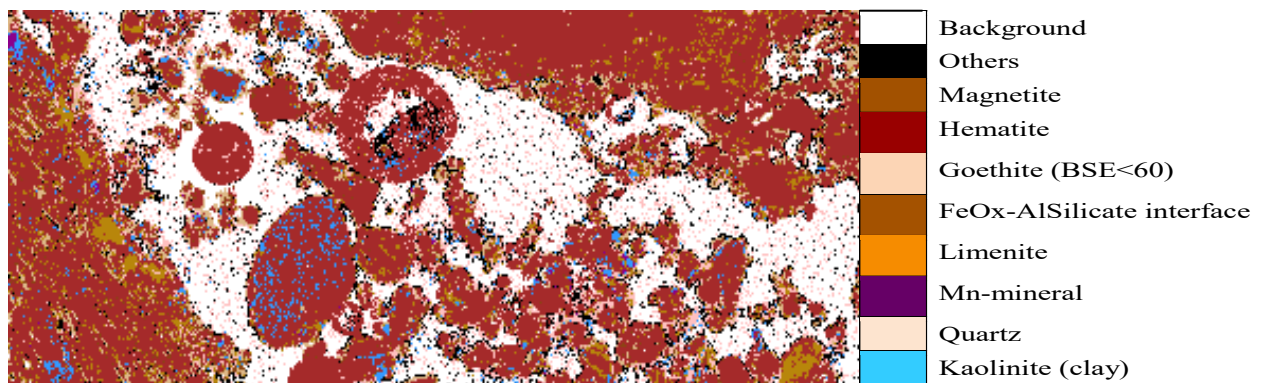


Fig. 5.34 Mineralogical analysis and phases in the blend feed sample by QEMSCAN

The specific gravity for the blend feed sample was determined by using the QEMSCAN. The specific gravity of the particles ranged between <5.10 and >4.75 in

which 82% was about hematite and about 18% was an association of quartz with hematite. From Fig. 5.35, it is evident that specific gravity range between <4.75 and >4 mainly consists of a major association of hematite with quartz interphase and kaolinite. For specific gravity <4 , it may consist of gangue particles.

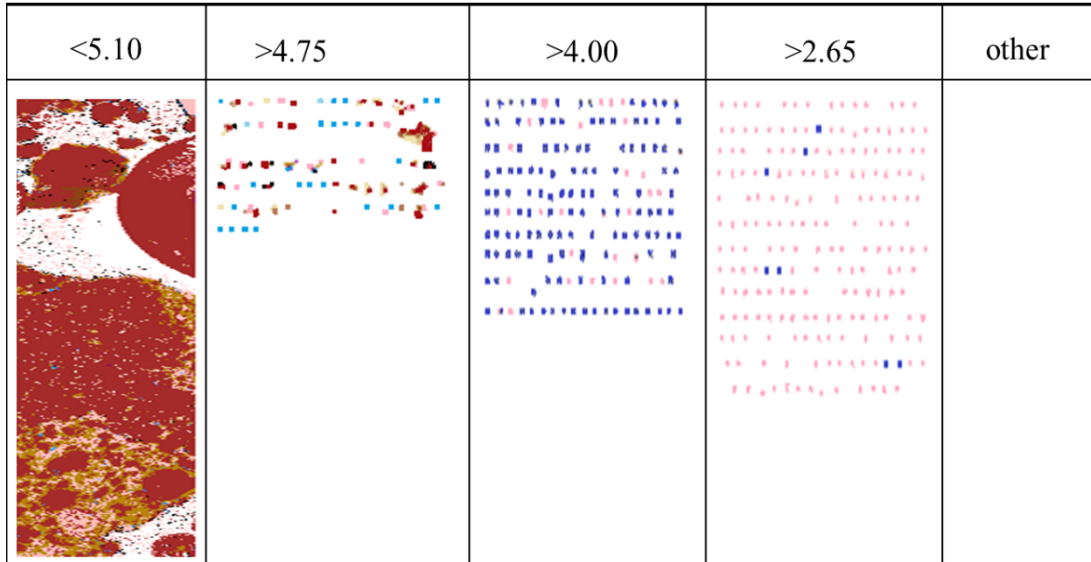


Fig. 5.35 Specific gravity classification analysis of blend feed sample by QEMSCAN

5.4.2 Grinding of blend sample in the BBM and LBM

The experimental results show that the blend has BWI of 10 KWh/t and TRT of 13 min. From Figs 5.29 to 5.31, the passing particle size at P_{80} for the HSHA, LSHA, and LSLA is very fine and not suitable for pellet making. So, for producing the desired particle size fraction a blend iron ore sample is prepared from HSHA, LSHA, and LSLA iron ore sample.

The quality of comminution is primarily determined by particle size analysis. Figure 5.36 presents the particle size analysis for the blend sample, which was ground for 11, 9, and 7 min in the LBM. From Fig. 5.36, it is clear that the grinding time of 11, 9, and 7 min of size fraction of 85, 120, and 148 μm , respectively, enabled to achieve 80% passing of particles. The grinding results in the LBM showed that with reduced grinding time, 80% passing of particles size increased. This may be because decreasing the milling time decreased the force acting on the ore leading to less grinding of the ore.

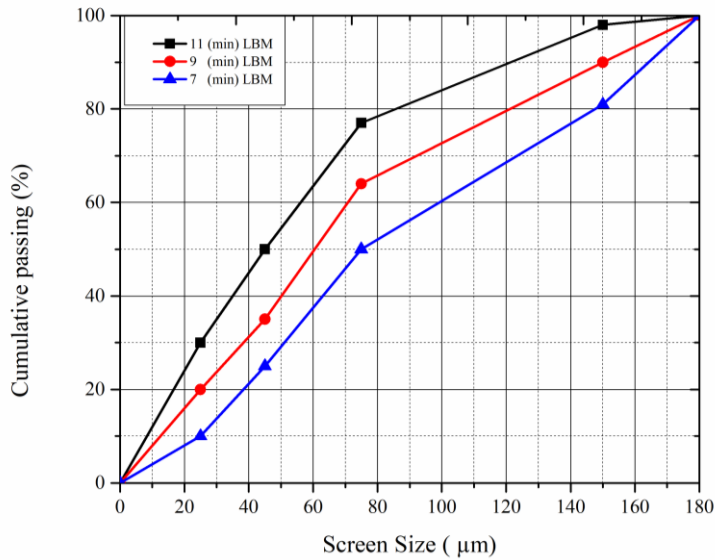


Fig. 5.36 Particle size analysis for blend sample ground in the LBM

5.4.3 Particle size analyses in OM for blend Product sample grounded in LBM at different grinding time

Figures 5.37, 5.38, 5.39 and Table 5.19 show particle size analyses in the OM for blend product sample grounded in the LBM at grinding times of 11, 9, and 7 min. Figure 5.37 shows that at grinding time of 11 min, the blended product is composed of very fine particles with approximate average size fraction less than 85 µm when compared with Figs 5.38 and 5.39. In addition, Fig. 5.39 shows that maximum particles of the blend product are coarse of approximate average size fraction of 130 µm. The OM analysis also indicates that with reduced grinding time of the mill, the particle size of the ground product increased as shown by the grey-white regions in Fig.5.39. However, the degree of hematite liberation from the locked-particles is not clear; therefore, additional study is required.

From Table 5.20, it can be observed that at grinding time of 13 to 9 min, about 33-42% of particle size fraction is less than -10 µm. The particle size analysis represents that grinding above 9 min produces excess fine particles (-10 µm). The presence of this excess fine (>30%) particles is not suitable for pellet making. But, at grinding time 7 min, about 76% of the ground product consisting of narrow size particles lie in the range of -150 to +10 µm size. Moreover, at grinding time 7 min, about 17% fine

particle size fraction of the total product is less than $-10\ \mu\text{m}$, and the weight percentage of the fine particles produced is in the acceptable range ($<30\%$) for pellet making (Hanumanthappa et al. 2020b).

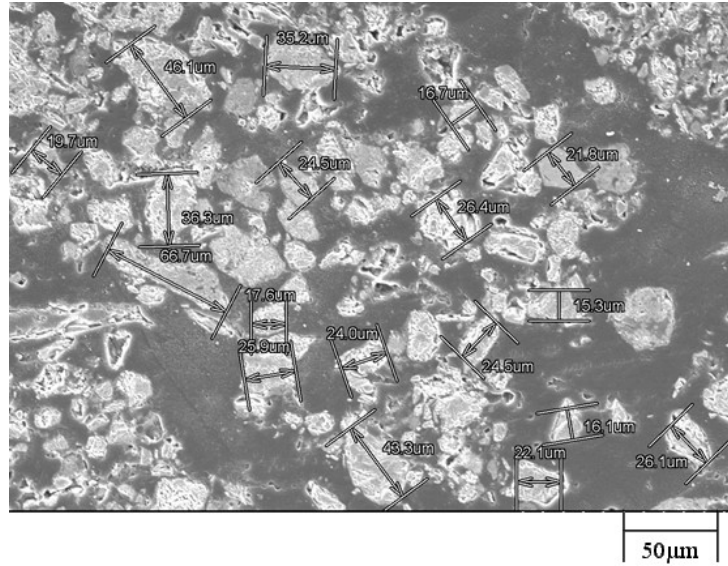


Fig. 5.37 Particle size analyses in OM for blend Product sample grounded in LBM at 11 min grinding time

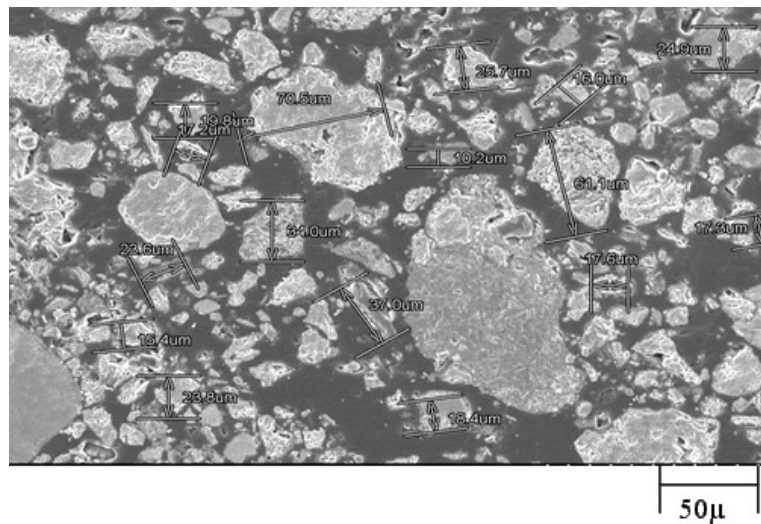


Fig. 5.38 Particle size analyses in OM for blend Product sample grounded in LBM at 9 min grinding time

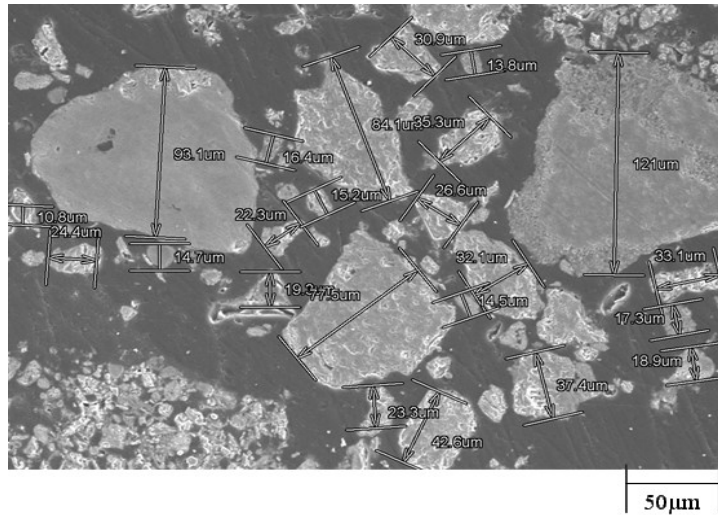


Fig. 5.39 Particle size analyses in OM for blend Product sample grounded in LBM at 7 min grinding time

Table 5.19 Physical properties of iron ore blend by using LBM

Sl. No.	Type of ore	P ₈₀ by LBM (µm)	Reduced grinding time in LBM (min)	Hematite Liberated Percentage (%)
1	Blend	85	11	79
		120	9	74
		148	7	70

Table 5.20 Weight percentage of narrow blend particle size fraction analysis of feed and product obtained in BBM and LBM

Type of sample	Type of ball mill	Total grinding time (min)	Wt.% of narrow band particle size fraction analysis (%)		
			+150 (µm)	-150/+10 (µm)	-10 (µm)
Feed analysis of blend			70	19	11
Product analysis of blend	BBM	13	0	45	55
	LBM	11	0	58	42
		7	7	67	33
			76	17	

5.4.4 Sink and float test for iron ore blend with varied grinding time

The sink and float was conducted to study the liberation of valuables from gangue particles by using a separating liquid having specific gravity of 3.3 g/cm^3 . Tests were conducted for the iron ore blend feed sample, and for products obtained at different grinding times. For this analysis, -3 mm feed blend was selected and the final product obtained at each varied grinding time was used. The results are shown in Table 5.21. From Fig. 5.40, it can be observed that, in feed sample float consist of less free alumina and silica is observed compared with ground iron ore blend. The feed float consists of 32.74% Fe. This indicates that few liberated small hematite particles are associated with the gangue particles. In the case of increasing grinding time, the ground sample float consists of increased free alumina or silica, and the alumina is increased from 18.33% to 28.5% and silica is increased from 30.48% to 44.43%. This indicates that with increasing grinding time, the gangue particles are liberated from the hematite. From Fig. 5.41, it can also be observed that in the sink with increasing grinding time, the Fe value increases from 54.28% to 61.16 %. The sink results clearly indicate that with increasing grinding time, the locked hematite in the gangue particles gets liberated. The results also show that at grinding time of 11 min, maximum grade is recorded compared with 9 min and 7 min grinding time, and the yield decreases as the grinding time increases.

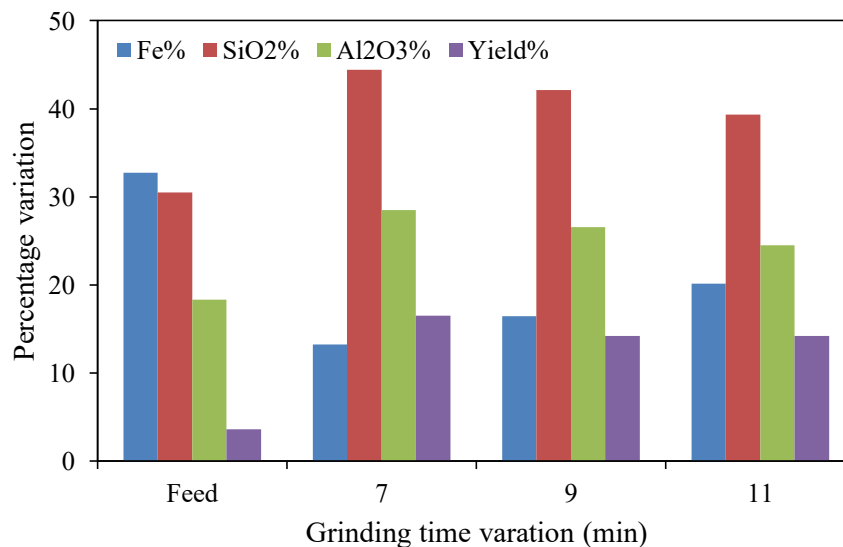


Fig. 5.40 Float analysis of iron ore blend with varied grinding time

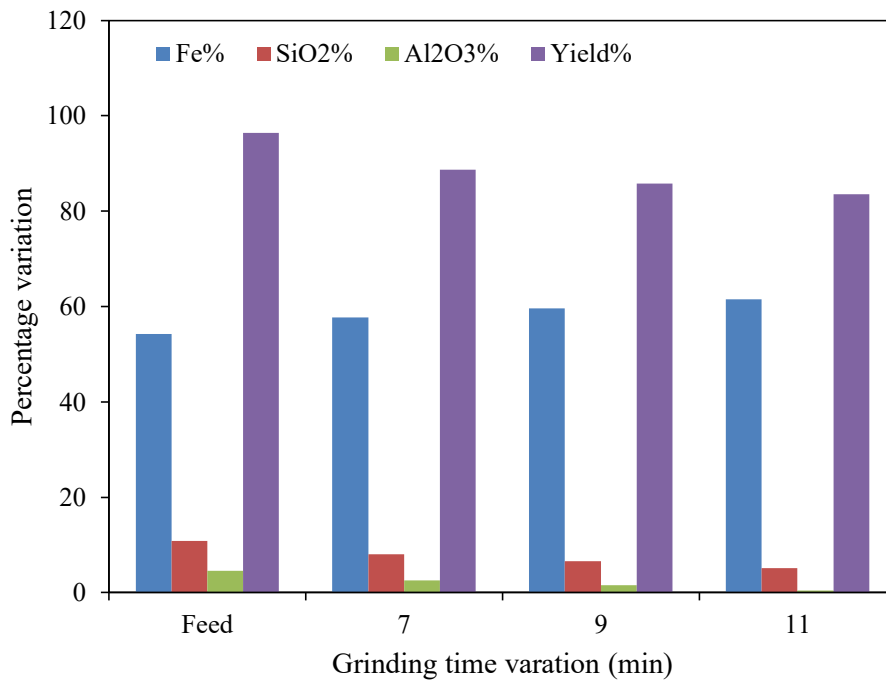


Fig. 5.41 Sink analysis of iron ore blend with varied grinding time

Table 5.21 Sink and float analysis for iron ore blend

Grinding Time (min)	Product	Fe (%)	SiO ₂ (%)	Al ₂ O ₃ (%)	Yield (%)
Feed Blend	Sink	54.28	10.89	4.61	96.4
	Float	32.74	30.48	18.33	3.6
11	Sink	61.46	5.11	0.48	83.5
	Float	13.2	44.43	28.5	16.5
9	Sink	59.64	6.55	1.55	85.8
	Float	16.41	42.14	26.58	14.2
7	Sink	57.75	8.06	2.62	88.69
	Float	20.14	39.36	24.52	14.2

5.4.5 Liberation analysis of blend product samples ground in LBM for different grinding times

For pellet making, the present practice is to obtain the desired particle size with acceptable hematite liberation at the grinding stage itself. Liberation in the ball milling refers to the mechanical reduction of rocks into valuable liberated particles. A

single particle is said to liberate from a mineral grain only when the particle size geometry is smaller than the mineral grain. In iron ore, the hematite phases may vary from ore- to- ore or within the ore body and the grinding of such ore leads to too high or too low liberation of hematite. Hence, it is very important to verify the degree of hematite liberation periodically during grinding.

Figure 5.42 and Table 5.21 show the OM results of the liberated hematite blend sink sample ground for 11, 9, and 7 min in the LBM. The degree of liberation in the iron ore sample was determined by using Equations (10) and (11). Figure 5.42(a) shows that at grinding time of 11 min, the blended product has maximum hematite liberation of 79% compared with hematite liberation obtained at grinding times of 9 and 7 min as shown in Figure 5.42(b) and (c). This may be due to; the hematite phase does not have any association with the phase FeOx-Alsilicate interphase as shown in Fig. 5.33, but has a clear association with quartz and kaolinite. As the grinding time increases, the fragmentation increases between the hematite phase and the gangue. The results clearly indicate increasing grinding time increases the reduction of the particles, which ultimately leads to increased liberation of hematite from quartz and kaolinite. Hence, with increasing grinding time up to a certain limit, the hematite liberation may increase.

Figure 5.42(c) shows that at grinding time of 7 min, the blend product has hematite liberation of 70%. For pellet making, the hematite liberation should be equal or greater than 70% (Umadevi et al. 2013). In the present study, the desired hematite liberation was achieved in 7 min grinding time compared with 11 min grinding time. The grinding results suggest that about 4 min grinding time can be reduced by using the new approach to obtain the desired hematite liberation, and it will also help avoid over grinding and minimize the energy required for grinding. Therefore, 7 min grinding time is the minimum grinding time required for a sufficient amount of hematite liberation from the iron ore blend.

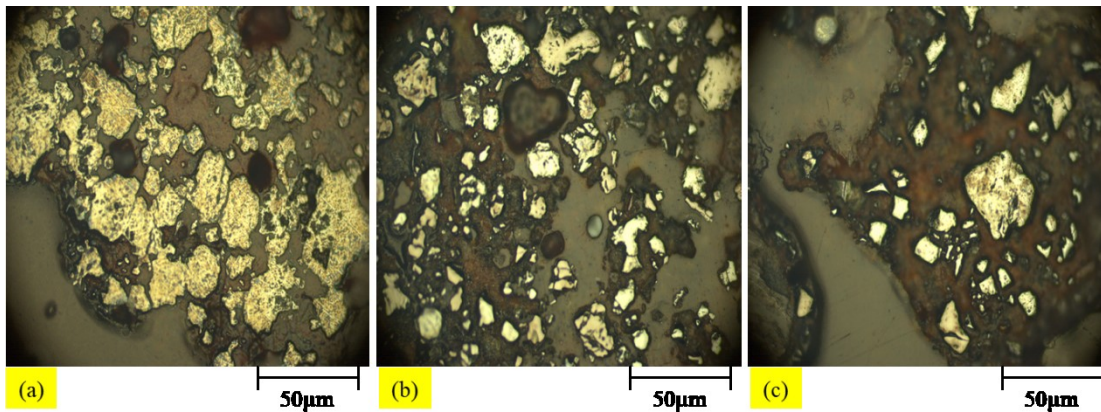


Fig. 5.42 Liberation analysis in OM of blend sink sample grounded in LBM at grinding time - (a) 11 min, (b) 9 min, and (c) 7 min

5.4.6 Variation of hematite liberation and PSD with respect to grinding time for iron ore blend product

Figure 5.43 shows the variation of hematite liberation and PSD with respect to grinding time for iron ore blends ground in the BBM and LBM. The results represent that increased grinding time increases the fines of the particle size with corresponding increase in hematite liberation. From Fig. 5.43, at grinding times 11 min and 9 min, 80% passing product particle size have finer size fraction, and the weight percentage of fine particles ($-10\ \mu\text{m}$) produced in the ground product exceeded the desired particle size range (i.e., $-10\ \mu\text{m}$ particles should be less than 30% weight percentage in the ground product as given in Table 5.21). If the ground product consists of more than 30% weight percentage of fine particles ($-10\ \mu\text{m}$), then the obtained ground product is not suitable for pellet making (Umadevi et al. 2013). Hence, grinding the iron ore blend at 11 min and 9 min is not desirable, since the amount of energy supplied at these two grinding times is more than the required energy for desired particle size reduction and leads to increased energy consumption by the ball mill, which is not economical.

In addition, from Fig. 5.43, at grinding time of 7 min, 80% passing product size is $148\ \mu\text{m}$ with 70% of hematite liberation, and the weight percentage of the desired particles ($-150/+10\ \mu\text{m}$) and fine particles ($-10\ \mu\text{m}$) produced are in the acceptable range. The results clearly show that for any ore blend, it is important to know the ore

RT before grinding in the ball mill to obtain the desired particle size fraction with acceptable hematite liberation. The new approach can be used in plant scale mill for iron ore blend grinding, and it also avoids over grinding compared with conventional methods of grinding.

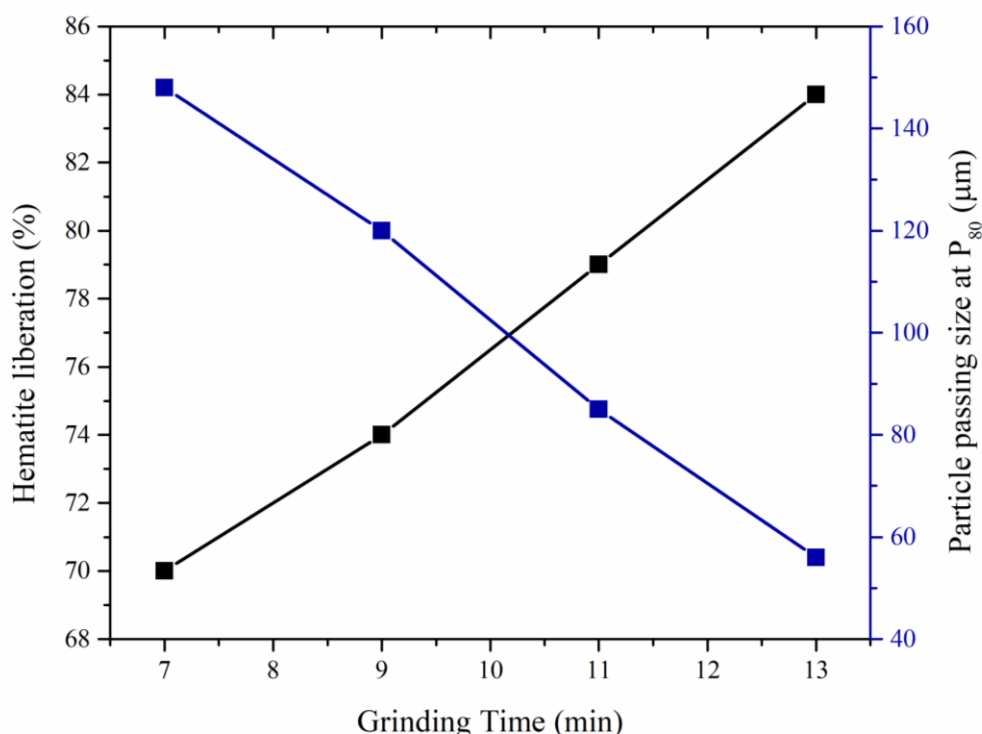


Fig. 5.43 Variation of hematite liberation and PSD with respect to grinding time for iron ore blend product

From dry grinding and characterization analysis of iron ore and its blend, to produce desired PSD from dry grinding was varying for each sample. The OM analysis of iron ores feed samples showed different mineralogical aspects. The results from BBM for HSHA, LSHA, LSLA and blend iron ore samples indicated that 80% passing product particle size varies from one another, and each iron ore sample takes different retention time for 250% circulating load in the BBM. The BBM and OM analysis showed that feeding the mill a single type of iron ore is not preferable due to significant variation in the physical composition of each ore.

The each iron ore samples takes different RT when grounded in the BBM for 250% circulating load with different 80% passing particle size. Also, the HSHA, LSHA,

LSLA and blend iron ore sample obtained from the BBM composed of a higher percentage of fines and is not suitable for pellet making. So, to obtain desirable particle size a new wet grind and classification machine was developed.

5.5 Comparative Analysis of a Newly Designed Ball Mill and the Conventional Ball Mill Performance With Respect to Particle Size Distribution and Recirculating Load at the Discharge End

The particle size distribution and percentage of the recirculating load obtained at the discharge were studied for different mill operating speeds, lifters and outlet-discharge mechanisms, as shown in Figs. 5.44, 5.45, and 5.46. The effect of the mill speed, with and without lifter arrangements at the discharge end of the mill, on the percentage of -150 μm particles passing, percentage of the recirculating load to the ball mill and passing particle size fraction at P_{80} is given in Table 5.22.

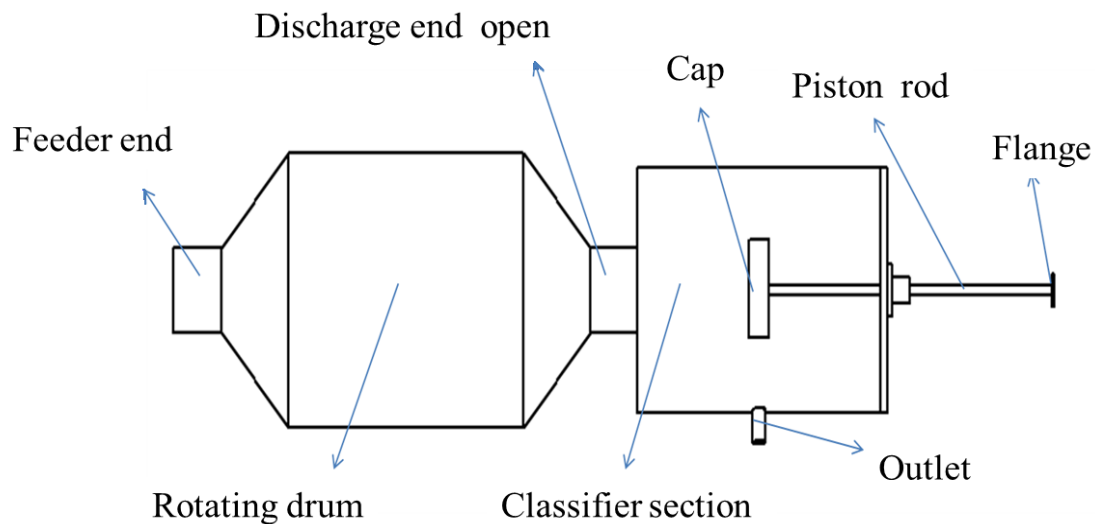


Fig. 5.44 Discharge end without lifters (discharge end open)

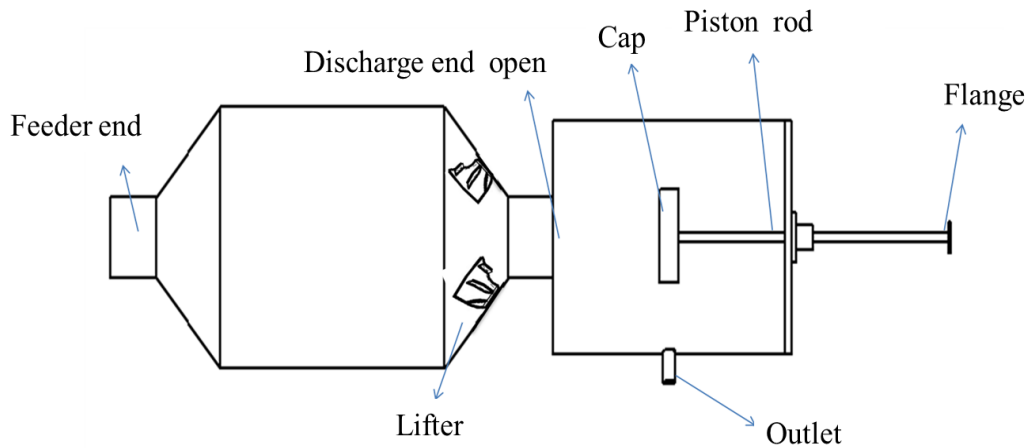


Fig. 5.45 Discharge end with lifters (discharge end open)

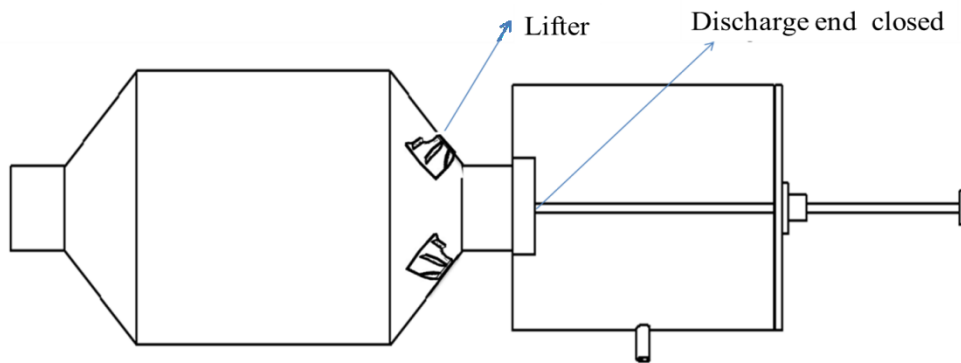


Fig. 5.46 Discharge end with lifters (discharge end closed)

5.5.1 Case 1: Effect of mill speed on the product particle size distribution and recirculating load of the ball mill without lifters and the discharge end open

Particle size analysis was carried out by plotting the mesh size/screen size along the x-axis and the cumulative percentage passing along the y-axis. The results of particle size analysis are shown in Fig. 5.47, which shows particle size distribution obtained for each mill speed. A diagram relating to this portent is illustrated in Fig. 5.44. From Figs 5.47 and 5.48 the particle size analysis results show that at a lower speed of the mill, very fine particles are discharged from the mill. This may be because at lower mill speed, particles with higher density in the slurry try to settle at the bottom of the shell and fine particles with lower density float on the upper surface of the slurry. Also, the particles move from bottom of the mill shell in anti-clock wise direction up

to 3 o'clock position, due to the cascading motion of particles and balls, where particles and balls cannot be further lifted up to shoulder position (Cleary, 2001c). Hence, the particles slip and slide back from the 3 o'clock position to the grinding section because of gravity (Cleary, 2015). At lower mill speed, fine particles that are floating are discharged due to the gradient difference between the inlet and outlet of the mill. Thus, the ball mill works at relatively low efficiency at lower mill speed, since the majority of particles moving at a low speed in the grinding section will not collide with higher energy.

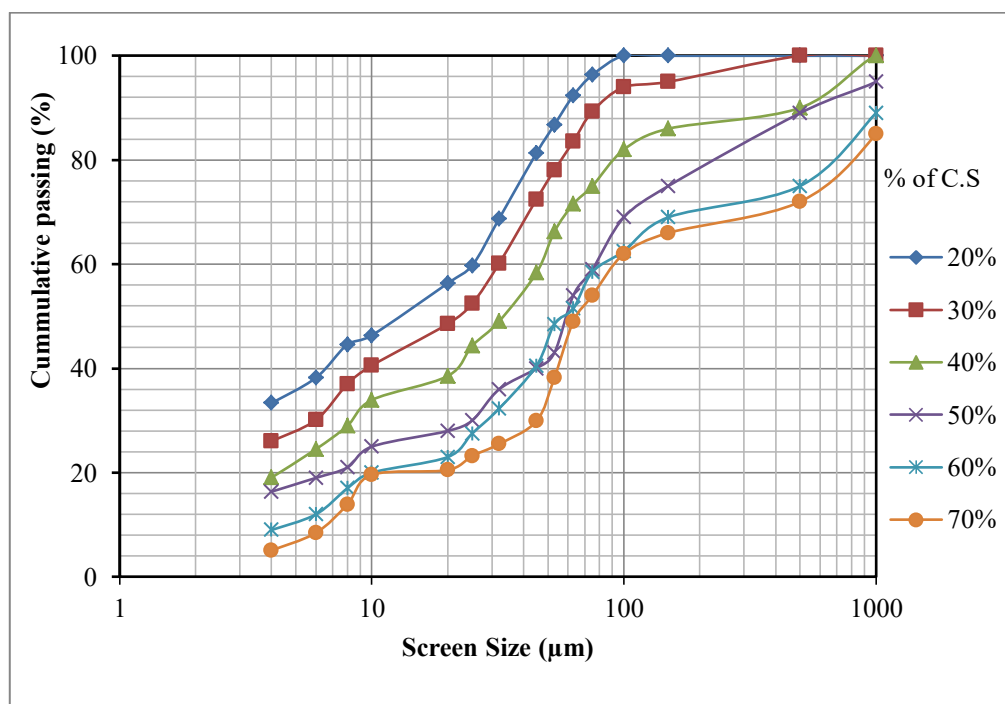


Fig. 5.47 Particle size analysis of discharge product when mill operated at different critical speeds (CS) without lifter and discharge end open

Figure 5.48 shows the oversize (+150µm), desired size (-150µm/+10 µm) and undersize particle size (-10µm) analysis of the discharge product when the mill is operating at different critical speeds without the lifter and the discharge end open. At 20% critical speed, about 81% of particle size distributions are fines, 19% is the desired size particles and no oversize particles were discharged. It is observed that, there was a variation of particle size distribution with each mill speed. At 60% of mill critical speed, the desired particle size distribution discharged from the mill was maximum compared to the mill operating at a different critical speed. However, above

60% of mill critical speed, there was an increase in the discharge percentage of oversize particles (+150 μm). This may be due to the fact that the mill without lifter arrangement in the discharge section cannot provide separation zone and leads to the discharge of maximum quantity of oversized particles. Also, the discharge end does not have any stopper to prevent unground particles from flowing back into the mill.

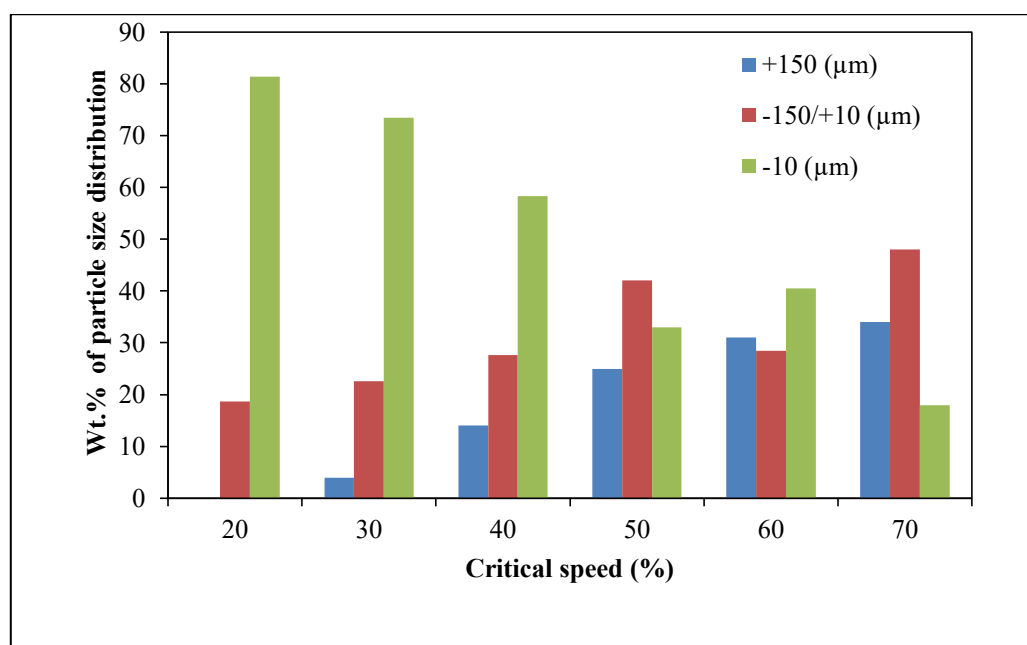


Fig. 5.48 Over size (+150 μm), narrow size (-150 μm /+10 μm) and undersize particle size (-10 μm) analysis of discharge product when mill operated at different critical speeds without lifter and discharge end open

Figure 5.49 shows the percentage of the recirculating load when the mill operates without the lifter and the discharge end is open. At the lower speed of the mill (less than 20% critical speed), the recirculating load is very low, since balls and the oversize particles in the mill will not rise up to shoulder position and will roll back to the bottom portion of the mill. This effect will reduce the grinding and also the recirculating load. However, when the mill speed was increasing above 60% critical speed, it was observed that the recirculating load was also increasing. This was due to large quantities of unground particles moving at high speed and with less contact of particles with the mill shell that lift the particles and balls, and that in turn prevent the unground particles from flowing back into the grinding section, leading to the

discharge of more unground particles from the mill (Gutierrez et al., 2018). Hence, operating a ball mill without lifter is not preferable, since the grinding efficiency of the mill reduces and the particles discharged from the mill do not undergo size reduction. Also, the discharged particles consist of oversize particles, which are not suitable for pellet making; the load to the mill increases by recirculating the unground product to the mill.

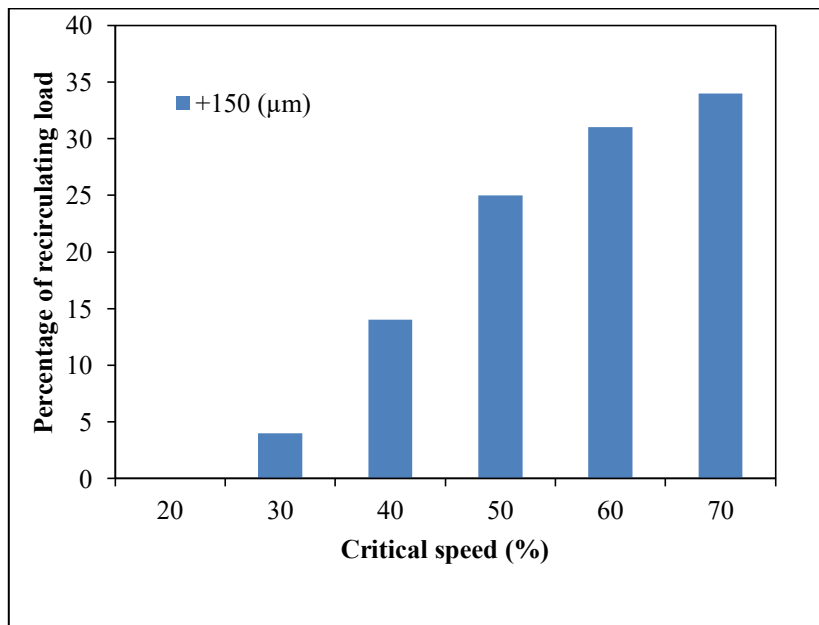


Fig. 5.49 Influence of mill speed on percentage of recirculating load when mill operated without lifter and discharge end open

5.5.2 Case 2: Effect of mill speed on the particle size distribution of the product and the recirculating load of the ball mill with lifters and the cap open at the discharge

Lifter design and mill speed play a very important role in the flow and discharge of particles from the mill. Lifters are mainly used to lift particles from the toe end to the shoulder position of the shell. The falling trajectory of the particles from the shoulder position to the grinding section depends on the design of the lifters and the speed of the mill (Cleary, 2001c). Lifters can also transfer the motion from the mill shell into the motion of the particles (Djordjevic et al., 2004).

In this case, a special type of lifters was used in the discharge section of the mill. Each lifter consists of primary, secondary and tertiary plates. The primary plate was fixed at a corner portion of the diaphragm. The profile of the primary plate is concave, which acts as a bucket when the lifter reaches the bottom portion of the mill. This kind of profile helps lift the desired particles from the bottom portion of the mill to the discharge end of the mill. Having lifters at the discharge end avoids coarse particles and balls to exit from the discharge end. The lifter blades are arranged in such a way that whenever a stream of cataracting balls and coarse particles come in contact with the lifter blades, the blades direct the balls and coarse particles back to the grinding section instead of allowing them to enter the discharge trunnion. The lifter blades are designed in such a way that the outer radius of the blade is not extended but terminated inside (Fig.5.1). This design has a special zone known as the zone of separation at the conical portion of the discharge end of the mill, which helps lift desire-sized particles from the mill; however, balls and coarse-sized particles cannot be picked in the separation zone. A pictorial representation to ball mill with lifters and open cap at the discharge is shown in Fig. 5.45.

For all the experiments, the discharge end was kept open for varying speeds of the mill. The variation of the particle size distribution at the discharge for the mill operating at different speeds, with the discharge end fitted with lifters, is shown in Fig. 5.50. From Fig. 5.50, for a particular mill speed, there is a change in particle size distribution for the mill operating with lifters.

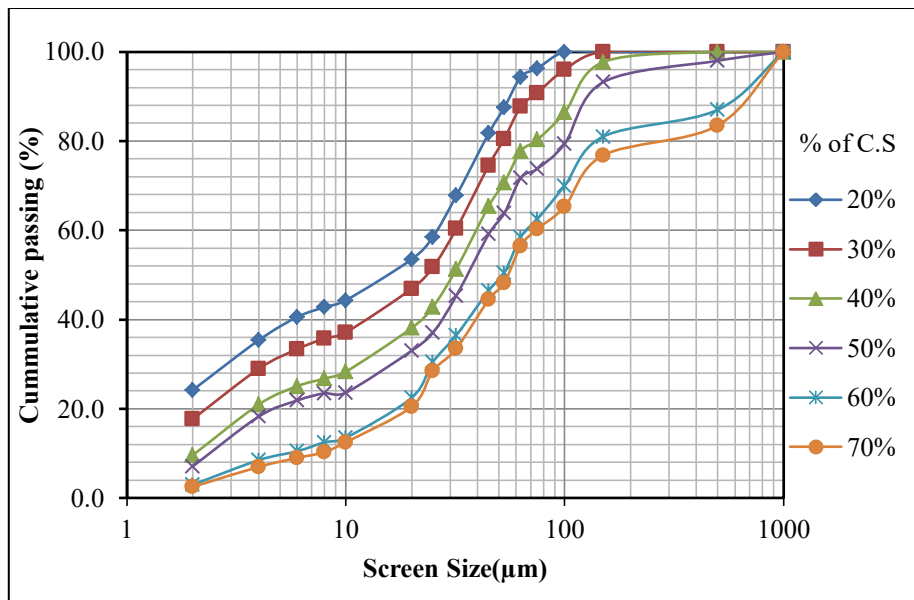


Fig. 5.50 Particle size analysis of discharge product when mill operated at different critical speeds (CS) with lifter and discharge end open

Figure 5.51 shows the oversize (+150 μm), desire size (-150 μm /+10 μm) and undersize particle size (-10 μm) analysis of the discharge product when the mill is operating at different critical speeds with lifters and the discharge end open. According to Fig.5.50, 70% instead of 60% critical speed seems to have produced the maximum amount of the desired size class. This may be due to the balls and particles' trajectory reaching at the discharge end began slipping from the shoulder position to the toe position when the mill was operated at 70% critical speed (Cleary, 2015; Bian et al., 2017). This kind of particle-profile stream at the discharge end helps the lifter plates classify the desired particle size range. The lifters are oriented in the grinding section in such a way that whenever the lifter reaches the bottom section of the mill shell, the primary plate lifts the selective-sized particles from the bottom end portion of the grinding chamber to the discharge end of the mill. Whereas, the secondary lifter plate, which is placed slightly away from the primary plate, lifts the particles present above the bottom section of the grinding end. The tertiary plate is placed at the inclined portion of the discharge end in such a way that it can help classify the particles. Hence, a new type of lifter design at the discharge end can be effectively used to classify the desire-sized particles from the mill.

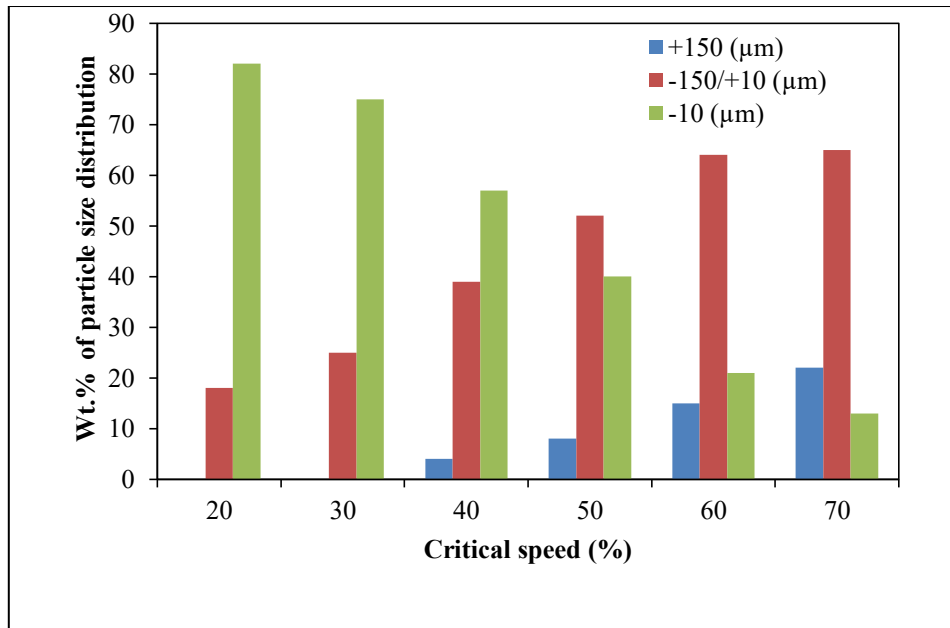


Fig. 5.51 Over size (+150 μm), narrow size (-150 μm /+10 μm) and undersize particle size (-10 μm) analysis of discharge product when mill operated at different critical speeds with lifter and discharge end open

From Fig. 5.51, at lower mill speeds (20 to 30%), very fine particles were discharged from the mill, since a large proportion of the particles move at a relatively low speed and the discharge takes place due to the gradient difference between the inlet and outlet of the mill. At high mill speed (70%), the percentage of oversize particles discharged from the mill is high compared to 60% critical speed. This may be due to the particle trajectory reaching the discharge end with high speed at a higher shoulder position and eventually falls to the toe position when the mill was operated above 70% critical speed (Cleary, 2015; Bian et al., 2017). The high-speed particle profile at the discharge end may make it difficult for the lifters to classify desired particle size distribution since the velocity of the particles is high when the mill is rotating at high speed (Gutierrez et al., 2018). Due to this, particles with high speeds have random motion at the discharge section, which leads to improper classification of particles in the lifters and leads to discharge of oversize particles from the discharge end without classification. Hence, at higher speeds of the mill, the percentage of oversize particles was higher than that of the desired particle size in the discharged product. The results suggest that, the new type of lifter design at discharge end can be effectively used to

classify the desired size particles from the mill when the mill is operated at 70% of critical speed.

Figure 5.52 shows the percentage of the recirculating load when the mill is operating with lifters and the discharge end is open. From Fig. 5.52, it is clear that with increasing mill speed, the recirculating load to the mill increases. The percentage of the recirculating load to the mill with lifters is less than the mill without lifters when the mill is operating at different critical speeds. There is about a 16% difference in the recirculating load between the mill with lifters and the one without.

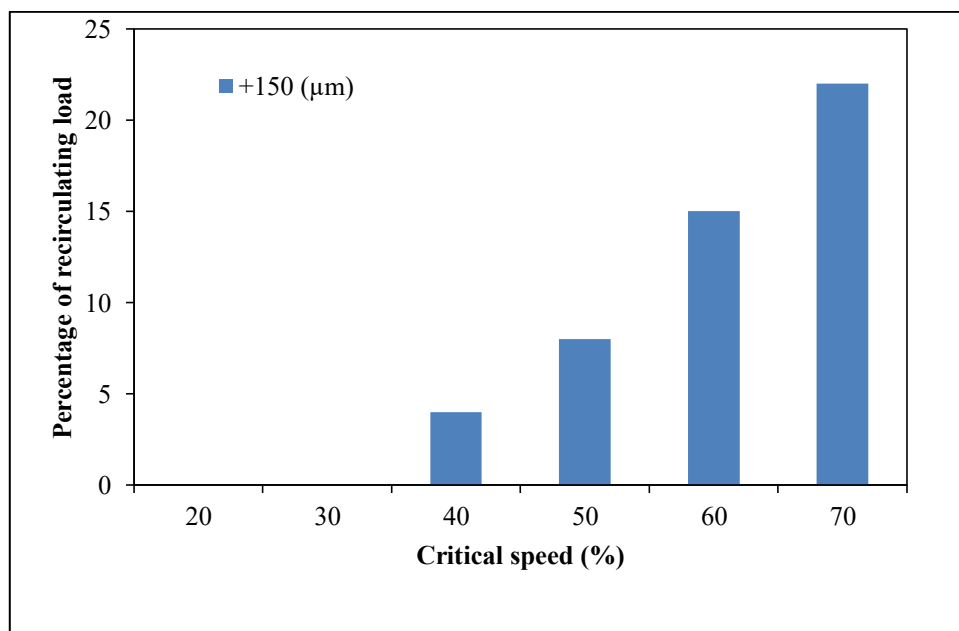


Fig. 5.52 Influence of mill speed on percentage of recirculating load when mill operated with lifter and discharge end open

5.5.3 Case 3: Effect of mill speed on the particle size distribution and recirculating load in the ball mill with lifters and the cap closed at discharge

The opening and closing of the discharge end mechanism with lifters arrangement are shown in Fig. 5.46. In this case, the lifters used at the discharge end are the same as that of the previous case (Section 4.5.2, Case 2). In the previous two cases, the discharge end was kept open during the grinding operation. However, in this case, the discharge end was intermittently opened and closed for every 30 seconds while

conducting the experiments. The opening and closing mechanism at the discharge end restricts slurry flow, leading to a lower rate of slurry discharge compared to the Case 1 and Case 2 mechanisms discussed earlier. Particle size distributions for different mill speeds are presented in Fig. 5.53.

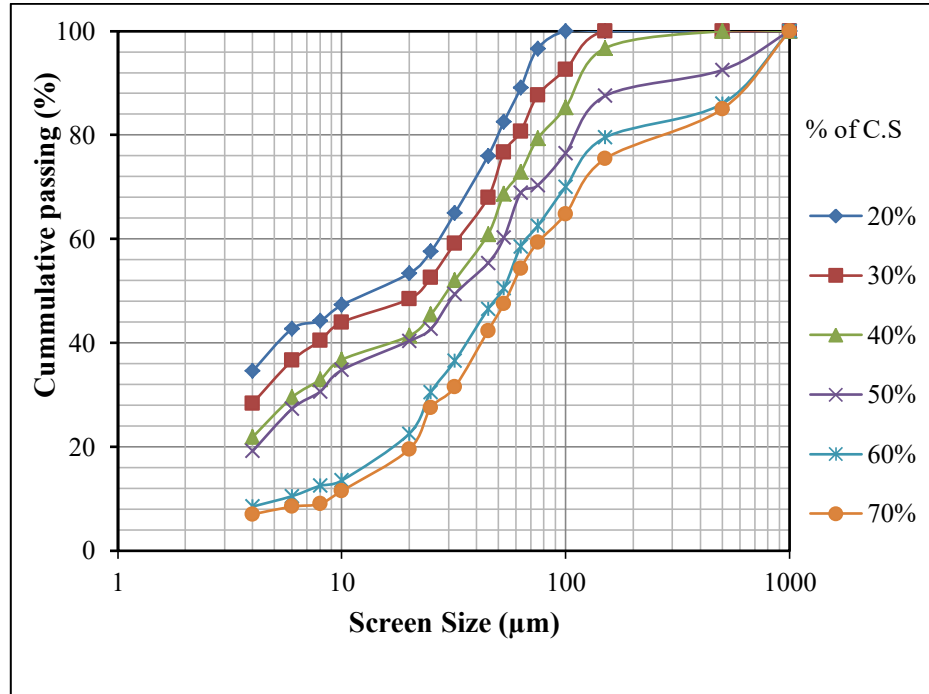


Fig. 5.53 Particle size analysis of discharge product when mill operated at different critical speeds (CS) with lifter and discharge end closed

Figure 5.54 shows the oversize, the desired size range and undersize particle size analysis of the discharge product when the mill was operated at different critical speeds with lifters and the discharge end closed. Also, Fig. 5.55 shows the percentage of the recirculating load when the mill was operated with lifters and the discharge end open. The results of particle size distribution and recirculating load to the mill, as obtained in Case 3, are almost similar to that of Case 2, indicating that the closing and opening of the discharge end for every 30 seconds may not have any effect on the particle size distribution from the discharge end of the mill.

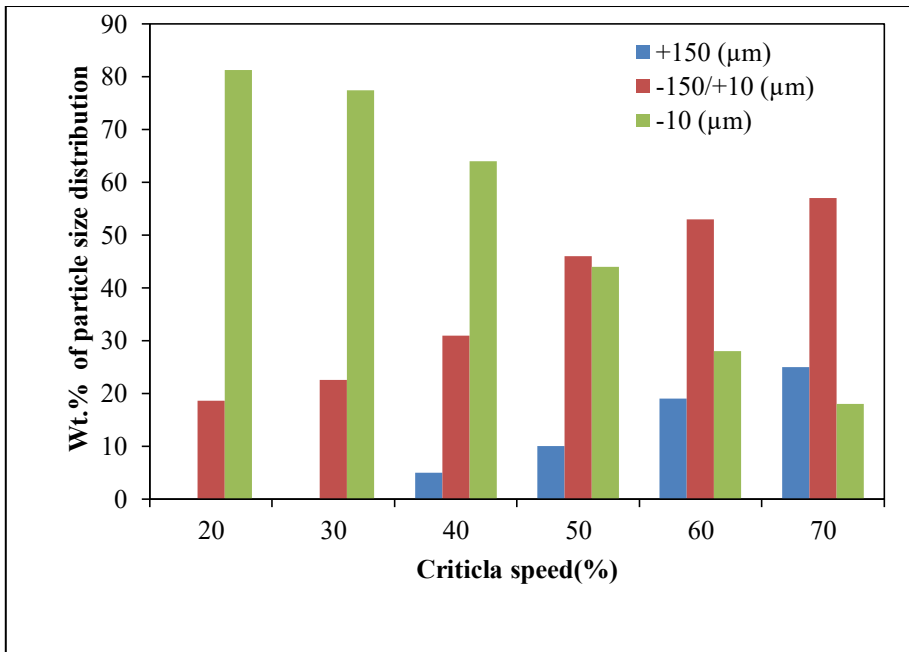


Fig. 5.54 Over size (+150μm), narrow size (-150μm/+10 μm) and undersize particle size (-10μm) analysis of discharge product when mill operated at different critical speeds with lifter and discharge end closed

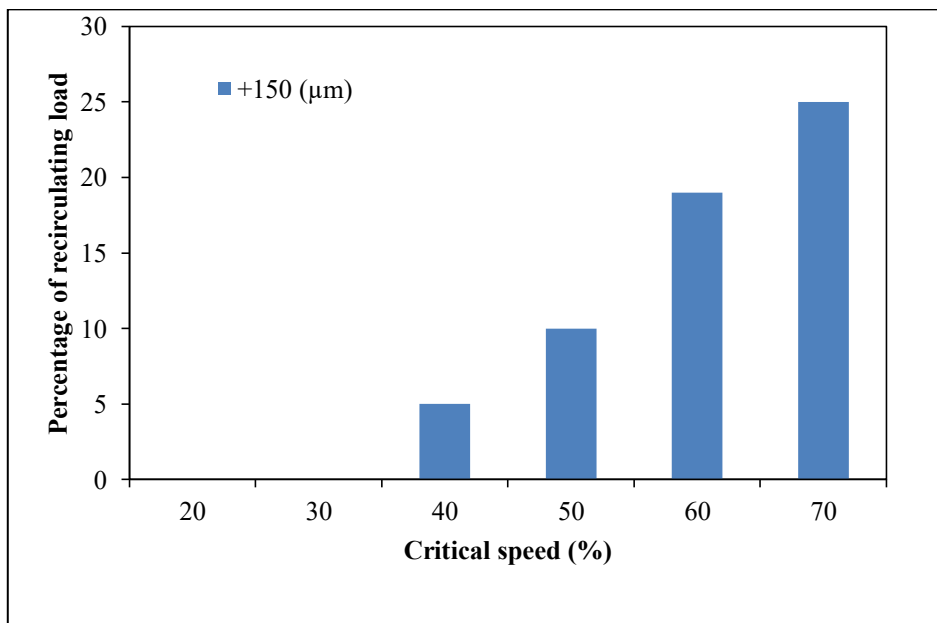


Fig. 5.55 Influence of mill speed on percentage of recirculating load when mill operated with lifter and discharge end closed

5.5.4 Comparison of Case 1, Case 2 and Case 3

From Fig. 5.56 (a & b), it is clear that the particle size distributions for Case 1, Case 2 and Case 3 are almost the same. The results obtained at 20% critical speed indicates that 80% passing size fraction in all the three cases is almost the same and that the particle size fraction at the discharge varies from 44 to 50 μm , as shown in Fig. 5.57. Also, from Fig. 5.58, at 20% critical speed, 100% passing size fraction in all the three cases is below 150 μm . This indicates that very low mill speeds do not have any impact on the size of the particles at the discharge end of the mill. The discharged products at lower mill speeds contain very fine particles, and the percentage of the desired particles discharged is very less (<65%) than the required feed size range for pellet making.

The particle size distribution in Case 1 has more coarse particles in the range of 90–840 μm compared to Case 2 and Case 3, wherein the particle size ranges from 75–290 μm when the mill operates at 50%–70% critical speed (Table 5.22, Fig. 5.56 c - Fig. 5.56 and Fig. 5.57). The results of Case 2 and Case 3 indicate that the percentage of the desired particle size range discharged from the mill is well within the desired fraction (-150 μm /+10 μm); it is 65% when the mill is operating at 60% critical speed, as shown in Fig. 5.51 and Fig. 5.54. Also, in Case 1, when the mill is operating at 60% critical speed, the percentage of desired particle size range discharged from the mill is about 34% lesser than that of Case 2 and about 25% lesser than that of Case 3, as shown in Fig. 5.48, Fig. 5.51 and Fig. 5.54. The results indicate that the lifters at the discharged end play an important role in discharging the desired band particles when the mill is operated at a particular operating speed (60% critical speed). This is again due to lifters at the discharge end, which acts as a separation zone in the discharge end of the mill. However, mills without lifters at the discharge end lead to uncontrolled particle size distribution in the discharge product, since there is no barricade to stop the movement of unground particles at the discharge end of the mill. Hence, the discharge will consist of fines and unground particles, which are unsuitable for further processing.

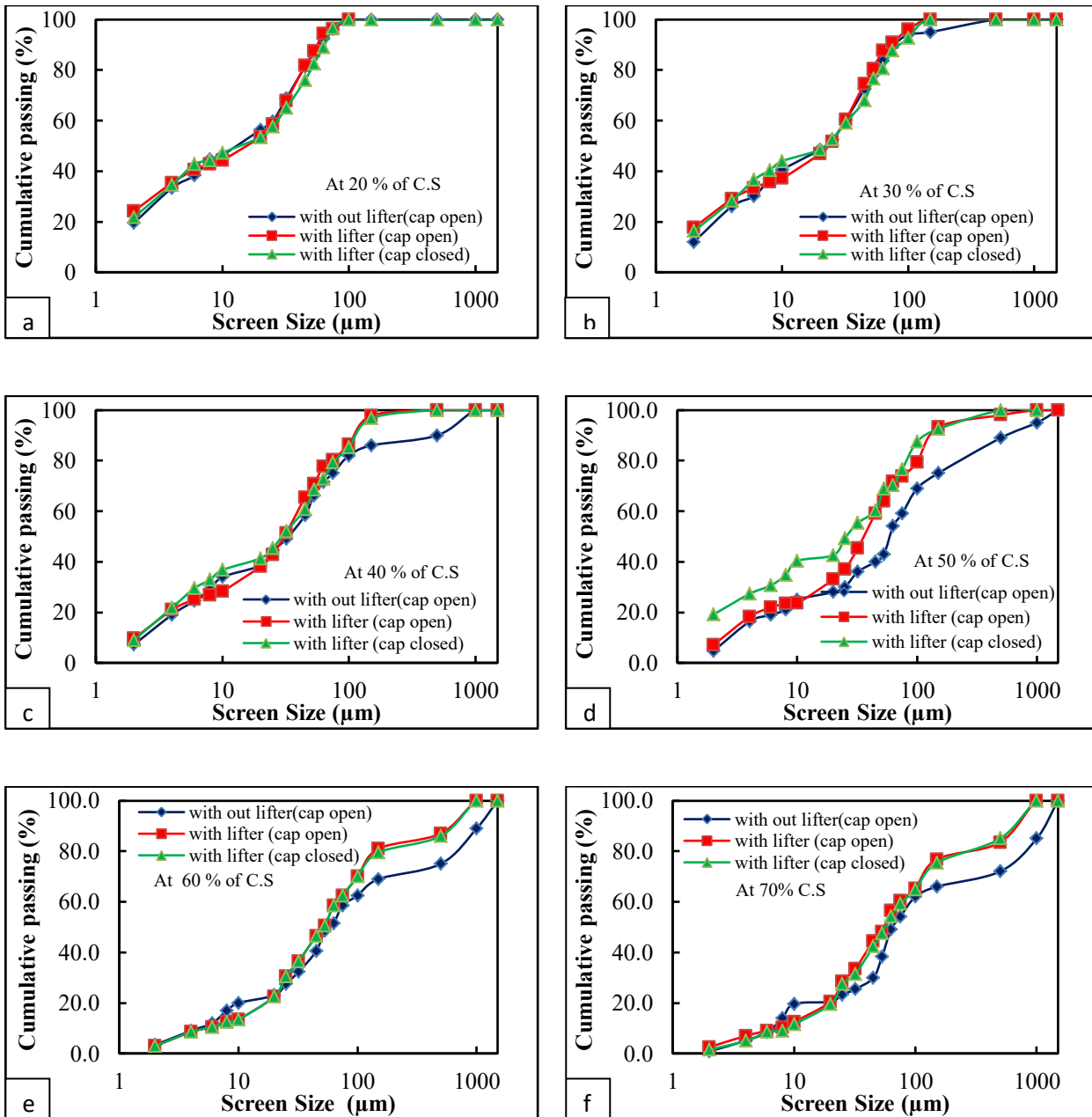


Fig. 5.56 Particle size distribution comparison for mill without lifter (cap open), with lifter (cap open), and with lifter (cap close) at different critical parentage speed (a) 20 % of C.S, (b) 30 % of C.S, (c) 40 % of C.S, (d) 50% of C.S, (e) 60 % of C.S, (f) 70 % of C.S

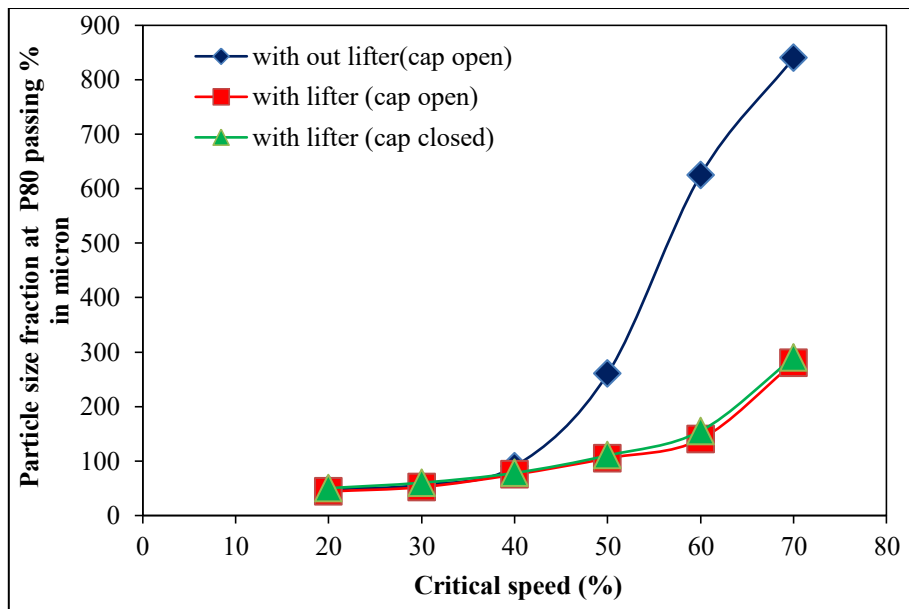


Fig. 5.57 Influence of mill speed on particle size fraction distribution with P₈₀ passing percentage

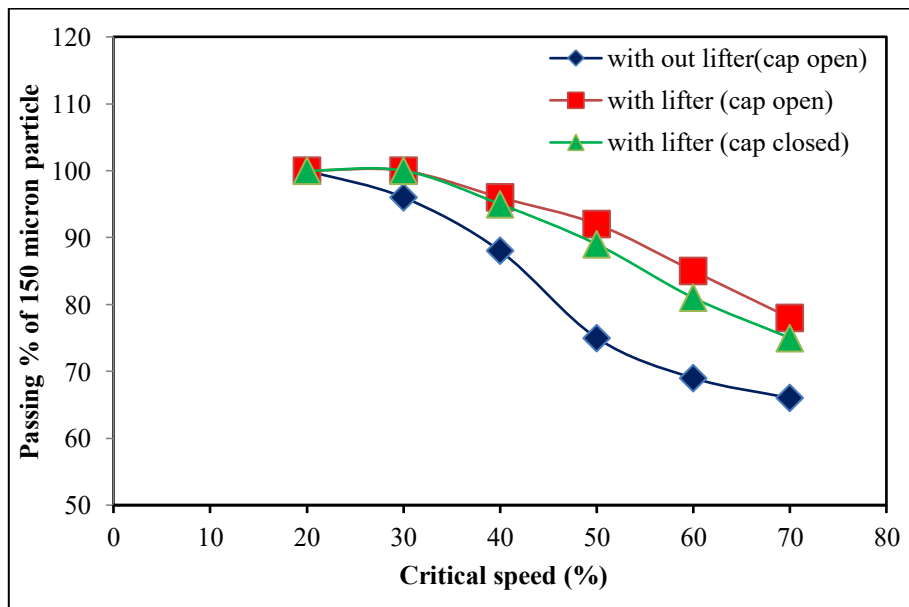


Fig. 5.58 Influence of mill speed on passing % of 150 μ m particle

It can be observed from Fig. 5.59 that for lower mill speeds of mills with and without lifters (open and closed condition) at the discharge end, a minimum percentage of the recirculating loads are yielded. A very smaller recirculating load was recorded at a mill speed of 20% with 80% passing particle size fraction varying from 44 to 50 μ m, as shown in Table 5.22, for all the three cases. In all the three cases, at a mill critical

speed above 70%, the percentage of the recirculating load to the mill increased with the increasing speed of the mill, as shown in Fig. 5.59. In Case 2 and Case 3, the percentage of the recirculating load at 60% critical speed is 15% and 19%, respectively, which is smaller compared to Case 1 with 31% recirculating load, as shown in Table 5.22. It can also be observed that for all the three cases when the mill was operated above 60% critical speed, the recirculating load exceeded more than 20%, thus, an increase in the circulating load to the mill decreases the performance of the mill. The results suggest that well-designed lifters with proper orientation in the discharge end can help to discharge the desired particle size with minimum recirculating load.

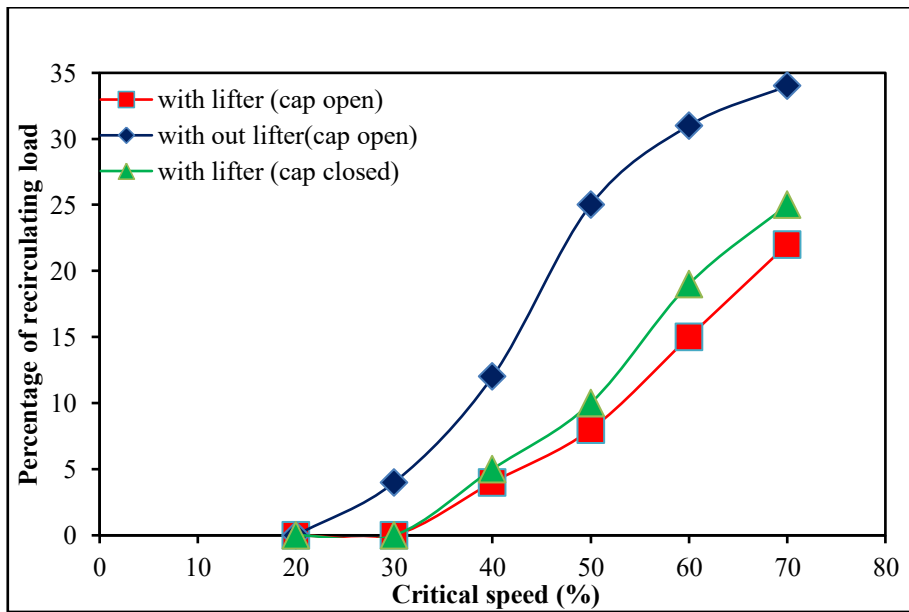


Fig. 5.59 Influence of mill speed on percentage of recirculating load to ball mill

Table 5.22 Effect of mill speed, with and without lifter arrangements at the discharge end of the mill on percentage passing of -150 μm particle, percentage of recirculating load to the ball mill and passing particle size fraction at P_{80}

Percentage of Critical speed (%)	% passing of -150 μm particle			% of recirculating load to the ball mill			Passing particle size fraction at P_{80} (μm)		
	Cap open		Cap closed	Cap open		Cap closed	Cap open		Cap closed
	without lifter	with lifter	with lifter	without lifter	with lifter	with lifter	without lifter	with lifter	with lifter
20	100	100	100	0	0	0	48	44	50
30	96	100	100	4	0	0	56	52	60
40	88	96	95	12	4	5	90	75	78
50	75	92	89	25	8	10	260	105	110
60	69	85	81	31	15	19	625	140	155
70	66	78	75	34	22	25	840	280	290

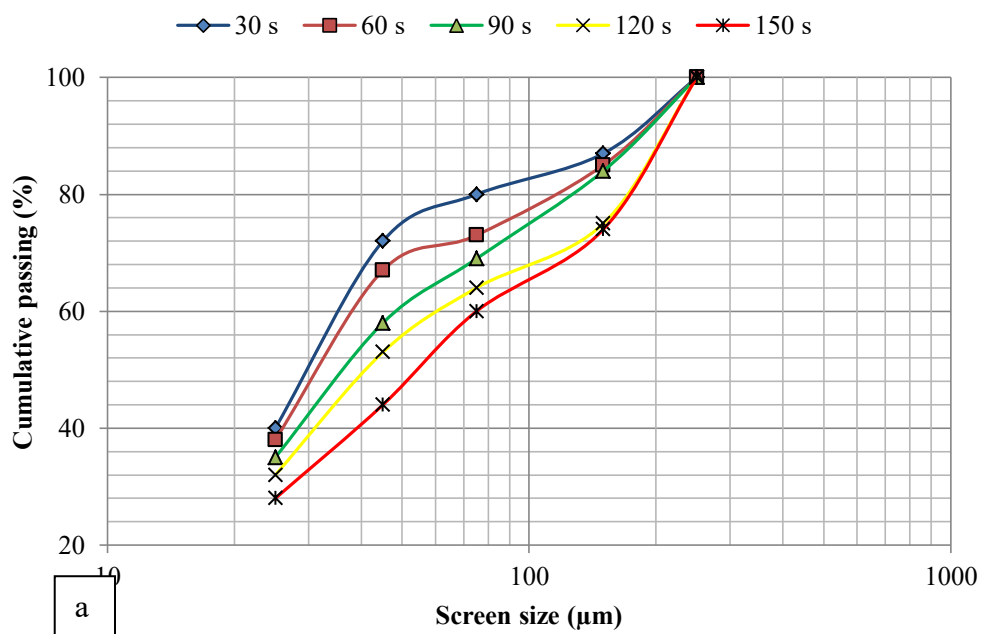
5.6 Evaluation of a New Ball Mill Hydro-Squeeze Classifier for Particle Size Reduction and Classification

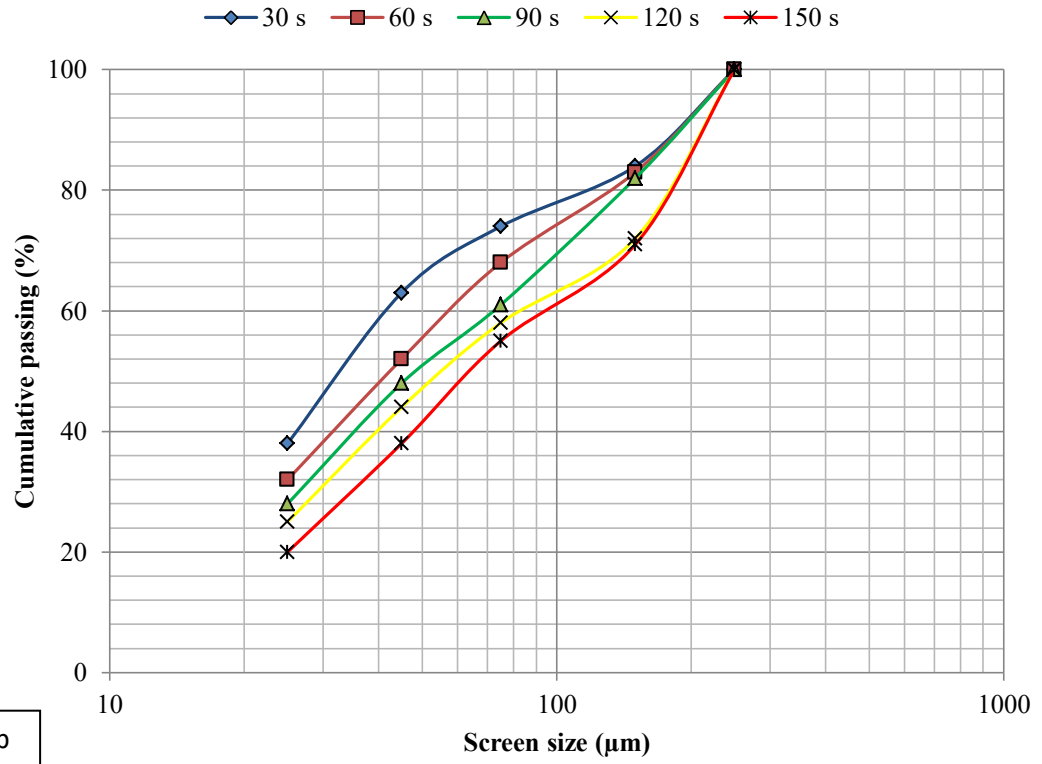
This experimental study covers the effect of the solid slurry concentration and the mill discharge end opening time on the size of particles discharged from the mill to the classifier section and the classifier classification efficiency.

5.6.1 Effect of the solid slurry concentration and the mill discharge end opening time on the size of particles discharged

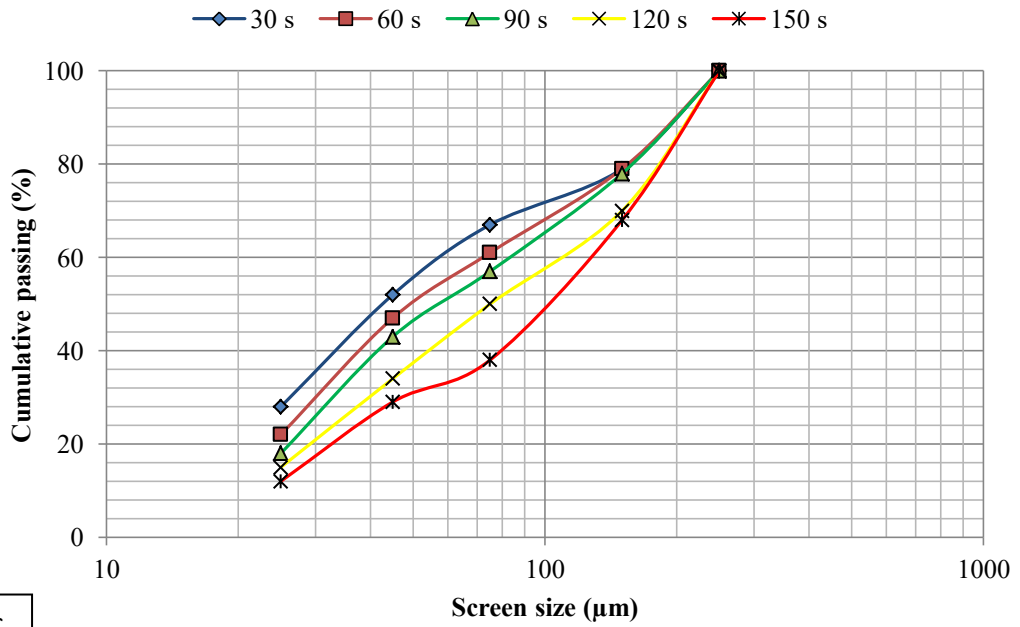
The slurry discharged from the ball mill to the classifier section which was subjected to particle size analysis. Particle size distribution for varying slurry solid concentrations and mill discharge end opening times are shown in Fig. 5.60a-e. In Figs. 5.60a-e and 5.61, it is clear that at 55% of the slurry solids concentration and 30 s discharge end opening, the mill discharges very fine particles. This may be explained that because, at a shorter discharge end opening time, the ore retention time in the mill increases, ultimately increasing impact forces on the ore. This effect leads to over-grinding of ore inside the mill and increases fines in the discharge product. Also, over-grinding of particles inside the mill leads to excess energy consumption.

The fine product discharge from the ball mill at lower slurry solid concentration and shorter discharge duration end opening is not suitable for pellet making (Hanumanthappa et al. 2020b). At a longer opening time (150 s) of the mill discharge end with an increasing slurry solid concentration, the power draw by the mill falls continuously with an increasing slurry solid to the mill for a longer period of time (Tangsathikulchai and Austin 1985). This power drop by the mill shows that there is a decline in the tumbling action of grinding media as the slurry viscosity increases with increasing slurry solid concentration to the mill²⁸. This effect led to decrease in particle size reduction in the mill. Hence, at a longer duration opening of mill discharge end with an increasing slurry solid concentration, coarser size particles are discharged from the mill as represented in Fig. 5.61. Therefore, with an increasing mill discharge end opening time and with an increasing slurry solid concentration to the mill, the recirculating load to the mill increases.

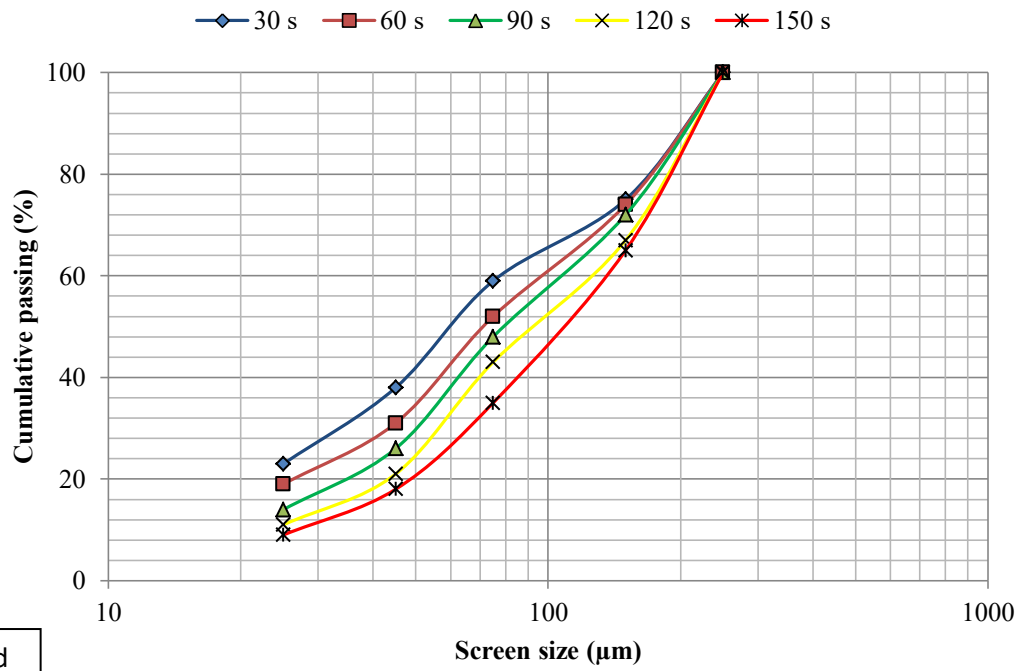




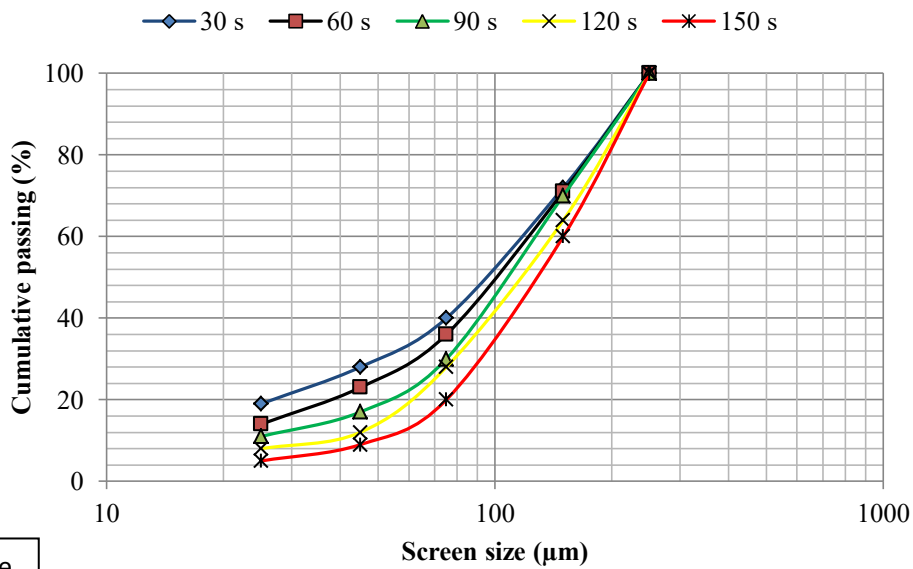
b



c



d



e

Fig. 5.60 Particle size analysis before squeezing in Chamber-1 –(a) for 55% solids, (b) for 60% solids, (c) for 65% solids, (d) for 70% solids, and (e) for 75% solids

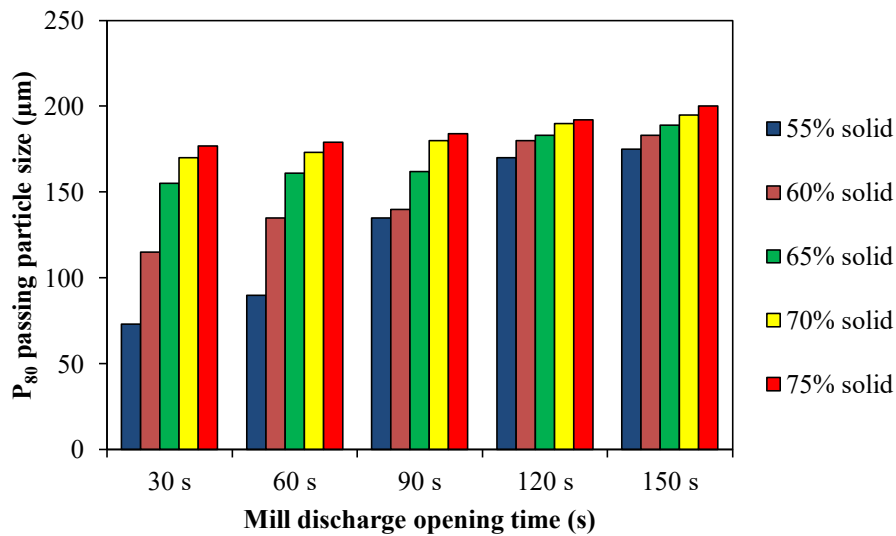


Fig. 5.61 P₈₀ passing percentage at different slurry solids percentage before squeezing in Chamber-1

Figure 5.62 shows +150 µm particles discharge from the ball mill to Chamber-1 of the classifier section when the mill is operating at different slurry solid concentrations. At 75% slurry solid concentration, +150 µm particles discharged from the mill to the classifier section were the highest among the selected range of the slurry solid concentration. However from Fig. 5.63, with increasing solid slurry concentration, there was a rise in the +150 µm particle discharge. Possibly, in case of the higher slurry solid concentration, large quantities of particles reside on the wall of the mill and are further crushed by the tumbling balls at the lower part of the ball load. Due to this, a small reduction in particle size can trigger a rapid increase in viscosity of the slurry (Tangsathikulchai and Austin 1989). As a result, the pulp stickiness at the mill shell increases quickly as higher quantities of fines are produced. This would also lead to a decrease in the material grinding level. Further, with an increasing slurry solid concentration, the particle size reduction is reduced due to increased damping of the slurry. As a result, the ball velocity in the slurry reduces; this effect leads to reduction of energy impacted from the balls to the particles. Also, at higher slurry solid concentrations, sedimentation of larger particles in the water increases its cushioning, resulting in a decrease in particle size reduction (El-Shall and Somasundaran 1984; Kotake et al. 2004; Tangsathikulchai and Austin 1985). Hence, on increasing the mill

slurry solid concentration, coarser particles will discharge from the mill to the classifier section.

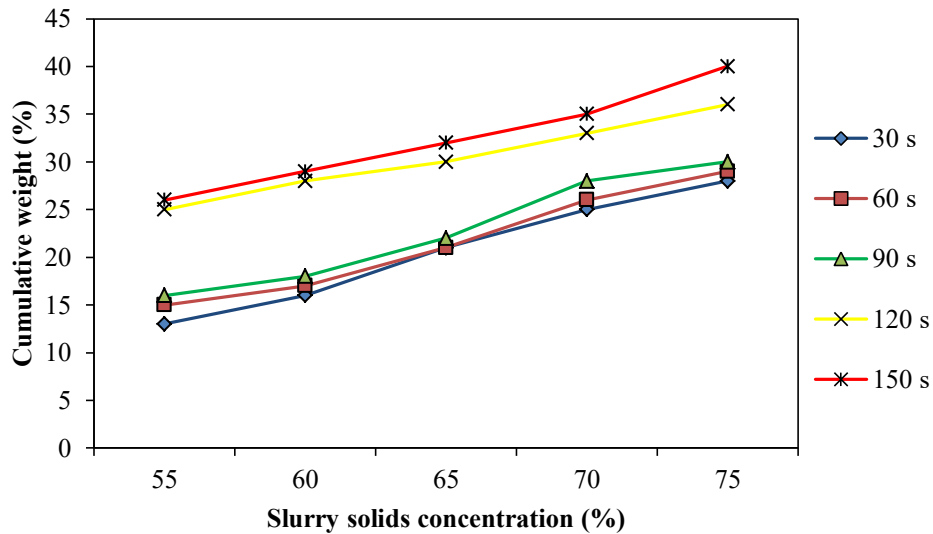


Fig. 5.62 Weight percentage of +150 μm particles collected in Chamber-1 (before squeezing) at different slurry solid concentrations

Figure 5.63 shows -150 μm particles discharge product from the ball mill to Chamber-1 of the classifier section when the mill is operating at different slurry solid concentrations. At the lower slurry solid concentration, the percentage of fine particles discharged increases. As coarse particles and fine particles are free from each other, these particles settle quickly at the bottom of the mill shell, while the fine particles float on the upper surface of the slurry (Bu et al. 2020; Klimpel 1989). This effect leads to the discharge of more fine particles from the mill discharge end to the classifier section at lower slurry solid concentrations. When the mill operated in the range of 55% to 75% slurry solid concentration, about 15% variation is observed in -150 μm particles discharged from the mill. The result suggests that the quantity of -150 μm particles discharged from the mill depends on the mill slurry solid concentration.

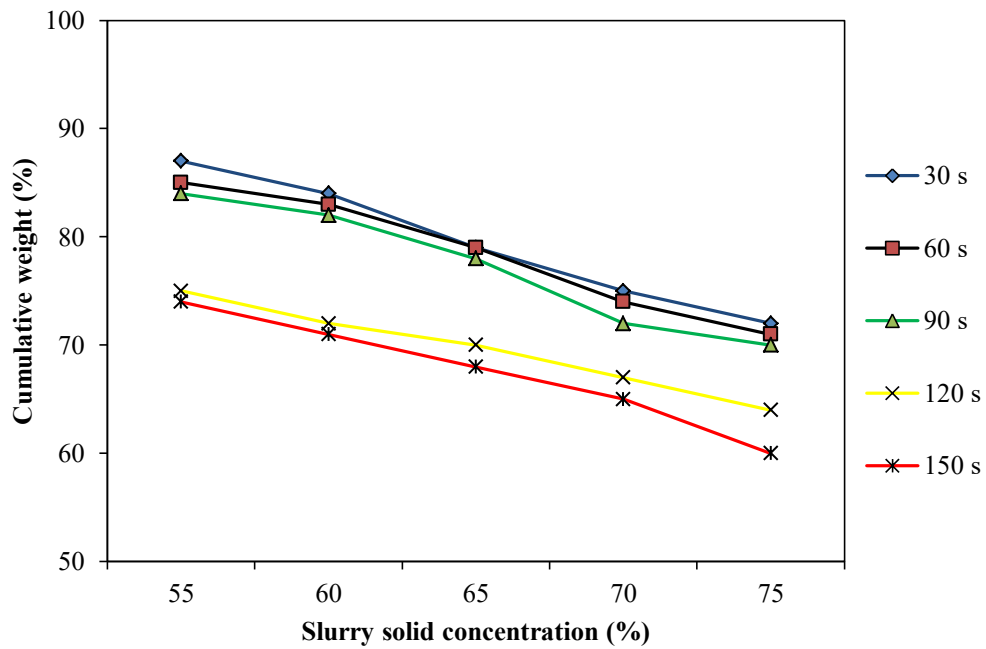


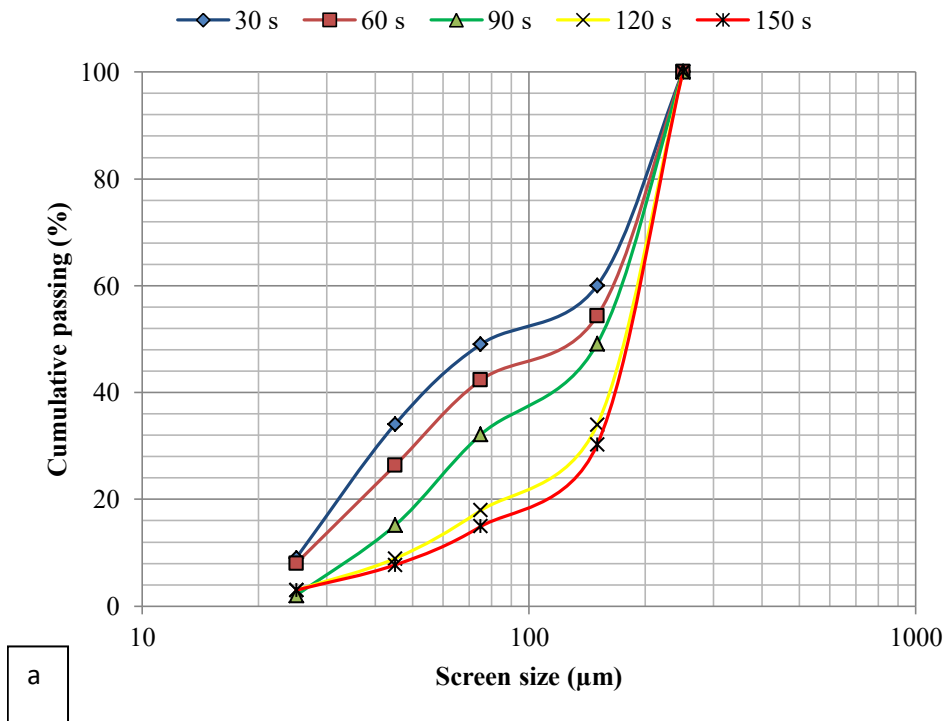
Fig. 5.63 Weight percentage of $-150\ \mu\text{m}$ particles collected in Chamber-1 (before squeezing) at different slurry solid concentrations

5.6.2 Particle size analysis of classified ground product in Chamber-1 and Chamber-2 after squeezing

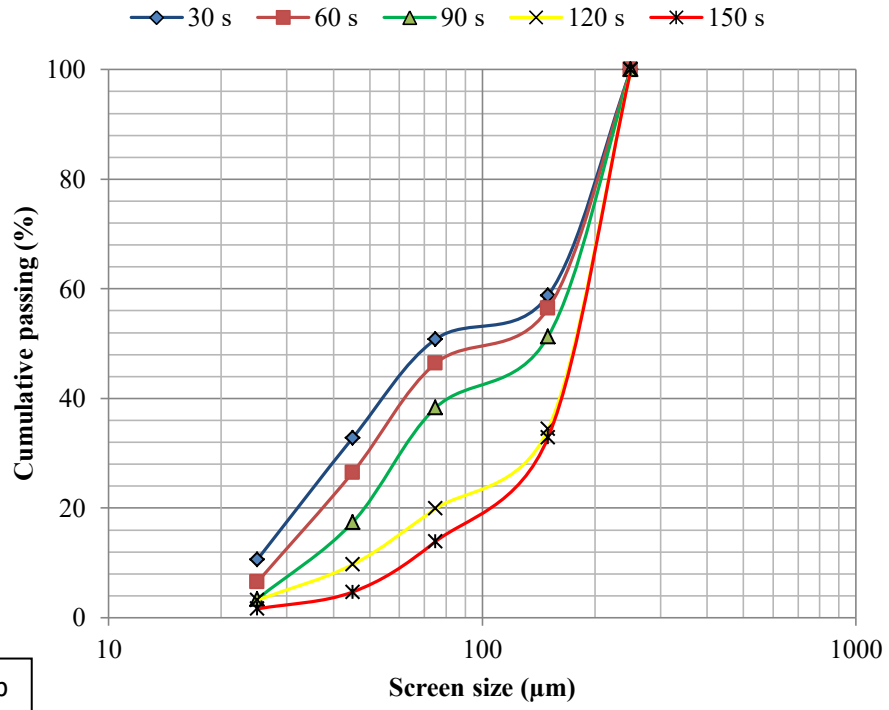
The classifier disc plays an important role in the separating of the $+150\ \mu\text{m}$ particles from $-150\ \mu\text{m}$ particles. The size of the particle separation depends on the screen size selected in the classifier disc. The screen size to classifier disc is selected based on the pellet feed size requirement. For pellets making, the size of a particle requires 100% passing $150\ \mu\text{m}$ particles (Hanumanthappa et al. 2020b). Hence, a $150\ \mu\text{m}$ screen size was used in the classifier disc. It has the flexibility to change the screen based on the particle size requirement. The classifier disc was placed inside the classifier section to divide the classifier section into two chambers, named Chamber-1 and Chamber-2. The slurry discharged from the ball mill to Chamber-1 of the classifier section was subjected to squeezing by the classifier disc. As the classifier disc moves towards the mill discharge end, the volume inside Chamber-1 reduces, which increases the compressive forces on the slurry inside the Chamber-1. This effect increases pressure

inside the Chamber-1, which helps to squeeze out the slurry from Chamber-1 to Chamber-2 through the classifier disc screen. After squeezing of slurry from Chamber-1 to Chamber-2, the leftover slurry residue in Chamber-1 was considered for particle size analysis.

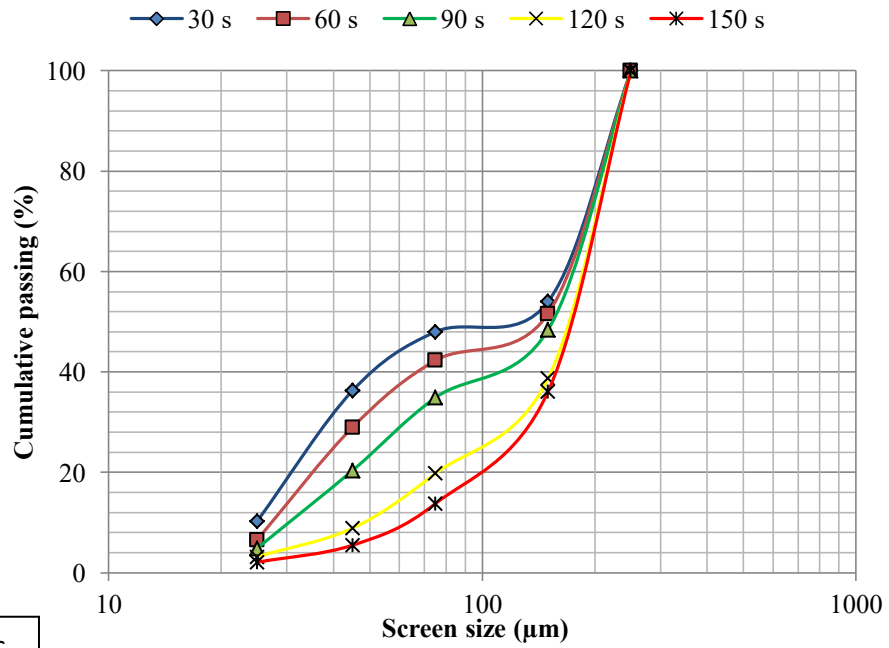
Figure 5.64a-e shows particle size analysis of the leftover product in Chamber-1 when the classifier section with slurry was squeezed at different slurry solid concentration and mill discharge end opening time. From Figs. 5.61 and 5.65, P80 passing size increased in Chamber-1 after squeezing of slurry when comparing to before squeezing. This indicates that $-150\ \mu\text{m}$ particles are squeezed out from Chamber-1 to Chamber-2. Hence, the classifier disc is successful in separating $-150\ \mu\text{m}$ particles from $+150\ \mu\text{m}$ particles after squeezing the slurry in Chamber-1.



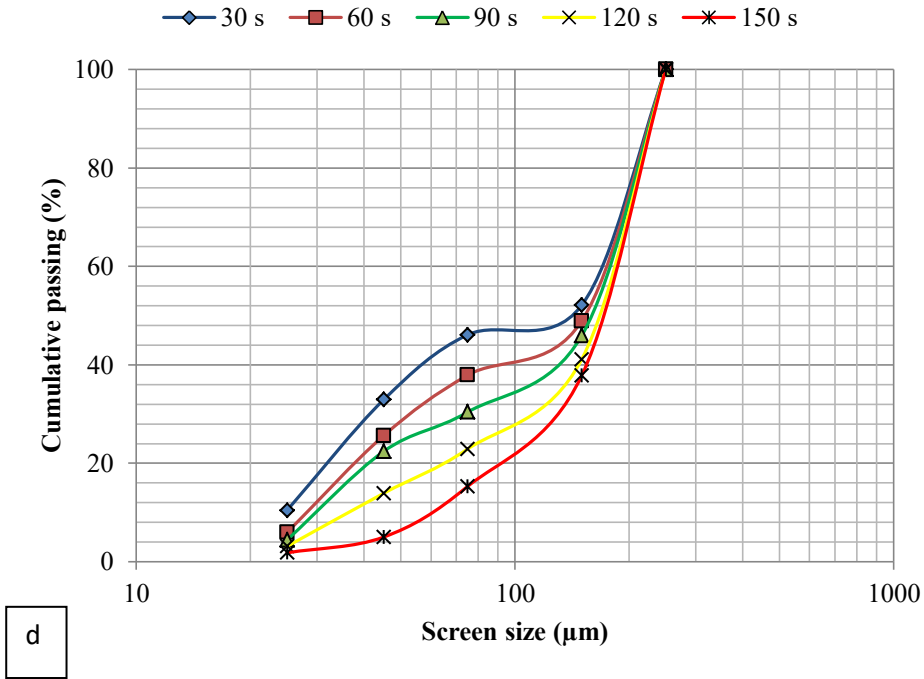
a



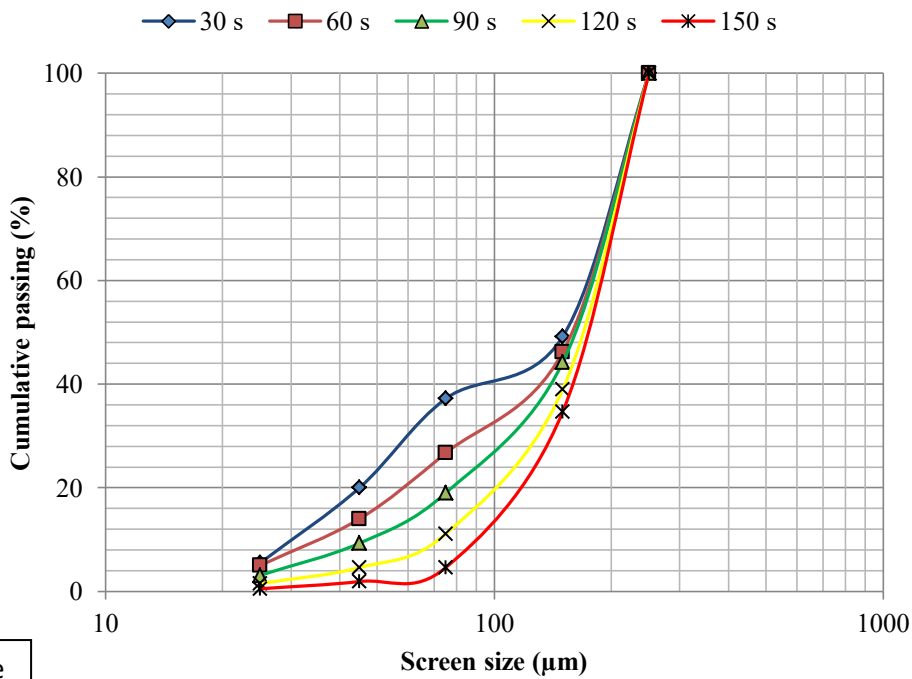
b



c



d



e

Fig. 5.64 Particle size analysis of leftover product in Chamber-1 after squeezing in Chamber-1 – (a) for 55% solids, (b) for 60% solids, (c) for 65% solids, (d) for 70% solids, and (e) for 75% solids

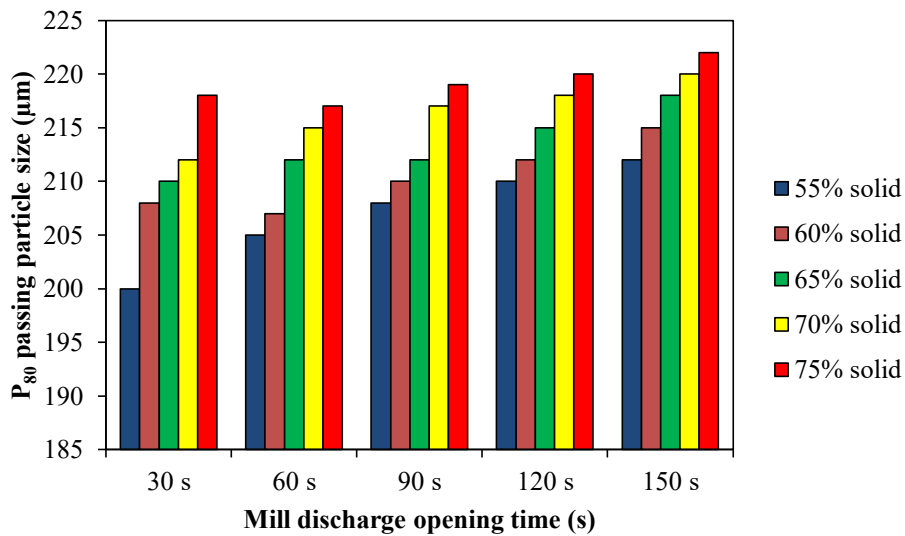


Fig. 5.65 P₈₀ passing percentage at different slurry solid percentages after squeezing in Chamber-1

Figures 5.62 and 5.66 show the weight percentage of +150 µm and -150 µm particles left in Chamber-1 after squeezing. The results indicate that, after squeezing off the slurry in Chamber-1, the quantity of -150 µm particles un-squeezed to Chamber-2 varied for each operating condition. Probably, at a lower slurry solid concentration with discharge end open for longer duration; the mill discharges slurry with low viscosity. At a lower slurry viscosity, the resistance of one particle to another particle is lower, which decreases the adhesive force between the particles in the slurry with a decreasing slurry solid concentration. At this condition, particles are free to move in the slurry, and squeezing of this slurry can easily separate -150 µm from +150 µm particles without any resistance. Hence, lower percentage of -150 µm particles is left in Chamber-1 while squeezing the slurry at the lower viscosity. However, mill discharge slurry of higher viscosity at a higher slurry solid concentration with the mill discharge end opens for a shorter duration. Due to the high slurry viscosity, the -150 µm and +150 µm particles adhere to each other, which further decrease the particle separation. Hence, the high percentage of -150 µm particles is un-squeezed from Chamber-1 to Chamber-2 after the squeezing process. This indicates that slurry viscosity plays a crucial role in the classification of particles during the classifier section squeezing process.

Figures 5.62 and 5.66 represent the recirculating load to the mill. From Fig. 5.66, the weight percentage of $-150\ \mu\text{m}$ particles recirculated to the mill is increasing with an increasing slurry solid concentration to the mill. This is due to the increase in slurry solid concentration to the mill; the viscosity of discharge slurry from the mill to Chamber-1 will be high. Due to the high viscosity of slurry, clogging of screen takes place. Therefore, fine particles collected in Chamber-1 will not be squeezed from Chamber-1 to Chamber-2. Hence, along with coarse particles, fine particles are also recirculated back to the mill at higher slurry solid concentration. Re grinding of these particles in the mill increases the ultra-fines, this in turn increases the energy utilization. So, the recirculation of excess undersize particles to the mill is not desirable. Since the mill output product consists of ultra-fines, which are not suitable for pellet making feed (Hanumanthappa et al. 2020c).

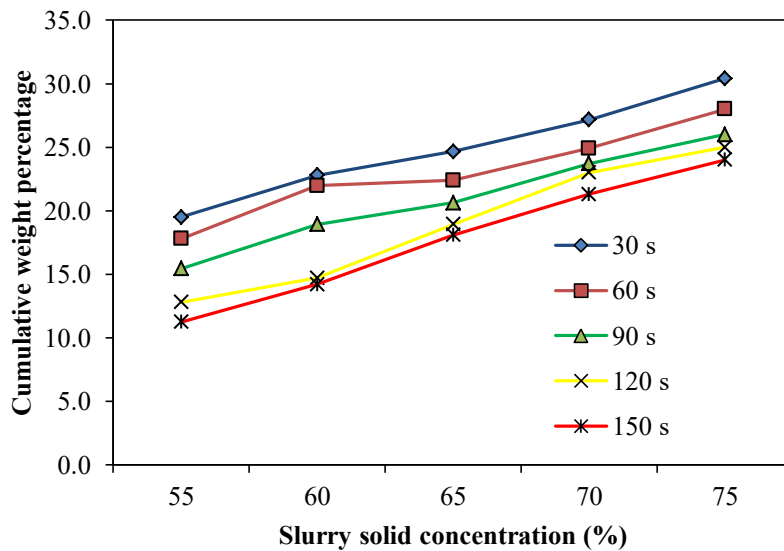
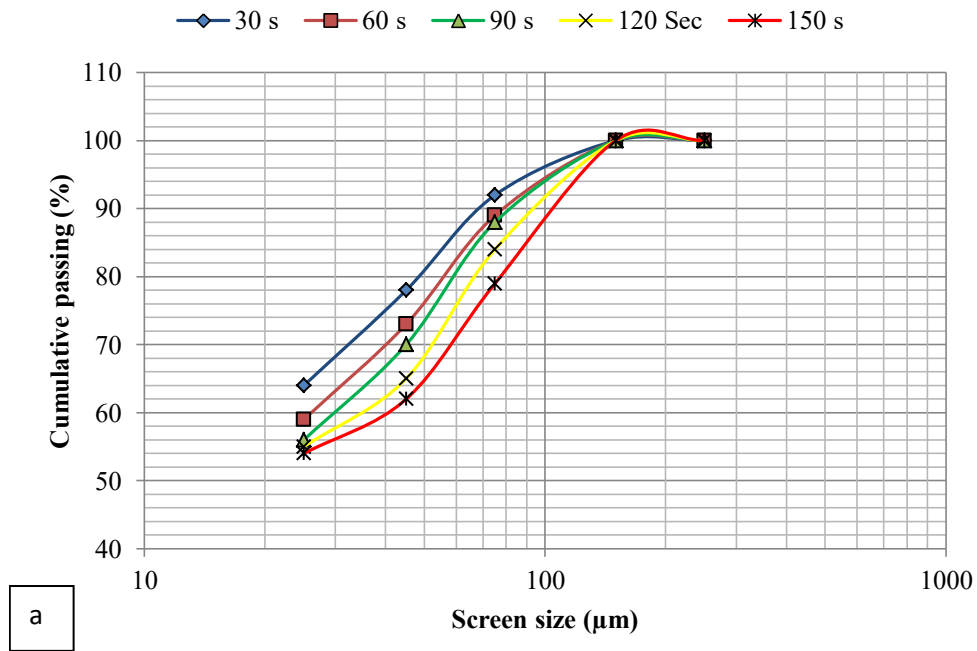


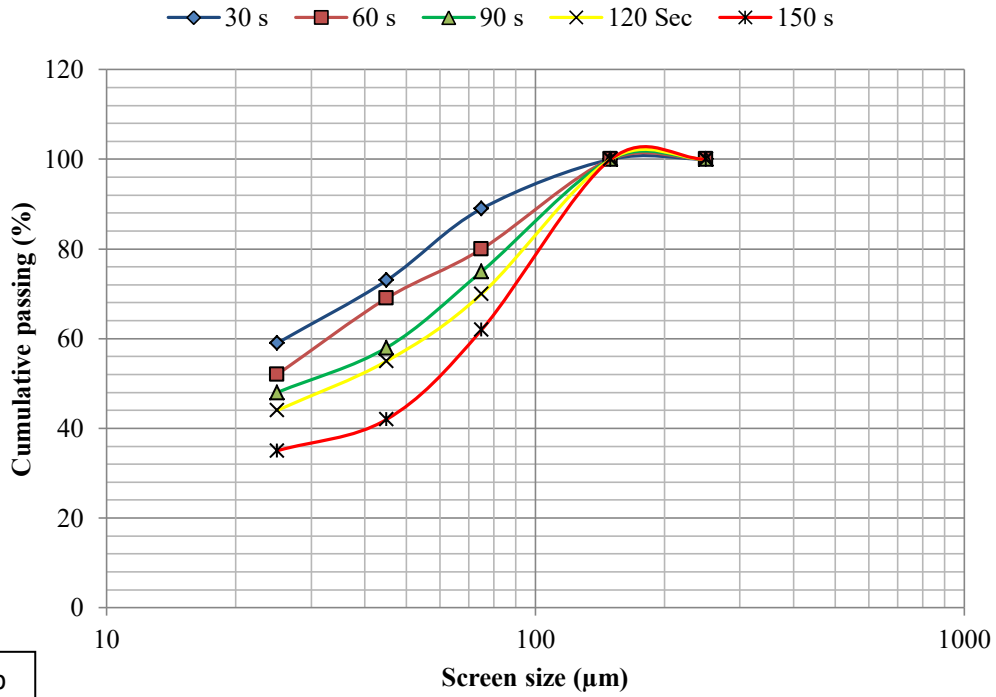
Fig. 5.66 Weight percentage of $-150\ \mu\text{m}$ particles collected in Chamber-1 (after Squeezing) at different slurry solid concentrations

Figures 5.67 and 5.68 shows that Chamber-2 consists of only $-150\ \mu\text{m}$ particles, indicating that $+150\ \mu\text{m}$ particles are restricted to Chamber-1, and Chamber-2 consists of 100% passing particle sizes are below $150\ \mu\text{m}$. It is observed from Fig. 5.69, the weight percentage of undersize particles collected in Chamber-2 varies with

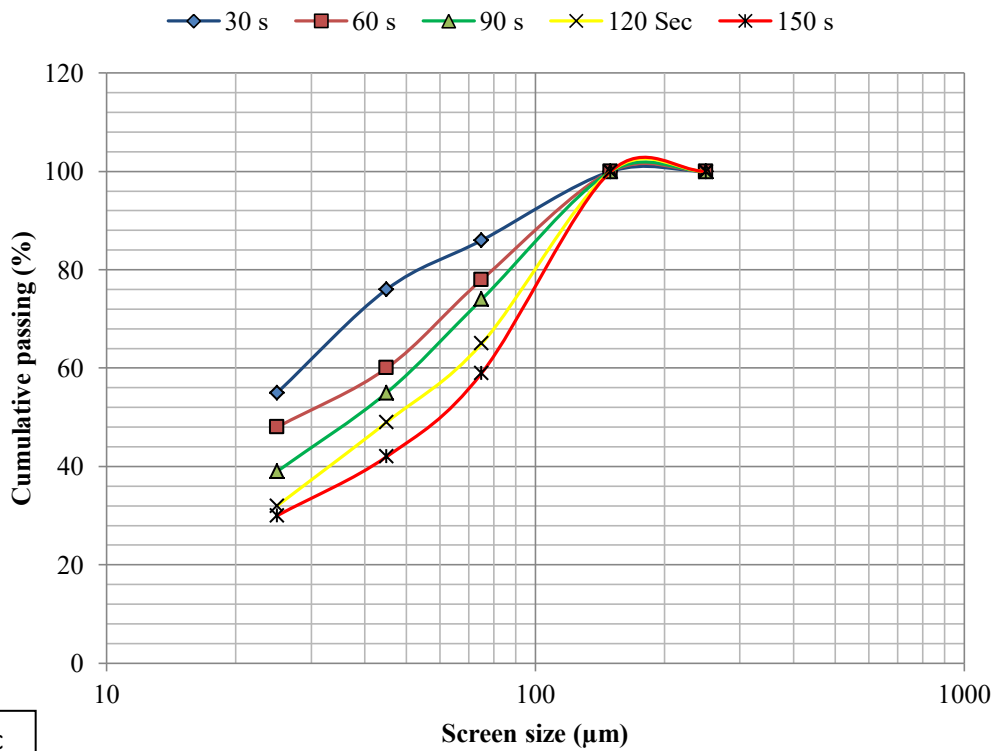
slurry solid concentration and mill discharge end opening time. At 55% slurry solid concentration, and at 90 s discharge end opening time, the highest weight percentage of undersize particles squeezed from Chamber-1 to Chamber-2 due to the increased mill discharge end opening time increases the slurry volume collected in the Chamber-1. It is known that the volume of slurry collected in Chamber-1 is linearly proportional to the internal pressure created inside Chamber-1 during the squeezing process. Therefore, the increased internal pressure in Chamber-1 is due to the increased slurry volume collected increases the classifier disc squeezing performance due to the increased compressive force on the slurry.



a



b



c

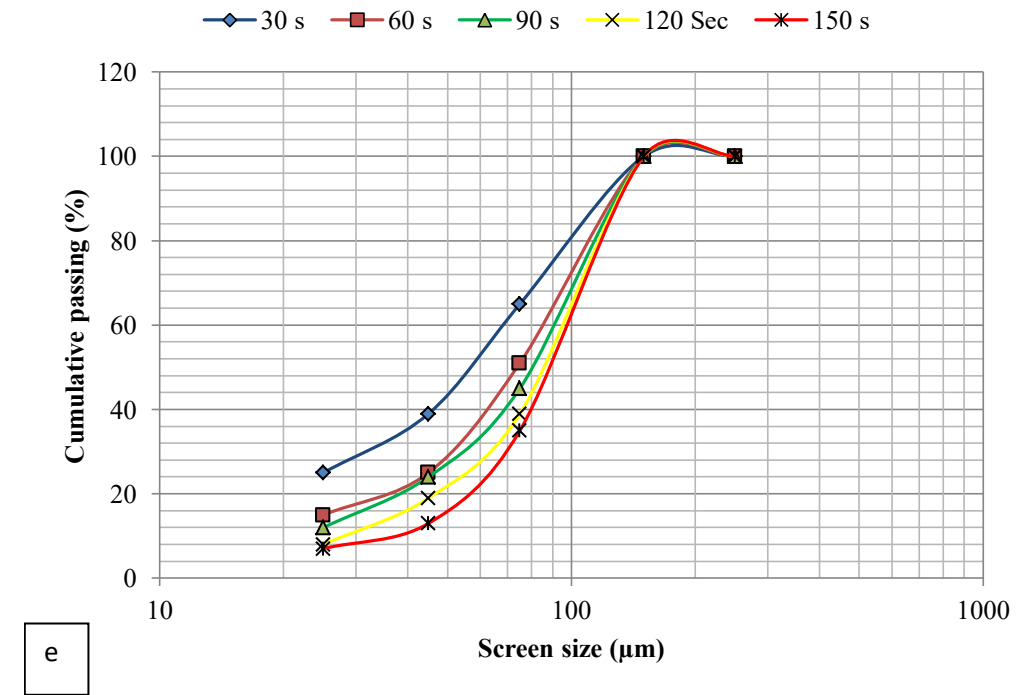
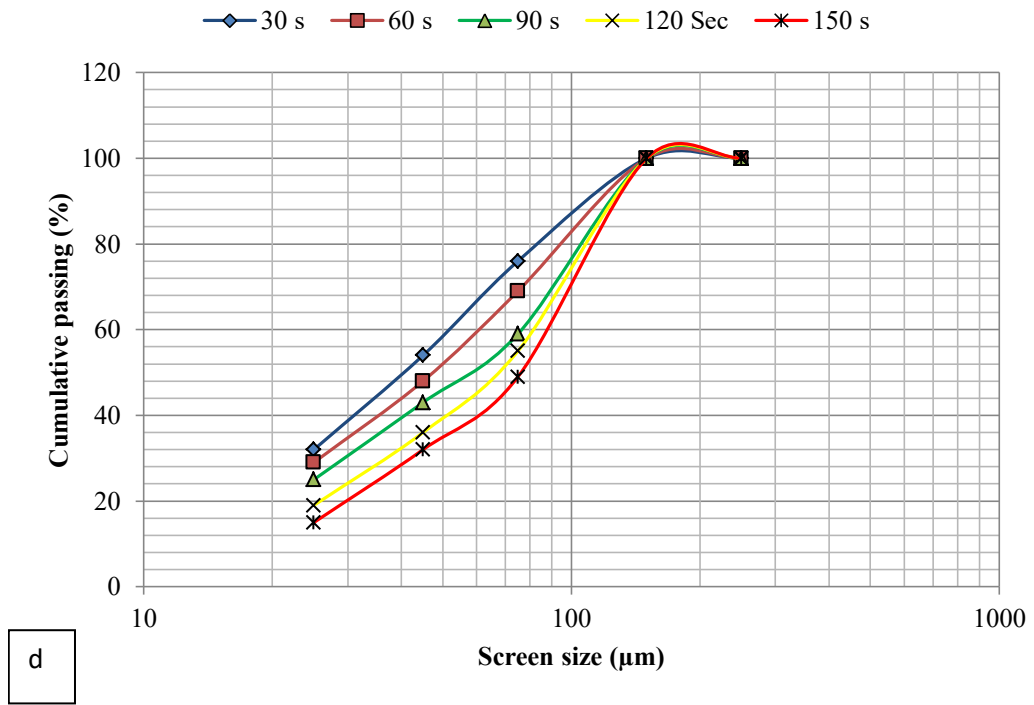


Fig. 5.67 Particle size analysis of collected product in Chamber-2– (a) for 55% solids, (b) for 60% solids, (c) for 65% solids, (d) for 70% solids, and (e) for 75% solids

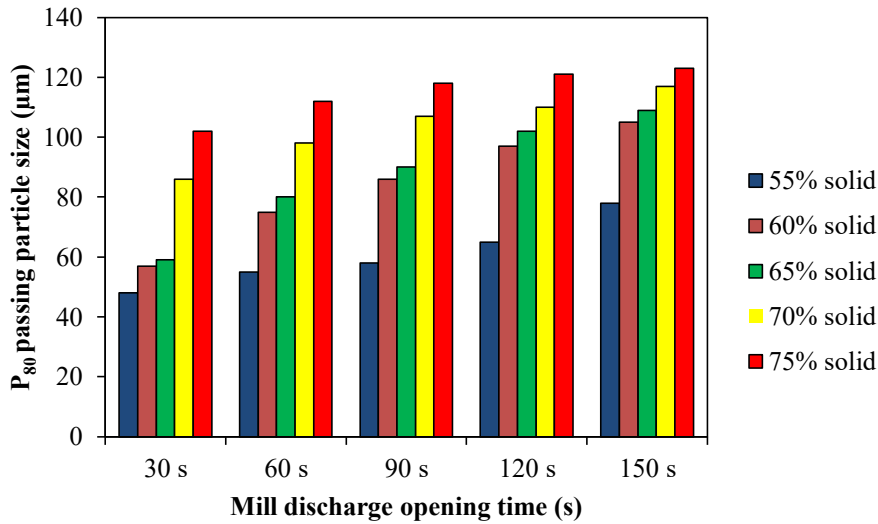


Fig. 5.68 P₈₀ passing percentage at different slurry solids percentages in Chamber-2 after squeezing in Chamber-1

From Fig. 5.69, with an increasing slurry solid concentration, the weight percentage of -150 µm particles squeezed from Chamber-1 to Chamber-2 decrease as it depends mainly on the slurry viscosity collected in Chamber-1. Hence, with an increasing slurry solids concentration, the viscosity of the slurry in Chamber-1 increases and decreases the Reynolds number 28. This effect will decrease the degree of turbulence in the slurry leading to an increase in adhesive forces between the particles in Chamber-1. Thus, the free particles in the slurry will reduce as slurry viscosity increases, resulting in decreased squeezing particles from Chamber-1 to Chamber-2, as seen in Fig. 5.69. Finally, classified particles collected in Chamber-2 can be directly used without any further processing for pellet making. Hence, a newly designed classifier can be used for both grinding and classification as a single unit.

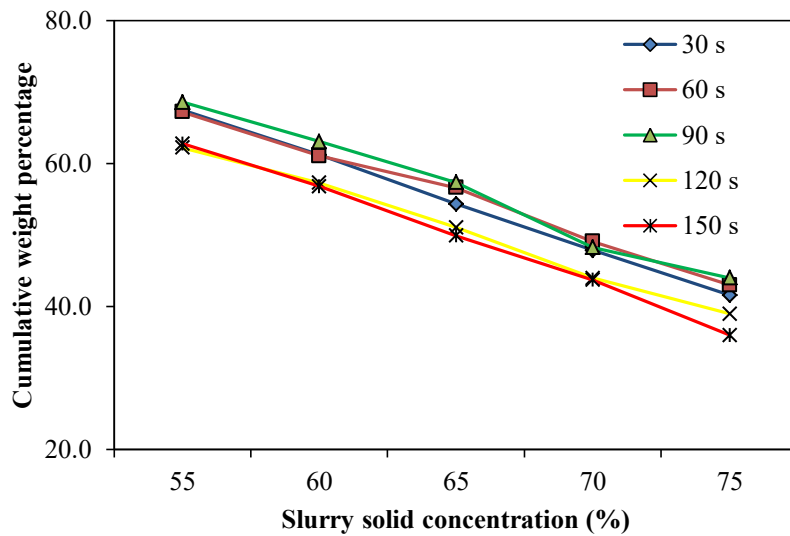


Fig. 5.69 Weight percentage of $-150 \mu\text{m}$ particles collected in Chamber-2 (after squeezing) at different slurry solid concentrations

5.6.3 Characterization analysis

Figure 5.70 shows the optical microscope images for feed particles and particles collected in Chamber-1 and 2. The feed particles show a good association of alumina and fine quartz grains within hematite. The association of fine quartz grains within hematite in the feed particles cannot be easily separated in the beneficiation process. Hence the feed particles were ground and classified in the newly designed ball mill. The particles collected after milling and classification were observed under an optical microscope, as shown in Fig.5.70b & c. The particles collected in Chamber-1 indicate that the association of fine quartz grains within hematite was reduced. But the classified product particles in Chamber-2 suggest that the association of fine quartz grains within hematite was reduced compared to the feed particles and particles collected in Chamber-1.

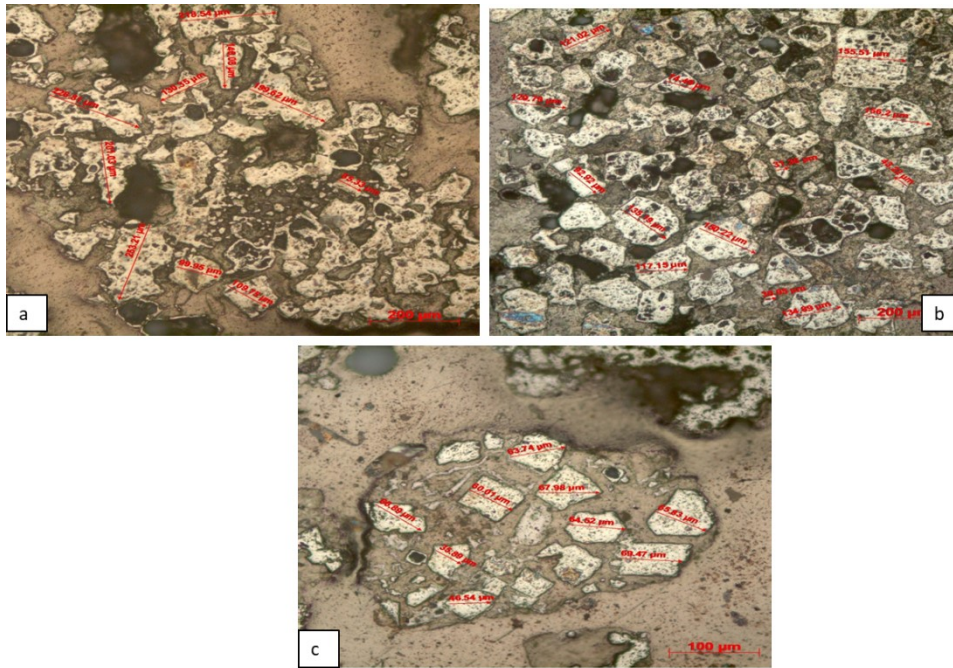


Fig. 5.70 Optical microscope images (a) for iron ore feed (b) for iron ore sample collected in Chamber-1, and (c) for iron ore sample collected in Chamber-2

Figure 5.71 shows the SEM and EDS images of iron ore feed particles, particles collected in Chamber-1, and particles collected in Chamber-2. Figure.5.71a shows the different size particles in the feed sample, and it consists of larger size particles compared to particles collected in Chamber-1 and 2 (Fig.5.71c,e). The SEM analysis of particles collected in Chamber-1 after classification indicates that the size of the particles reduced in the ball mill. Comparing Fig.5.71a with Fig.5.71c, e, particles collected in Chamber-1 and 2 show smaller particles than the feed particles due to milling. Also, Chamber-1 consists a maximum of +150 μm particles compared to -150 μm particles after the squeezing process. This analysis indicates that -150 μm particles are squeezed from Chamber -1 to Chamber-2. Figure.5.71e shows all particles are below -150 μm and indicating that the +150 μm particles are restricted to Chamber-1. The analysis suggests that the particles are reduced in the ball mill, and reduced particles are successfully classified in the classifier section.

The EDS analysis from Fig.5.71b shows the silica and alumina in large quantities than the iron element in the selected area, observed from their peaks intensity. This

represents that the iron is associated with silica and alumina. Also, from Fig. 5.71f, the iron element shows a large quantity in peak intensity than the silica and alumina elements. The EDS analysis represents that reducing particle size will reduce the association of iron with alumina and silica. The EDS and optical microscope analysis indicate that with the ball milling, hematite's liberation takes place from locked quartz and can be easily separated in the downstream process.

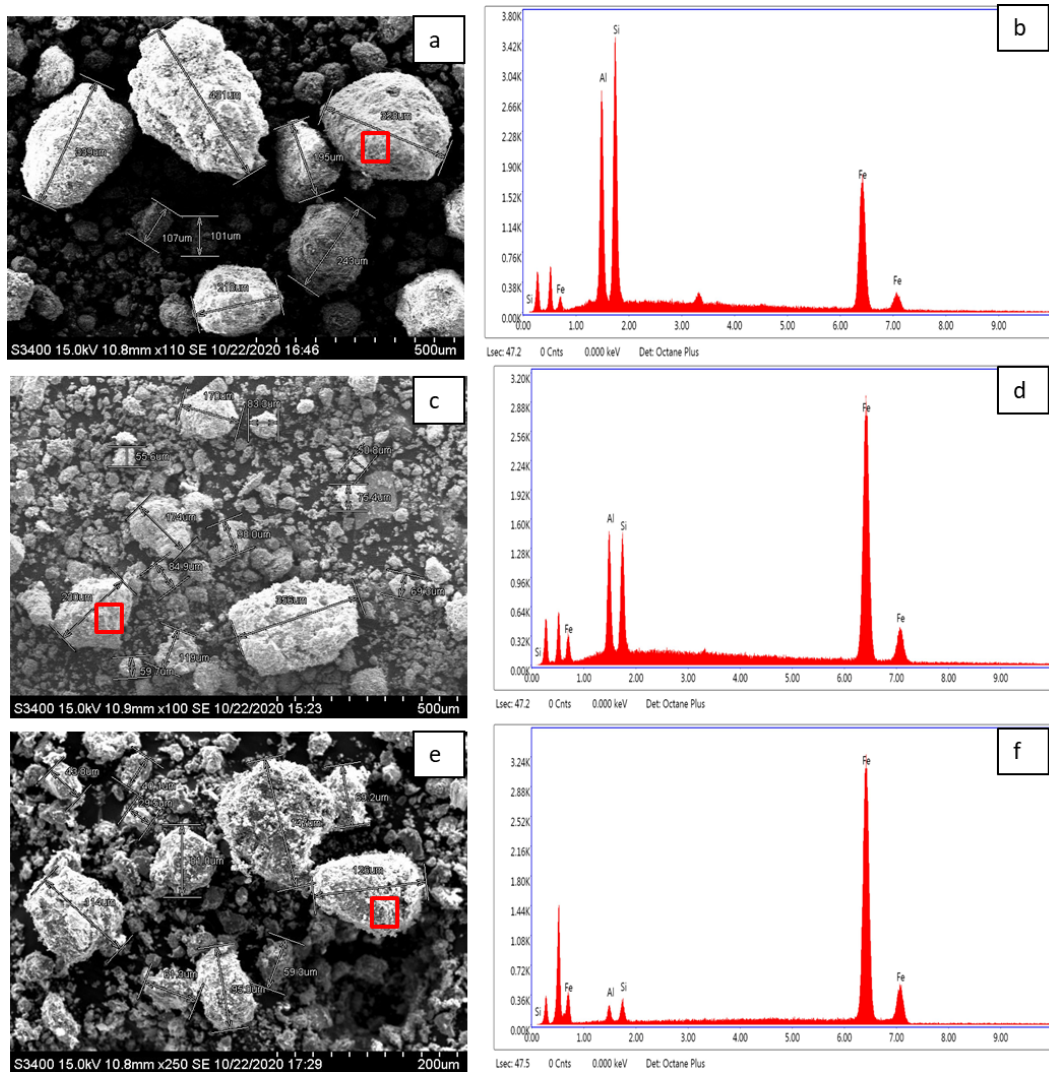


Fig. 5.71 SEM with EDS images (a) SEM image of the iron ore feed (b) EDS image of the iron ore feed (c) SEM image of the iron ore sample collected in Chamber-1 (d) EDS image of the iron ore sample collected in Chamber-1 (e) SEM image of the iron ore sample collected in Chamber-2 and (f) EDS image of the iron ore sample collected in Chamber-2.

5.6.4 Effect of internal pressure created on particle size classification efficiency

The measurement of internal pressure created inside Chamber-1 before and after squeezing helps to understand the classifier disc squeezing performance. As the pressure gauge position in the classifier section plays a vital role in tapping the pressure created inside Chamber-1, it is connected at the top of Chamber-1, which is near the mill discharge end (Fig. 5.2). Initially, the internal pressure inside Chamber-1 was taped by moving the classifier disc from its parking position to the discharge end of the mill without slurry inside Chamber-1. The pressure created inside the Chamber-1 of classifier section was nil at the classifier disc parking position. As the classifier disc moves from the parking position to the mill discharge end, the pressure gauge reading gradually increased with the classifier disc movement to the mill discharge end. The pressure gauge records maximum pressure of 1.2 bars when the classifier disc reaches the discharge end of the mill in Chamber-1. This indicates that the air present in Chamber-1 is compressed as the classifier disc moves from the parking position to the mill discharge end. The pressure gauge reading represents that the compressed air inside Chamber-1 generates internal pressure, which further squeezes the slurry. Figure 5.72 indicates the pressure created in Chamber-1 (after squeezing) at different slurry solid concentrations and at varying mill discharge end closing time. Also, comparing squeezing of classifier disc in Chamber-1 with and without slurry, the pressure created (>1.2 bar) in Chamber-1 while squeezing with slurry is greater than the pressure created (<1.2 bar) without a slurry. This pressure difference in Chamber-1 suggests that semi-liquid-solid media in Chamber-1 generates higher internal pressure than the air media. Hence, for the classifier section of optimum operation, it is essential to record the pressure generated during squeezing.

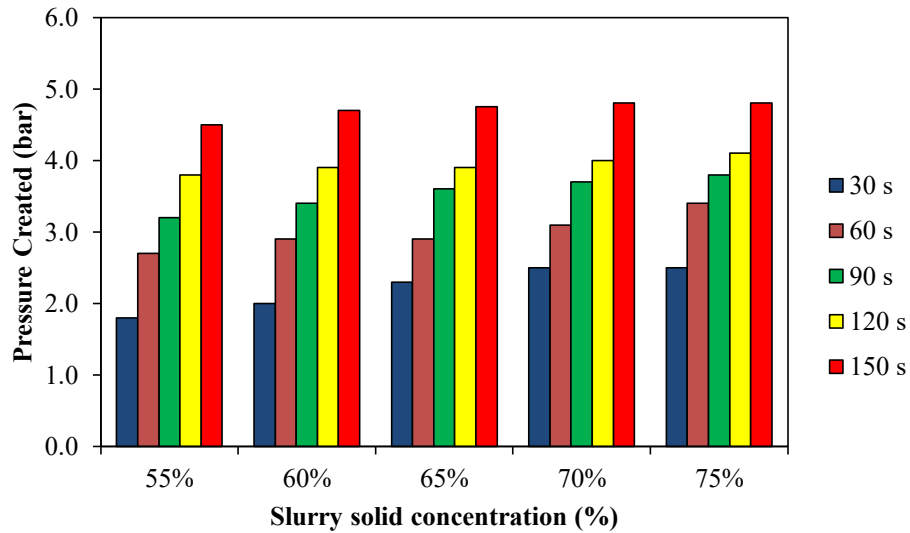


Fig. 5.72 Pressure created in Chamber-1 (after squeezing) at different slurry solid concentrations for varying the mill discharge end closing time

The classification efficiency of the classifier disc depends on the amount of pressure-induced inside Chamber-1 of classifier section. It is observed with increased slurry feed solid concentration to the ball mill from 55% to 75% reduces the squeezing efficiency from 84.8% to 57.8%. The results indicate that a decrease in the squeezing efficiency by 19.6% was observed for a solid slurry concentration of 75% compared with 55%. Even though the pressure created in Chamber-1 is high at 75% slurry solid concentration, the classifier disc classification efficiency is less compared with 55% slurry solid concentration. Since, at 75% slurry solid concentration, the slurry with high viscosity will be collected from ball mill to Chamber-1 of classifier section, squeezing of this slurry with classifier disc will clog the classifier disc screen. Also, as the classifier disc moves from parking position to discharge end of the mill, the slurry present in Chamber-1 will be subjected to high compressive forces. Due to the screen clogging and high compressive forces inside Chamber-1, there may be very less provision for the pressure to release from chamber-1. Hence, high internal pressure is created inside Chamber-1 of classifier section when squeezing of slurry with 75% slurry solid concentration. Further, with an increasing slurry solids concentration, particle segregations near the screen increases. This effect further increases in screen clogging and decreases the classifier disc squeezing performance. Hence, the

classifier disc squeezing efficiency is low at high slurry solids concentrations than at low slurry solid concentrations.

The mill discharge end closing time will also affect the classifier disc squeezing efficiency, as shown in Fig. 5.73. It is noted that when squeezing of slurry at different discharge end closing time with 55% solid concentration, the pressure gauge records different internal pressure. The pressure gauge also records high internal pressure at 150 s compared to 30 s discharge end closing time. As the discharge end is opened for a short duration, the volume of slurry collected in the stationary section (Chamber-1) is less compared with the discharge end open for a longer period. Even though, at 150 s discharge end open time, the internal pressure created in Chamber-1 is high at 75% slurry solid concentration compared to 55%. The classifier disc squeezing efficiency is more at 55% slurry solid concentration compared to 75%, because the slurry with 55% slurry solid concentration (low viscosity slurry) consists of majority free particles compared to the slurry with 75% slurry solid concentration (high viscosity slurry). Therefore, the slurry with lower viscosity can be easily squeezed from Chamber-1 to Chamber-2, because the resistance between the particles to particles and particles to the classifier disc screen is less. Hence, the maximum squeezing efficiency was obtained when the classifier disc squeezes the slurry with 55% solid concentration at 150 s discharge end closing time. Finally, it can be concluded that the classifier disc squeezing efficiency depends on the viscosity of the slurry in Chamber-1 and the volume of the slurry collected in Chamber-1.

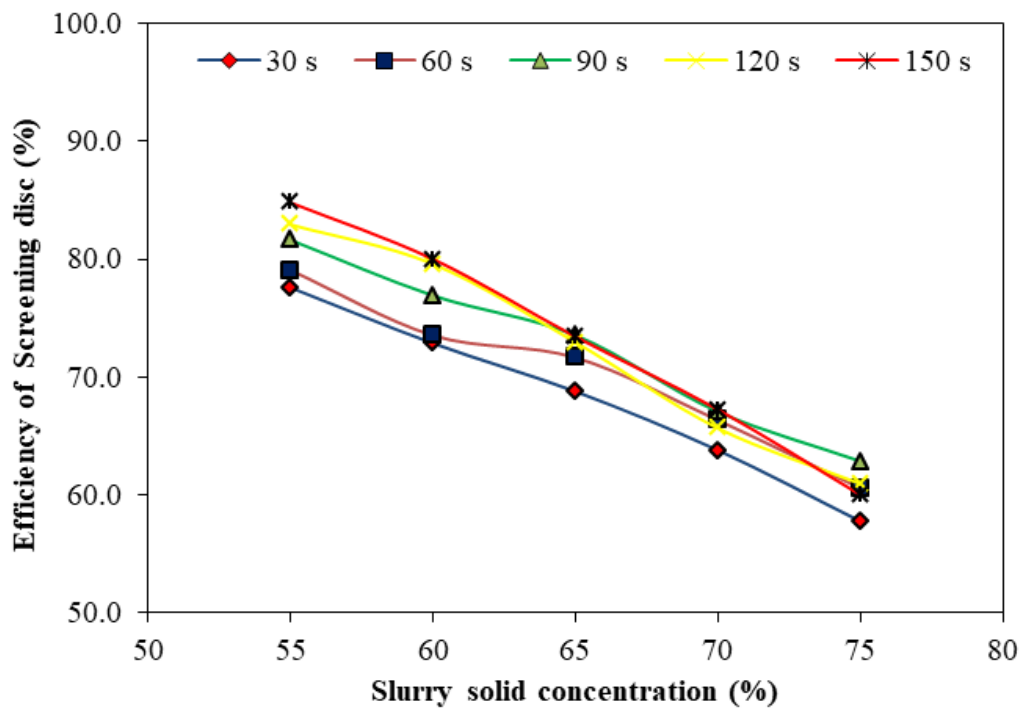


Fig. 5.73 Squeezing efficiency of disc at different slurry solid concentrations

The fine particles ($-150 \mu\text{m}$) collected in Chamber-2 after squeezing show that, the classifier completely restricts coarser size particles to Chamber-1. This indicates that, the fine particle collected in Chamber-2 can be directly used in downstream process without any further processing. Also, as classification system recirculates fewer amounts of fines to the mill, which reduces the over grinding of fine particle to ultra-fine particles in the mill which ultimately reduces the energy utilization for grinding. So, the new ball mill hydro-classification unit can be used as a single unit to grind and classify the desired particle size.

CHAPTER 6

6 CONCLUSIONS AND RECOMMENDATIONS FOR FUTURE WORK

6.1 Conclusions

Based on the experimental investigations carried out for the development of Hydro-Squeeze Classifier Assisted Grinding Ball Mill for Narrow Size Particle Separation, following conclusions are arrived on below aspects:

In this research, a new ball mill hydro-squeeze classifier was designed, fabricated and tested to overcome drawbacks of existing ball mill to obtain desired particle size for varying iron ore sample. HSHA, LSHA, and LSLA iron ore samples were selected for testing the performance of new ball mill hydro-squeeze classifier. The comparative analysis was conducted for the newly designed discharge end of the mill with and without lifters for iron ore size reduction and particle size classification. It was found that the slurry solids concentration has a significant effect on the particle size reduction and classification. The mill with high slurry solids concentration reduces the particle size and discharges coarse particles to the classification section.

The discharge end without lifter arrangement led to a higher recirculating load of 34% when the mill was operated at 70% critical speed. At the same operating speed, the discharge end with lifter arrangements (Case 2 and Case 3) led to 22–25% recirculation, which is lesser compared with discharge end without a lifter. The discharge end with lifter arrangement discharged maximum percentage of the desired particle size with minimum percentage of recirculating load to the mill when the mill was operated at 60% critical speed. The experimental results suggest that with appropriate design and placement of lifter in the discharge end, the output can attain the desired particle size distribution with the minimum recirculating load to the mill, ultimately decreasing the regrinding of ore in the mill.

Slurry solids concentration has a significant effect on the particle size reduction and classification. The mill with high slurry solids concentration reduces the particle size

and discharges coarse particles to the classification section. The squeezing of this slurry increases the recirculating load to the mill. The mill discharge end opening time has a significant effect on the size of the particles discharged. At a shorter duration opening of the mill discharge end, the mill increases the fine particles inside it, thereby increasing the mill discharge slurry viscosity. The squeezing of this slurry reduces the squeezing efficiency of the classifier disc. The optical microscopic and EDS analysis of the iron ore feed samples showed the association of fine quartz grains within hematite. The product sample collected in Chamber-1 and 2 indicated that the association of fine quartz grains within hematite was reduced compared to the feed sample. Optical microscopic and SEM shows that the particles are reduced in the ball mill, and reduced particles are successfully classified from Chamber-1 to Chamber-2.

The classification disc records the minimum classification efficiency of 57.8% at a solid slurry concentration of 75% at 30 s discharge end opening time. The squeezing of slurry at low volume in Chamber-1 with high viscosity leads to increased particle segregation and clogging near the screen, leading to a decreased squeezing efficiency of the classifier disc during the squeezing process. The classification disc records a maximum squeezing classification efficiency of 84.8% at a slurry solid concentration of 55% at 150 s discharge end opening time. The squeezing of low viscosity slurry at high volume in Chamber-1 increases internal pressure inside this chamber, which acts on the slurry to squeeze out maximum undersize particles from Chamber-1 to Chamber-2 without any resistance during the squeezing process.

The new ball mill hydro-classifier produces the desired particle size and classification for pellet feed making with the minimum recirculating load. The new equipment could be used as a single unit for particle size reduction, classification, and may also replace other classification units in the comminution circuits.

6.2 Recommendations for Future Work

- i. Experimental investigations can be carried out with different types of ores to evaluate the performance of newly designed ball mill hydro-squeeze classifier.

- ii. Multiple classifier discs can be used in classifier section of the ball mill hydro-squeeze classifier to obtain narrow size particles which can be used in downstream process like flotation where it helps to increase separation efficiency of flotation equipment.
- iii. Screw rod mechanism in the ball mill hydro-squeeze classifier can be replaced with hydraulic system, which helps to increase classification efficiency of classifier disc.
- iv. The control of the ball mill hydro-squeeze classifier can be further increased by automating the opening and closing of discharge end of the mill, and out let valves of classifier section.

REFERENCES

- Abazarpoor, A., and Halali, M. (2017). "Investigation on the particle size and shape of iron ore pellet feed using ball mill and HPGR grinding methods." *Physicochem. Probl. Miner. Process.*, 53(2), 908–919.
- Abouzeid, A. Z. M. A., Mika, T. S., Sastry, K. V., and Fuerstenau, D. W. (1974). "The influence of operating variables on the residence time distribution for material transport in a continuous rotary drum." *Powder Technol.*, 10(6), 273–288.
- Aguado, J. M. M., Velázquez, A. L. C., Tijonov, O. N., and Díaz, M. A. R. (2006). "Implementation of energy sustainability concepts during the comminution process of the Punta Gorda nickel ore plant (Cuba)." *Powder Technol.*, 170(3), 153–157.
- Ahmadi, R., and Shahsavari, S. (2009). "Procedure for determination of ball Bond work index in the commercial operations." *Miner. Eng.*, 22(1), 104–106.
- Angadi, S. I., Jeon, H. S., Mohanthy, A., Prakash, S., and Das, B. (2012). "Analysis of Wet High-Intensity Magnetic Separation of Low-Grade Indian Iron Ore using Statistical Technique." *Sep. Sci. Technol.*, 47(8), 1129–1138.
- Austin, L. G., and Bagga, P. (1981). "An analysis of fine dry grinding in ball mills." *Powder Technol.*, 28(1), 83–90.
- Ballantyne, G. R., Hilden, M., Peter, F., and Meer, V. Der. (2018). "Improved characterisation of ball milling energy requirements for HPGR products." *Miner. Eng.*, 116(January 2017), 72–81.
- Barkhuysen, N. J. (2009). "Implementing strategies to improve mill capacity and efficiency through classification by particle size only, with case studies." *South African Inst. Min. Metall. Base Met. Conf.*, 101–114.
- Bian, X., Wang, G., Wang, H., Wang, S., and Lv, W. (2017). "Effect of lifters and mill speed on particle behaviour , torque , and power consumption of a tumbling ball mill : Experimental study and DEM simulation." *Miner. Eng.*, 105, 22–35.

Bond FC. (1960). “Crushing and grinding calculations.” *Br. Chem. Eng.*, 80(378–391.), 543–548.

Bu, X., Chen, Y., Ma, G., Sun, Y., Ni, C., and Xie, G. (2019). “Differences in dry and wet grinding with a high solid concentration of coking coal using a laboratory conical ball mill: Breakage rate, morphological characterization, and induction time.” *Adv. Powder Technol.*, 30(11), 2703–2711.

Bu, X., Chen, Y., Ma, G., Sun, Y., Ni, C., and Xie, G. (2020). “Wet and dry grinding of coal in a laboratory-scale ball mill: Particle-size distributions.” *Powder Technol.*, 359, 305–313.

Chapman, N. A., Shackleton, N. J., Malysiak, V., and O’Connor, C. T. (2011). “The effect of using different comminution procedures on the flotation of Platinum-Group Minerals.” *Miner. Eng.*, 24(8), 731–736.

Chen, X., Peng, Y., and Bradshaw, D. (2014). “The effect of particle breakage mechanisms during regrinding on the subsequent cleaner flotation.” *Miner. Eng.*, 66–68, 157–164.

Chimwani, N., Glasser, D., Hildebrandt, D., Metzger, M. J., and Mulenga, F. K. (2013). “Determination of the milling parameters of a platinum group minerals ore to optimize product size distribution for flotation purposes.” *Miner. Eng.*, 43–44, 67–78.

Chimwani, N., Mulenga, F. K., Hildebrandt, D., Glasser, D., and Bwalya, M. M. (2015). “Use of the attainable region method to simulate a full-scale ball mill with a realistic transport model.” *Miner. Eng.*, 73, 116–123.

Cho, H., and Austin, L. G. (2002). “The equivalence between different residence time distribution models in ball milling.” 124, 112–118.

Cleary, P. W. (2001). “Charge behaviour and power consumption in ball mills : sensitivity to mill operating conditions , liner geometry and charge composition.” 79–114.

- Coello Velázquez, A. L., Menéndez-Aguado, J. M., and Brown, R. L. (2008). “Grindability of lateritic nickel ores in Cuba.” *Powder Technol.*, 182(1), 113–115.
- Danha, G., Hildebrandt, D., Glasser, D., and Bhondayi, C. (2015). “Application of basic process modeling in investigating the breakage behavior of UG2 ore in wet milling.” *Powder Technol.*, 279, 42–48.
- Deniz, V., Umucu, Y., and Çayirli, S. (2012). “Estimation of the Bond Grindability Index From the Sink-Float Test Data of Two Different Particulate Pumices Estimation of the Bond Grindability Index From the Sink-Float Test Data of Two Different Particulate Pumices.” 6351.
- Devasahayam, S. (2015). “Predicting the liberation of sulfide minerals using the breakage distribution function.” *Miner. Process. Extr. Metall. Rev.*, 36(2), 136–144.
- Djordjevic, N., Shi, F. N., and Morrison, R. (2004). “Determination of lifter design , speed and filling effects in AG mills by 3D DEM.” 17, 1135–1142.
- Donskoi, E., Suthers, S. P., Fradd, S. B., Young, J. M., Campbell, J. J., Raynlyn, T. D., and Clout, J. M. F. (2007). “Utilization of optical image analysis and automatic texture classification for iron ore particle characterisation.” *Miner. Eng.*, 20(5), 461–471.
- Dueck, J., Farghaly, M., and Neesse, T. (2014). “The theoretical partition curve of the hydrocyclone.” *Miner. Eng.*, 62, 25–30.
- Dwarapudi, S., Devi, T. U., Mohan Rao, S., and Ranjan, M. (2008). “Influence of Pellet Size on Quality and Microstructure of Iron Ore Pellets.” *ISIJ Int.*, 48(6), 768–776.
- El-Shall, H., and Somasundaran, P. (1984). “Physico-chemical aspects of grinding: a review of use of additives.” *Powder Technol.*, 38(3), 275–293.
- Engneermg, P. (1990). “Graphical Assessment of a Random Breakage Model for Mineral Liberation.” 60, 83–97.

Eswaraiyah, C., Angadi, S. I., and Mishra, B. K. (2012). “Mechanism of particle separation and analysis of fish-hook phenomenon in a circulating air classifier.” *Powder Technol.*, 218, 57–63.

Frachon, M., and Cilliers, J. J. (1999). “A general model for hydrocyclone partition curves.” *Chem. Eng. J.*, 73(1), 53–59.

Fuerstenau, D. W., De, A., and Kapur, P. C. (2004). “Linear and nonlinear particle breakage processes in comminution systems.” *Int. J. Miner. Process.*, 74(SUPPL.).

Gao, P., Yuan, S., Han, Y., Li, Y., and Chen, H. (2017). “Experimental Study on the Effect of Pretreatment with High-Voltage Electrical Pulses on Mineral Liberation and Separation of Magnetite Ore.” *Minerals*, 7(9), 153.

Gilvarry, J. J., and Bergstrom, B. H. (1961). “Fracture of brittle solids. ii. Distribution function for fragment size in single fracture (Experimental).” *J. Appl. Phys.*, 32(3), 400–410.

Gupta, A., and Yan, D. S. (2016). “Introduction to Mineral Processing Design and Operation.” *Elsevier*.

Gupta, V. K., and Hussain, M. (2017). “Estimation of the Specific Energy Requirement for Size Reduction of Solids in Ball Mills.” *Trans. Indian Inst. Met.*, 70(2), 303–311.

Gupta, V. K., and Patel, J. P. (2015). “A one-parameter model for describing the residence time distribution of closed continuous flow systems characterized by nonlinear reaction kinetics : Rod and ball mills.” *Powder Technol.*, 274, 163–172.

Gutiérrez, A., Ahues, D., González, F., and Merino, P. (2018). “Simulation of Material Transport in a SAG Mill with Different Geometric Lifter and Pulp Lifter Attributes Using DEM.”

Hacıfazlıoğlu, H., and Korkmaz, A. V. (2019). “Performance comparison of stirred media mill and ball (BOND) mill in bauxite grinding bauxite grinding.” *Part. Sci.*

Technol., 0(0), 1–5.

Hagni, A. M. (2008). “Phase identification, phase quantification, and phase association determination utilizing automated mineralogy technology.” *Jom*, 60(4), 33–37.

Hanumanthappa, H., Vardhan, H., Mandela, G. R., Kaza, M., Sah, R., and Shanmugam, B. K. (2020a). “Estimation of Grinding Time for Desired Particle Size Distribution and for Hematite Liberation Based on Ore Retention Time in the Mill.” *Mining, Metall. Explor.*, 37(2), 481–492.

Hanumanthappa, H., Vardhan, H., Mandela, G. R., Kaza, M., Sah, R., and Shanmugam, B. K. (2020b). “A comparative study on a newly designed ball mill and the conventional ball mill performance with respect to the particle size distribution and recirculating load at the discharge end.” *Miner. Eng.*, 145(October 2019), 106091.

Hanumanthappa, H., Vardhan, H., Mandela, G. R., Kaza, M., Sah, R., Shanmugam, B. K., and Pandiri, S. (2020c). “Investigation on Iron Ore Grinding based on Particle Size Distribution and Liberation.” *Trans. Indian Inst. Met.*, 73, 1853–1866.

Harish, H., Vardhan, H., Raj, M. G., Kaza, M., Sah, R., Sinha, A., and Kumar, S. B. (2020). “Investigation of iron ores based on the bond grindability test.” *AIP Conf. Proc.*, 040006.

Hassanzadeh, A., and Hassanzadeh, A. (2018). “A new statistical view to modeling of particle residence time distribution in full-scale overflow ball mill operating in closed-circuit full-scale overflow ball mill operating in closed-circuit.” *Geosystem Eng.*, 9328, 1–11.

He, F., Wang, H., Wang, J., Li, S., Fan, Y., and Xu, X. (2020). “Experimental study of mini-hydrocyclones with different vortex finder depths using Particle Imaging Velocimetry.” *Sep. Purif. Technol.*, 236, 116296.

Hlungwani, O., Rikhotso, J., Dong, H., and Moys, M. H. (2003). “Further validation of DEM modeling of milling : effects of liner profile and mill speed.” 16, 993–998.

Hoal, K. O., Stammer, J. G., Appleby, S. K., Botha, J., Ross, J. K., and Botha, P. W. (2009). “Research in quantitative mineralogy: Examples from diverse applications.” *Miner. Eng.*, 22(4), 402–408.

Horst, W. E., and E. J. F. (1998). . “Mathematical modeling of a continuous comminution process.’ Trans. SME-AIME 252 (1972): 160-167.” *Miner. Eng.*, 11(12), 1143–1160.

Horst, and Freeh. (1972). “Mathematical modeling of a continuous comminution process.” *Trans. SME-AIME*, 252, 160–167.

Jankovic, A., Suthers, S., Wills, T., and Valery, W. (2015). “Evaluation of dry grinding using HPGR in closed circuit with an air classifier.” *Miner. Eng.*, 71, 133–138.

Klimpel, L. G. A. and R. C. (1989). “An investigation of wet grinding in a laboratory overflow ball mill.” *Miner. Metall. Process.*, 6(February), 1–19.

Kotake, N., Kawaguchi, T., Koizumi, H., and Kanda, Y. (2004). “A fundamental study of dry and wet grinding in bending tests on glass - Effect of repeated impact on fracture probability.” *Miner. Eng.*, 17(11–12), 1281–1285.

Kotake, N., Kuboki, M., Kiya, S., and Kanda, Y. (2011). “Influence of dry and wet grinding conditions on fineness and shape of particle size distribution of product in a ball mill.” *Adv. Powder Technol.*, 22(1), 86–92.

Kraipech, W., Chen, W., Parma, F. J., and Dyakowski, T. (2002). “Modelling the fish-hook effect of the flow within hydrocyclones.” *Int. J. Miner. Process.*, 66(1–4), 49–65.

Kraipech, W., Nowakowski, A., Dyakowski, T., and Suksangpanomrung, A. (2005). “An investigation of the effect of the particle-fluid and particle-particle interactions on the flow within a hydrocyclone.” *Chem. Eng. J.*, 111(2–3), 189–197.

Kumar, C. R., Tripathy, S., and Rao, D. S. (2009). “Characterisation and Pre-

concentration of Chromite Values from Plant Tailings Using Floatex Density Separator.” *J. Miner. Mater. Charact. Eng.*, 08(05), 367–378.

Kumar, R. (2017). “Characterisation of Minerals and Ores: On the Complementary Nature of Select Techniques and Beyond.” *Trans. Indian Inst. Met.*, 70(2), 253–277.

Lane, G. R., Martin, C., and Pirard, E. (2008). “Techniques and applications for predictive metallurgy and ore characterization using optical image analysis.” *Miner. Eng.*, 21(7), 568–577.

Latchireddi, S., and Morrell, S. (2003). “Slurry flow in mills : grate-pulp lifter discharge systems (Part 2).” *Miner. Eng.*, 16, 635–642.

Latchireddi, S. R., and Morrell, S. (1997). “A laboratory study of the performance characteristics of mill pulp lifters.” *Miner. Eng.*, 10(11), 1233–1244.

Magdalinovic, N., Trumic, M., Trumic, G., Magdalinovic, S., and Trumic, M. (2012). “Determination of the Bond work index on samples of non-standard size.” *Int. J. Miner. Process.*, 114–117, 48–50.

Majumder, A. K., Shah, H., Shukla, P., and Barnwal, J. P. (2007). “Effect of operating variables on shape of ‘fish-hook’ curves in cyclones.” *Miner. Eng.*, 20(2), 204–206.

Majumder, A. K., Yerriswamy, P., and Barnwal, J. P. (2003). “The ‘fish-hook’ phenomenon in centrifugal separation of fine particles.” *Miner. Eng.*, 16(10), 1005–1007.

Makokha, A. B., and Moys, M. H. (2007). “Effect of cone-lifters on the discharge capacity of the mill product : Case study of a dry laboratory scale air-swept ball mill.” 20, 124–131.

Markauskas, D., and Kruggel-Emden, H. (2019). “Coupled DEM-SPH simulations of wet continuous screening.” *Adv. Powder Technol.*, 30(12), 2997–3009.

Mishra, B. K., and Rajamai, R. K. (1994). “Simulation of charge motion in ball mills . Part 2 : numerical simulations.” 40, 187–197.

Mishra, B. K., and Rajamani, R. K. (1992). "The discrete element method for the simulation of ball mills." 16(March), 598–604.

Mori, H., Mio, H., Kano, J., and Saito, F. (2004). "Ball mill simulation in wet grinding using a tumbling mill and its correlation to grinding rate." *Powder Technol.*, 143–144, 230–239.

Morrell, S. (2004). "An alternative energy-size relationship to that proposed by Bond for the design and optimisation of grinding circuits." *Int. J. Miner. Process.*, 74(1–4), 133–141.

Morrell, S. (2008). "A method for predicting the specific energy requirement of comminution circuits and assessing their energy utilisation efficiency." *Miner. Eng.*, 21(3), 224–233.

Morrell, S., and Stephenson, I. (1996). "Slurry discharge capacity of autogenous and semi-autogenous mills and the effect of grate design." *Int. J. Miner. Process.*, 46, 53–72.

Mosher, J. B., and Tague, C. B. (2001). "Conduct and precision of Bond grindability testing." *Miner. Eng.*, 14(10), 1187–1197.

Moys, M., and Smit, I. (1998). "The effect of discharge arrangement, load volume, slurry rheology and mill speed on power and slurry hold-up in rotary mills." *Chem. Technol.*, 27–31.

Mulenga, F. K., and Chimwani, N. (2013). "Introduction to the use of the attainable region method in determining the optimal residence time of a ball mill." *Int. J. Miner. Process.*, 125, 39–50.

Mulenga, F. K., Mkonde, A. A., and Bwalya, M. M. (2016). "Effects of load filling , slurry concentration and feed flowrate on the attainable region path of an open milling circuit." 89, 30–41.

Mulenga, F. K., and Moys, M. H. (2014). "Effects of slurry filling and mill speed on

the net power draw of a tumbling ball mill.” *Miner. Eng.*, 56, 45–56.

Napier-Munn, T. J., and Lynch, A. J. (1992). “The modelling and computer simulation of mineral treatment processes - current status and future trends.” *Miner. Eng.*, 5(2), 143–167.

Napier-Munn, T. J., Morrell, S., Morrison, R. D., and Kojovic, T. (1996). “Mineral Comminution Circuits Their Operation and Optimisation.” <<https://espace.library.uq.edu.au/view/UQ:357349>> (Feb. 16, 2021).

Narayanan, S. S., and Whiten, W. J. (1988). “Determination of comminution characteristics from single-particle breakage tests and its application to ball-mill scale-up.” *Trans. Inst. Min. Metall.*, (97), C115–C124.

Nasr-El-Din, H. A., Afacan, A., Masliyah, J. H., and Foster, J. (1992). “Slurry transport in horizontal rotary drums with an end-constriction.” *Powder Technol.*, 71(3), 251–261.

Nkwanyana, S., and Loveday, B. (2018). “Addition of pebbles to a ball-mill to improve grinding efficiency – Part 2.” *Miner. Eng.*, 128(August), 115–122.

Nomura, S. (2012). “Dispersion properties for residence time distributions in tumbling ball mills.” *Powder Technol.*, 222, 37–51.

Petrakis, E., Stamboliadis, E., and Komnitsas, K. (2017). “Evaluation of the relationship between energy input and particle size distribution in comminution with the use of piecewise regression analysis.” *Part. Sci. Technol.*, 35(4), 479–489.

Powell, M. S., Morrell, S., and Latchireddi, S. (2001). “Developments in the understanding of South African style SAG mills.” *Miner. Eng.*, 14(10), 1143–1153.

Rao, S. S., Rao, D. S., Prabhakar, S., Raju, G. B., and Kumar, T. V. V. (2015). “Mineralogy and Geochemistry of A Low Grade Iron Ore Sample from Bellary-Hospet Sector, India and Their Implications on Beneficiation.” *J. Miner. Mater. Charact. Eng.*, 08(02), 115–132.

Rath, S. S., Dhawan, N., Rao, D. S., Das, B., and Mishra, B. K. (2016). “Beneficiation studies of a difficult to treat iron ore using conventional and microwave roasting.” *Powder Technol.*, 301, 1016–1024.

Rezaeizadeh, M., Fooladi, M., Powell, M. S., and Mansouri, S. H. (2010). “Experimental observations of lifter parameters and mill operation on power draw and liner impact loading.” *Miner. Eng.*, 23(15), 1182–1191.

Rodríguez, B. Á., García, G. G., Coello-Velázquez, A. L., and Menéndez-Aguado, J. M. (2016). “Product size distribution function influence on interpolation calculations in the Bond ball mill grindability test.” *Int. J. Miner. Process.*, 157, 16–20.

Rogers, R. S. C., and Austin, L. G. (1984). “Residence time distributions in ball mills.” *Part. Sci. Technol.*, 2(2), 191–209.

Roldán-Villasana, E. J., Williams, R. A., and Dyakowski, T. (1993). “The origin of the fish-hook effect in hydrocyclone separators.” *Powder Technol.*, 77(3), 243–250.

Saeidi, N., Noaparast, M., Azizi, D., Aslani, S., and Ramadi, A. (2013). “A developed approach based on grinding time to determine ore comminution properties.” *J. Min. Environ.*, 4(2), 105–112.

Shanmugam, B. K., Vardhan, H., Raj, M. G., Kaza, M., Sah, R., and H, H. (2019a). “Screening performance of coal of different size fractions with variation in design and operational flexibilities of the new screening machine.” *Energy Sources, Part A Recover. Util. Environ. Eff.*, 00(00), 1–9.

Shanmugam, B. K., Vardhan, H., Raj, M. G., Kaza, M., Sah, R., and H, H. (2019b). “Evaluation of a new vibrating screen for dry screening fine coal with different moisture contents.” *Int. J. Coal Prep. Util.*, 0(0), 1–10.

Shanmugam, B. K., Vardhan, H., Raj, M. G., Kaza, M., Sah, R., and Hanumanthappa, H. (2020). “Experimentation and statistical prediction of screening performance of coal with different moisture content in the vibrating screen.” *Int. J. Coal Prep. Util.*, 1–14.

- Shanmugam, B. K., Vardhan, H., Raj, M. G., Kaza, M., Sah, R., and Hanumanthappa, H. (2021). "Artificial neural network modeling for predicting the screening efficiency of coal with varying moisture content in the vibrating screen." *Int. J. Coal Prep. Util.*, 1–19.
- Shoji, K., Austin, L. G., Smaila, F., Brame, K., and Luckie, P. T. (1982). "Further studies of ball and powder filling effects in ball milling." *Powder Technol.*, 31(1), 121–126.
- Shoji, K., Lohrasb, S., and Austin, L. G. (1980). "The variation of breakage parameters with ball and powder loading in dry ball milling." *Powder Technol.*, 25(1), 109–114.
- Sichalwe, K., Govender, I., and Mainza, A. N. (2011). "Characterising porosity of multi-component mixtures in rotary mills." *Miner. Eng.*, 24(3–4), 276–281.
- Singh, V., Dixit, P., Venugopal, R., and Venkatesh, K. B. (2018). "Ore pretreatment methods for grinding: journey and prospects." *Miner. Process. Extr. Metall. Rev.*, 40(1), 1–15.
- Soleymani, M. M., Fooladi, M., and Rezaeizadeh, M. (2016). "Effect of slurry pool formation on the load orientation, power draw, and impact force in tumbling mills." *Powder Technol.*, 287, 160–168.
- Solomon, N., Becker, M., Mainza, A., Petersen, J., and Franzidis, J. P. (2011). "Understanding the influence of HPGR on PGM flotation behavior using mineralogy." *Miner. Eng.*, 24(12), 1370–1377.
- Srivastava, M. P., Pan, S. K., Prasad, N., and Mishra, B. K. (2001). "Characterization and processing of iron ore fines of Kiruburu deposit of India." *Int. J. Miner. Process.*, 61(2), 93–107.
- Sutherland, D. N., and Gottlieb, P. (1991). "Application of automated quantitative mineralogy in mineral processing." *Miner. Eng.*, 4(7–11), 753–762.

Tangsathitkulchai, C. (2002). “Acceleration of particle breakage rates in wet batch ball milling.” *Powder Technol.*, 124(1–2), 67–75.

Tangsathitkulchai, C., and Austin, L. G. (1985). “The effect of slurry density on breakage parameters of quartz, coal and copper ore in a laboratory ball mill.” *Powder Technol.*, 42(3), 287–296.

Tangsathitkulchai, C., and Austin, L. G. (1989). “Slurry density effects on ball milling in a laboratory ball mill.” *Powder Technol.*, 59(4), 285–293.

Tavares, L. M., Carvalho, R. M. De, and Guerrero, J. C. (2012). “Simulating the Bond rod mill grindability test.” *Miner. Eng.*, 26(1), 99–101.

Tue Nenu, R. K., and Yoshida, H. (2009). “Comparison of separation performance between single and two inlets hydrocyclones.” *Adv. Powder Technol.*, 20(2), 195–202.

Ulusoy, U., and Igathinathane, C. (2016). “Particle size distribution modeling of milled coals by dynamic image analysis and mechanical sieving.” *Fuel Process. Technol.*, 143, 100–109.

Umadevi, T., Kumar, M. G. S., Kumar, S., Prasad, C. S. G., and Ranjan, M. (2013). “Influence of raw material particle size on quality of pellets Influence of raw material particle size on quality of pellets.” *Ironmak. Steelmak.*, 35(5), 327–337.

Vakamalla, T. R., Koruprolu, V. B. R., Arugonda, R., and Mangadoddy, N. (2017). “Development of novel hydrocyclone designs for improved fines classification using multiphase CFD model.” *Sep. Purif. Technol.*, 175, 481–497.

Vinnett, L., Contreras, F., Lazo, A., Morales, M., Díaz, F., and Waters, K. E. (2018). “The use of radioactive tracers to measure mixing regime in semi-autogenous grinding mills.” *Miner. Eng.*, 115(October 2017), 41–43.

Vizcarra, T. G., Wightman, E. M., Johnson, N. W., and Manlapig, E. V. (2010). “The effect of breakage mechanism on the mineral liberation properties of sulphide ores.”

Miner. Eng., 23(5), 374–382.

Wang, C., Chen, J., Shen, L., Mainul, M., Ge, L., and Evans, M. (2018). “Inclusion of screening to remove fish-hook effect in the three products hydro-cyclone screen (TPHS).” *Miner. Eng.*, 122(March), 156–164.

Weerasekara, N. S., and Powell, M. S. (2014). “Performance characterisation of AG / SAG mill pulp lifters using CFD techniques.” *Miner. Eng.*, 63, 118–124.

Yang, J., Li, S., Chen, X., and Li, Q. (2010). “Disturbance rejection of ball mill grinding circuits using DOB and MPC.” *Powder Technol.*, 198(2), 219–228.

Yianatos, J. B., Lisboa, M. A., and Baeza, D. R. (2002). “Grinding capacity enhancement by solid concentration control of hydrocyclone underflow.” *Miner. Eng.*, 15(5), 317–323.

Yin, Z., Peng, Y., Zhu, Z., Ma, C., Yu, Z., and Wu, G. (2019). “Effect of mill speed and slurry filling on the charge dynamics by an instrumented ball.” *Adv. Powder Technol.*, 30(8), 1611–1616.

APPENDIX-I

LIST OF PUBLICATIONS BASED ON Ph.D RESEARCH WORK

1. Hanumanthappa, H., Vardhan, H., Mandela, G. R., Kaza, M., Sah, R., and Shanmugam, B. K. (2020b). “A comparative study on a newly designed ball mill and the conventional ball mill performance with respect to the particle size distribution and recirculating load at the discharge end.” *Minerals Engineering*, 145(1), 106091. <https://doi.org/10.1016/j.mineng.2019.106091> (SCI, Scopus) (Elsevier, Impact factor – **5.479**)
2. Hanumanthappa, H., Vardhan, H., Mandela, G. R., Kaza, M., Sah, R., and Shanmugam, B. K. (2020a). “Estimation of Grinding Time for Desired Particle Size Distribution and for Hematite Liberation Based on Ore Retention Time in the Mill.” *Mining, Metallurgy & Exploration*, 37(2), 481–492. <https://doi.org/10.1007/s42461-019-00167-8>. (SCI, Scopus) (Springer, Impact factor – **1.695**)
3. Hanumanthappa, H., Vardhan, H., Mandela, G. R., Kaza, M., Sah, R., Shanmugam, B. K., and Pandiri, S. (2020c). “Investigation on Iron Ore Grinding based on Particle Size Distribution and Liberation.” *Transactions of the Indian Institute of Metals*, 73, 1853–1866. <https://doi.org/10.1007/s12666-020-01999-5> (SCIE, Scopus) (Springer, Impact factor – **1.499**)
4. Harish, H., Vardhan, H., Raj, M. G., Kaza, M., Sah, R., Sinha, A., and Kumar, S. B. (2020). “Investigation of iron ores based on the bond grindability test.” *AIP Conf. Proc.*, 040006. (**Scopus**)
5. Harish, H., Vardhan, H., Raj, M. G., Kaza, M., Sah, R., and Kumar, S. B. (2019). “Ball mill performance study: A review.” *Proceedings of International*

Conference on Innovations and Emerging Trends in Mechanical Engineering, March 26-27.

6. Hanumanthappa, H., Vardhan, H., Mandela, G. R., Kaza, M., Sah, R., and Shanmugam, B. K. (2020). "Influence of crushed raw materials and crushed-sieved raw materials on grindability to obtain required product particle size distribution" 2nd International Conference on Opencast Mining Technology & Sustainability in association with IIT (BHU) and Springer Nature, December 13-14.

PATENT BASED ON Ph.D RESEARCH WORK

S. No	Title	Inventor(s)	Patent No.	Date and Country
1	System for material beneficiation involving hydro-squeeze classifier assisted grinding ball mill	Mr.Harish Hanumanthappa, Dr. Maruthiram Kaza, Dr. Harsha Vardhan, Dr.Govinda Raj Mandela, Dr. Rameshwar Sah, Mr. Abhishek Kumar, Dr. Arindam Roy Choudary, Mr. Chaitanya Naik, Mr. Suhas Nayak	Patent application number - TEMP/E-1/51796/2018-MUM Application No. 201821047543	15-12-2018 (Patent filled) 19-06-2020 (Patent published) 2022/08/26 Patent first examination report completed

APPENDIX-II

I. Fabrication Methods for New Ball Mill Hydro-Squeeze Classifier



Fig. I.1 Rolling of classifier shell



Fig. I.2 welding of classifier shell



Fig. I.3 Identification of cracks after welding in classifier shell

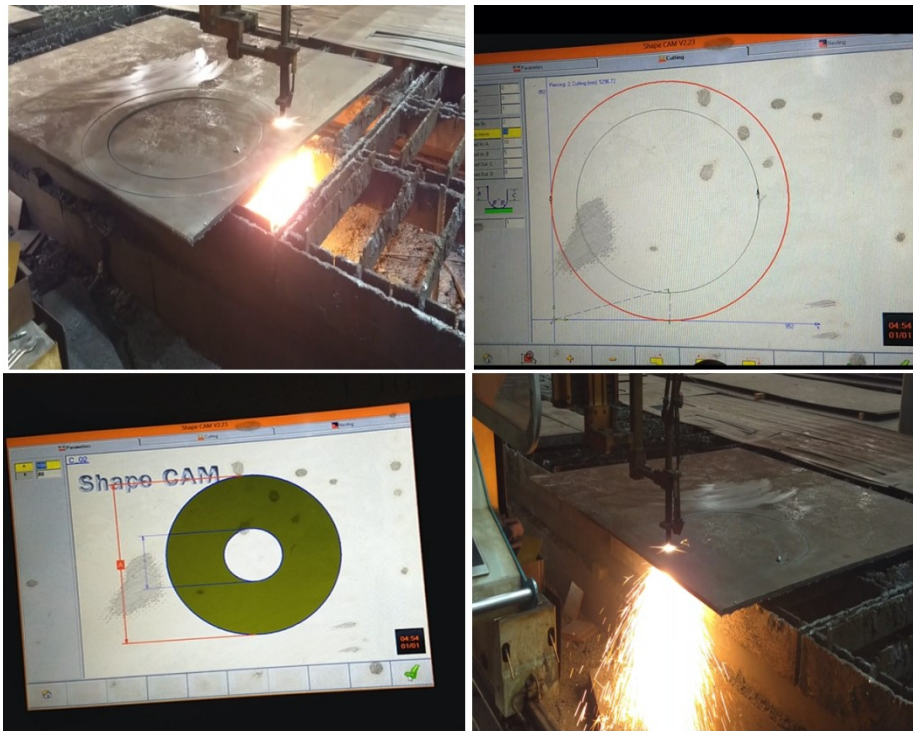


Fig. I.4 closing plate cutting for classifier shell by using oxy gas cutter



Fig. I.5 Supporting rings for classifier shell



Fig. I.6 Machining of internal surface of classifier shell



Fig. I.7 Drilling of out let valves in classifier shell by using magnetic drill machine



Fig. I.8 Machining of screw and guide rod



Fig. I.9 Spare parts



Fig. I.10 Machining of classifier disc



Fig. I.11 Assembly of classifier discs



Fig. I.12 Assembly of classifier section



Fig. I.13 Drive system for rotating drum



Fig. I.14 Assembly of rotating drum



Fig. I.15 Assembly of rotating drum and classifier shell

BIODATA

1. Name : Harish H
2. Father's Name : Hanumanthappa V
3. Date of Birth : 07-09-1986
4. Nationality : Indian
5. Marital Status : Married
6. Present Position : Research Scholar
7. Address for Communication : M Gollahalli (village), Chintamani (TQ),
Chikkabalapur (dist), Karnataka, India.
8. Mobile : +91-9535555832
9. E-mail : hari.harish86@gmail.com

10. Academic Qualifications:

Degree	University/ Board	Year of awarding degree
M.Tech (Machine Design)	NCET, Bangalore	2012
B. E (Mechanical Engineering)	NCET, Bangalore	2010

PUBLICATIONS

1. **Hanumanthappa, H.**, Vardhan, H., Mandela, G. R., Kaza, M., Sah, R., and Shanmugam, B. K. (2020a). "Estimation of Grinding Time for Desired Particle Size Distribution and for Hematite Liberation Based on Ore Retention Time in the Mill." Mining, Metall. Explor., 37(2), 481–492. **(SCI, Scopus)**
2. **Hanumanthappa, H.**, Vardhan, H., Mandela, G. R., Kaza, M., Sah, R., and Shanmugam, B. K. (2020b). "A comparative study on a newly designed ball mill and the conventional ball mill performance with respect to the particle

size distribution and recirculating load at the discharge end.” *Miner. Eng.*, 145(1), 106091. (SCIE, Scopus)

3. **Hanumanthappa, H.**, Vardhan, H., Mandela, G. R., Kaza, M., Sah, R., Shanmugam, B. K., and Pandiri, S. (2020c). “Investigation on Iron Ore Grinding based on Particle Size Distribution and Liberation.” *Trans. Indian Inst. Met.*, 73, 1853–1866. (SCIE, Scopus)
4. Shanmugam, B. K., Vardhan, H., Raj, M. G., Kaza, M., Sah, R., and **H, H.** (2019a). “Screening performance of coal of different size fractions with variation in design and operational flexibilities of the new screening machine.” *Energy Sources, Part A Recover. Util. Environ. Eff.*, 00(00), 1–9. (SCIE, Scopus)
5. Shanmugam, B. K., Vardhan, H., Raj, M. G., Kaza, M., Sah, R., and **H, H.** (2019b). “Evaluation of a new vibrating screen for dry screening fine coal with different moisture contents.” *Int. J. Coal Prep. Util.*, 0(0), 1–10. (SCIE, Scopus)
6. Shanmugam, B. K., Vardhan, H., Raj, M. G., Kaza, M., Sah, R., and **Hanumanthappa, H.** (2020). “Experimentation and statistical prediction of screening performance of coal with different moisture content in the vibrating screen.” *Int. J. Coal Prep. Util.*, 1–14. (SCIE, Scopus)
7. Shanmugam, B. K., Vardhan, H., Raj, M. G., Kaza, M., Sah, R., and **Hanumanthappa, H.** (2021). “Artificial neural network modeling for predicting the screening efficiency of coal with varying moisture content in the vibrating screen.” *Int. J. Coal Prep. Util.*, 1–19. (SCIE, Scopus)
8. Mohanraj, G. T., Rahman, M. R., Joladarashi, S., **Hanumanthappa, H.**, Shanmugam, B. K., Vardhan, H., and Rabbani, S. A. (2021). “Design and fabrication of optimized magnetic roller for permanent roll magnetic separator

(PRMS): Finite element method magnetics (FEMM) approach.” *Advanced Powder Technology*, 32(2), 546-564. ***(SCI, Scopus)***

9. Chethan M C , Harish H , Bharath V G, and Kumar K, (2014). “Structural Evaluation of Steel Adapter and Door Type Ring Stiffener in Wind Turbine Tower for Certification.” *International Journal Of Engineering Research & Technology (IJERT)*, 07.
10. Vijay Kumar S, Manjunath C, Lakshmiddevamma M. M, and **Harish.H** (2017). “Prediction of Vortex Flow Visualization using different Fluids by Towing Tank Method.” *Greenze Scientific Society*, 1-5.
11. Bharath S B, Prashantha Kumar S T and **Harish H** (2015) “Structural Chassis Design and Finite Element Optimization of a Truck for Road Vibration”. *International Journal for Ignited Minds*, 2, 160-167.
12. Bipin J, Hanumanthlal S and **Harish H** (2015) “Finite Element Analysis and Optimization of Loading Bin and Mining Platform”. *International Journal for Ignited Minds*, 2, 146-152.
13. Veeresh P, Harish H and Prashantha Kumar S T (2015) “Finite Element Analysis of Casing Stability and Radial Growth of a Steam Turbine Disc”. *International Journal for Ignited Minds*, 2, 138-145.

INTERNATIONAL CONFERENCES

1. **Harish, H.**, Vardhan, H., Raj, M. G., Kaza, M., Sah, R., Sinha, A., and Kumar, S. B. (2020). “Investigation of iron ores based on the bond grindability test.” *AIP Conf. Proc.*, 040006. ***(Scopus)***
2. Shanmugam, B. K., Vardhan, H., Raj, M. G., Kaza, M., Sah, R., and **Hanumanthappa, H** (2020). “The screening efficiency of linear vibrating

screen-An experimental investigation.” In AIP Conference Proceedings, 040002. (*Scopus*)

3. **Harish, H.**, Vardhan, H., Raj, M. G., Kaza, M., Sah, R., and Kumar, S. B. (2019).”Ball mill performance study: A review.” Proceedings of International Conference on Innovations and Emerging Trends in Mechanical Engineering, March 26-27.
4. **Hanumanthappa, H.**, Vardhan, H., Mandela, G. R., Kaza, M., Sah, R., and Shanmugam, B. K. (2020). “Influence of crushed raw materials and crushed-sieved raw materials on grindability to obtain required product particle size distribution” 2nd International Conference on Opencast Mining Technology & Sustainability in association with IIT (BHU) and Springer Nature, December 13-14.
5. Shanmugam, B. K., Vardhan, H., Raj, M. G., Kaza, M., Sah, R., and **Hanumanthappa, H.** (2020). “Shortcomings of Vibrating Screen and Corrective Measures: A Review.” International Conference on Emerging Trends in Engineering (ICETE), 345-351.

WORKSHOPS

- 5th August 2013 to 08th August 2013: Participated 4 days VTU-VGST Faculty Development Programme on "**Finite Element Methods In Structural Mechanics**", S.E.A college of Engineering and Technology, Bangalore.
- 5th to 6th Nov.2012: Participated in the "**Finite Element Methods & its Applications**" **National seminar**" at Dept. Of Mechanical engg., CMR institute of Technology, B'lore.
- 16th&17th APR 2012: Participated two days' workshop on "**Noise and Vibration Control**"Nagarjuna College of Engg & technology, Bangalore.
- 28th& 29th Aug 2009: Participated two days workshop on "**Recent Advancement in Refrigeration and Air conditioning**" Nagarjuna College of Engg & technology(ISHRAE), Bangalore.

S. No	Title	Inventor(s)	Patent No.	Date and Country
1	System for material beneficiation involving hydro-squeeze classifier assisted grinding ball mill	Mr. Harish, Hanumanthappa, Dr. Maruthiram Kaza, Dr. Harsha Vardhan, Dr. Govinda Raj Mandela, Dr. Rameshwar Sah, Mr. Abhishek Kumar, Dr. Arindam Roy Choudary, Mr. Chaitanya Naik, Mr. Suhas Nayak	Patent application number - TEMP/E-1/51796/2018-MUM Application No. 201821047543	15-12-2018 (Patent filled) 19-06-2020 (Patent published) (India)
2	A system for mineral separation and a processthereof combining froth flotation and gravity separation.	Mr. Varma raju, Dr. Harsha Vardhan, Dr. Govinda Raj Mandela, Dr. Rameshwar Sah, Mr. Harish Hanumanthappa, Mr. Shanmugam Bharath Kumar	TEMP/E-1/4060/2021-MUM Application No. 202121003890	28-01-2021 (Patent filled)
3	Hydro-squeeze separator system for material beneficiation.	Mr. Harish Hanumanthappa, Dr. Harsha Vardhan, Dr. Govinda Raj Mandela, Dr. Rameshwar Sah, Mr.		In filling process

S. No	Title	Inventor(s)	Patent No.	Date and Country
		Shanmugam Bharath Kumar, Mr. Varma raju		
4	A process of hydrosqueeze pressure filtering for the efficient beneficiation of coal material	Mr. Shanmugam Bharath Kumar, Dr. Harsha Vardhan, Dr. Govinda Raj Mandela, Dr. Rameshwar Sah, Mr. Harish Hanumanthappa , Mr. Varma Raju, Mr. Harish Kumar N S		In filling process